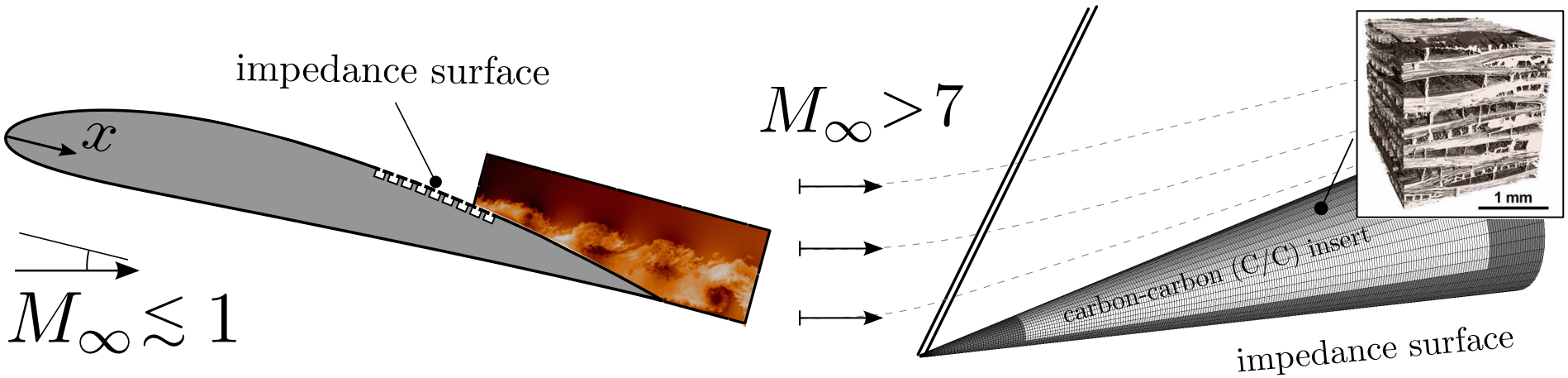
Resonant mode control from transonic to hypersonic boundary layers over complex wall impedance

Dr. Carlo Scalo

School of Mechanical Engineering, Purdue University, IN, USA



AFOSR
AIR FORCE OFFICE OF SCIENTIFIC RESEARCH

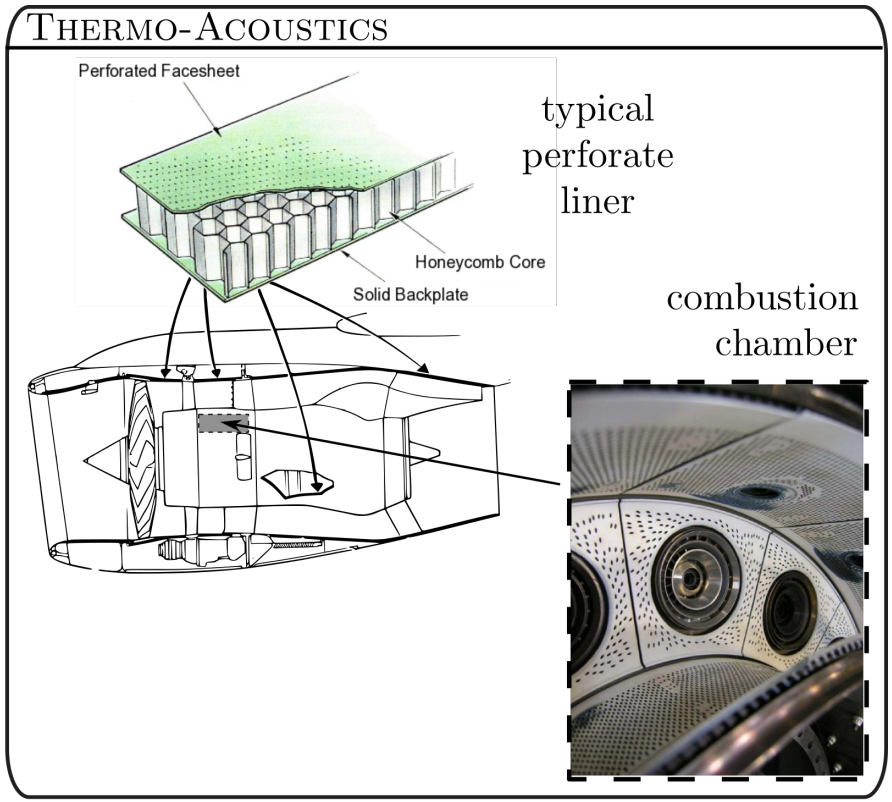
Award FA9550-16-1-0209

Advanced Modeling & Simulation (AMS) Seminar Series

NASA Ames Research Center
Building N258, Auditorium (Rm 127)
Moffett Field, California
August 7, 2017

PURDUE MECHANICAL ENGINEERING

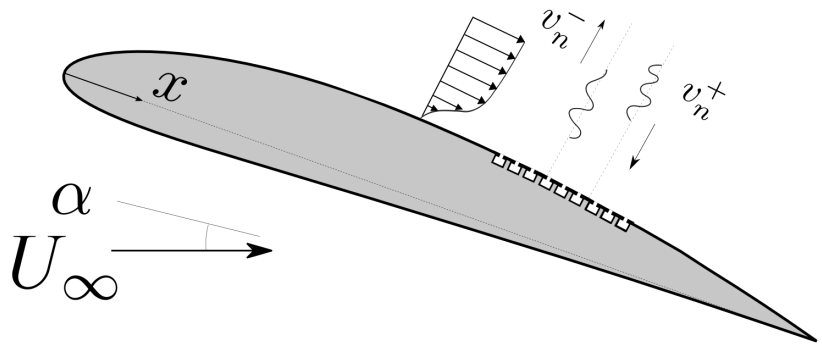
Porous surfaces in aeronautical applications



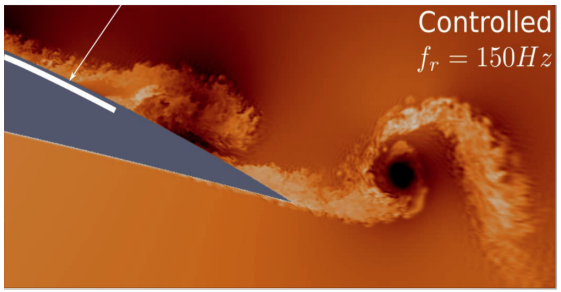
Background

Porous surfaces in aeronautical applications

Flow-Separation Control

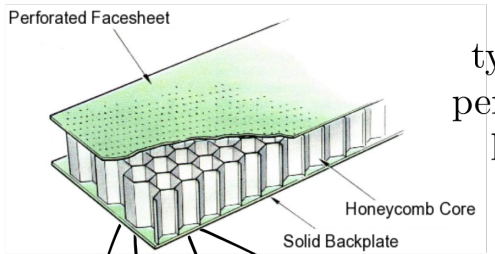


impedance strip



Bodart & Scalo, AIAA-SciTech, 2017

Thermo-Acoustics



typical perforate liner

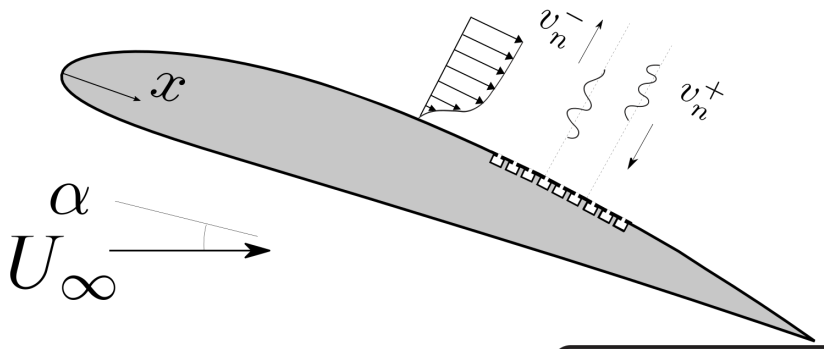
combustion chamber



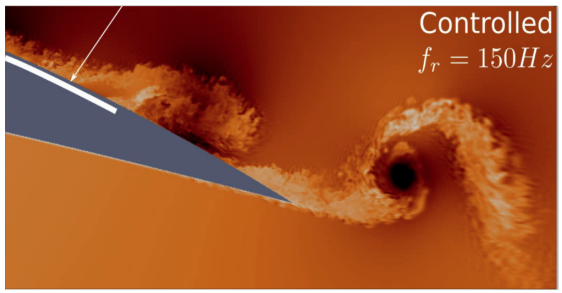
Background

Porous surfaces in aeronautical applications

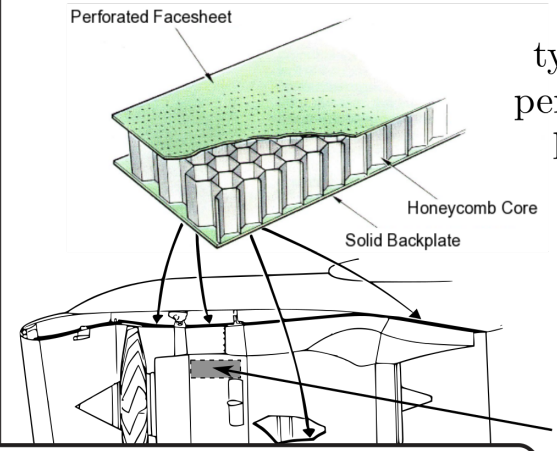
Flow-Separation Control



impedance strip



Thermo-Acoustics

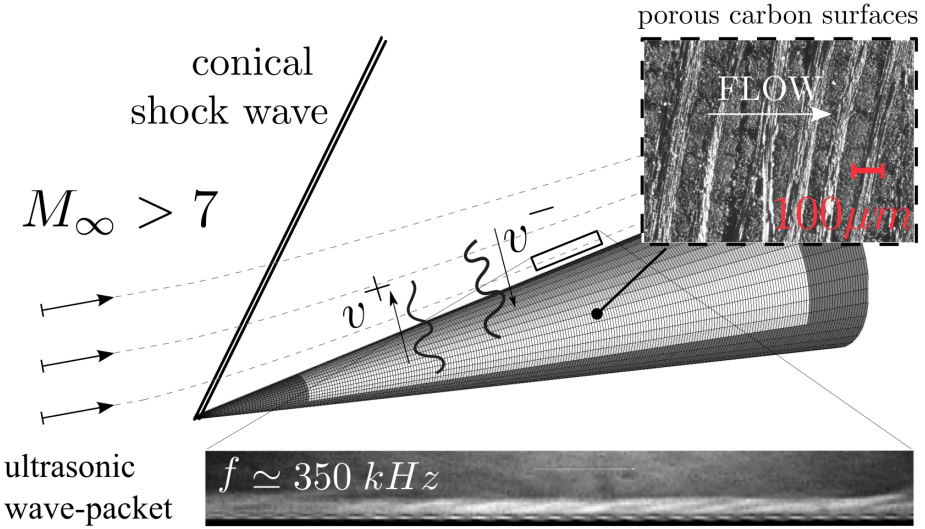


typical perforate liner

combustion chamber



Hypersonic Transition Control



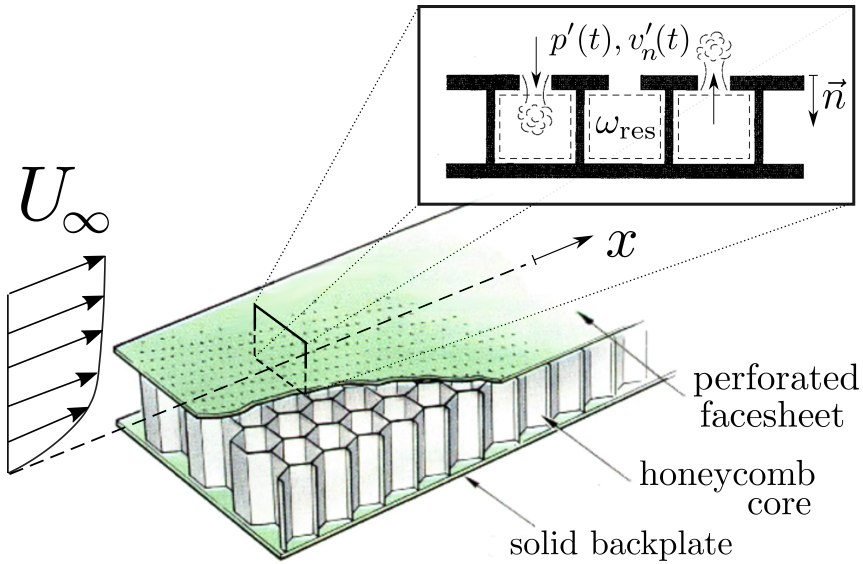
AFOSR grant FA9550-16-1-0209

Impedance Boundary Conditions (IBC)

- Frequency response of porous surfaces is defined via acoustic impedance, $Z(\omega)$:

$$\hat{p} = \rho_0\, a_0 Z(\omega)\hat{v}_n, \quad Z(\omega) = \underbrace{R(\omega)}_{\text{resistance}} + i\underbrace{X(\omega)}_{\text{reactance}}, \quad \text{(hereafter:} \quad \rho_0\, a_0 = 1)$$

where $\hat{p}$ and $\hat{v}$ are the Fourier transforms of pressure and transpiration velocity



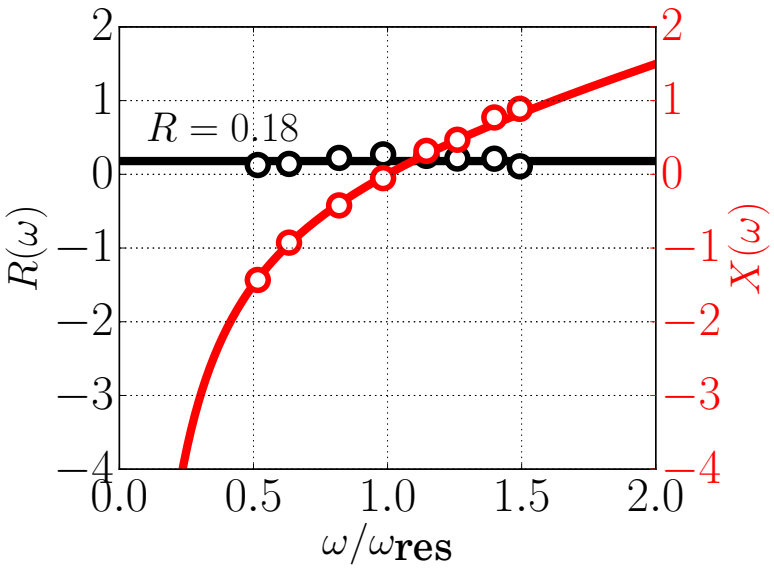
PURDUE UNIVERSITY

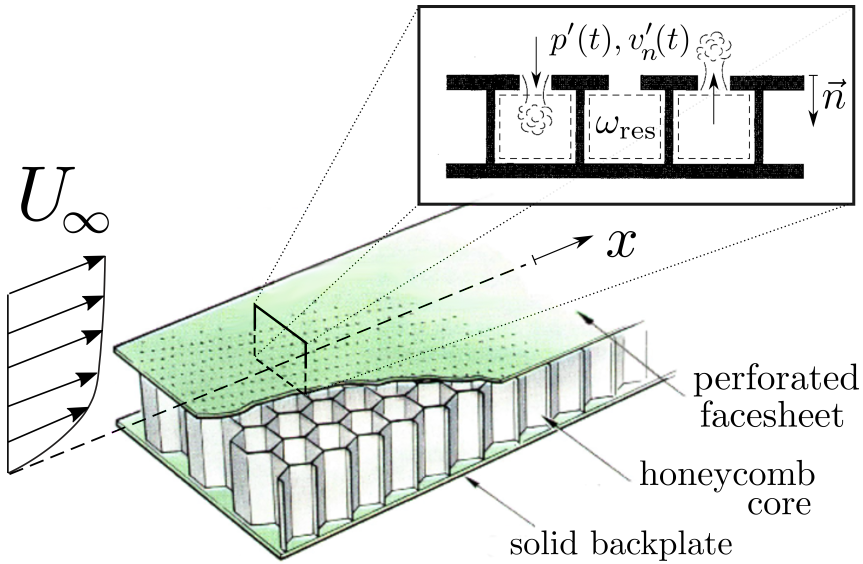
Impedance Boundary Conditions (IBC)

- Frequency response of porous surfaces is defined via acoustic impedance, $Z(\omega)$:

$$\hat{p} = \rho_0\, a_0 Z(\omega)\hat{v}_n, \quad Z(\omega) = \underbrace{R(\omega)}_{\text{resistance}} + i\underbrace{X(\omega)}_{\text{reactance}}, \quad \text{(hereafter:} \quad \rho_0\, a_0 = 1)$$

where $\hat{p}$ and $\hat{v}$ are the Fourier transforms of pressure and transpiration velocity





- Three-parameter model (Tam and Auriault, AIAA, 1996)

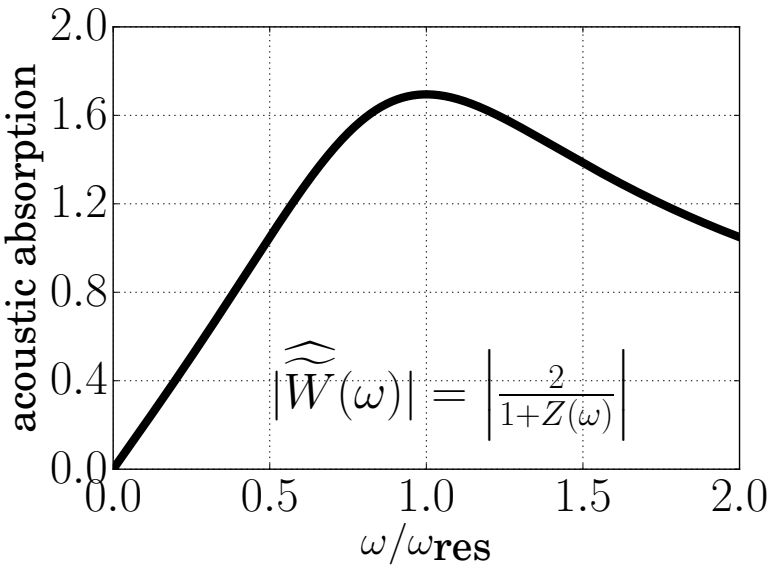
$$Z(\omega) = R - i\left(X_{(-1)}/\omega - X_{(+1)}\omega\right), \quad \text{where} \quad \omega_{\text{res}} = \sqrt{\frac{X_{(-1)}}{X_{(+1)}}}$$

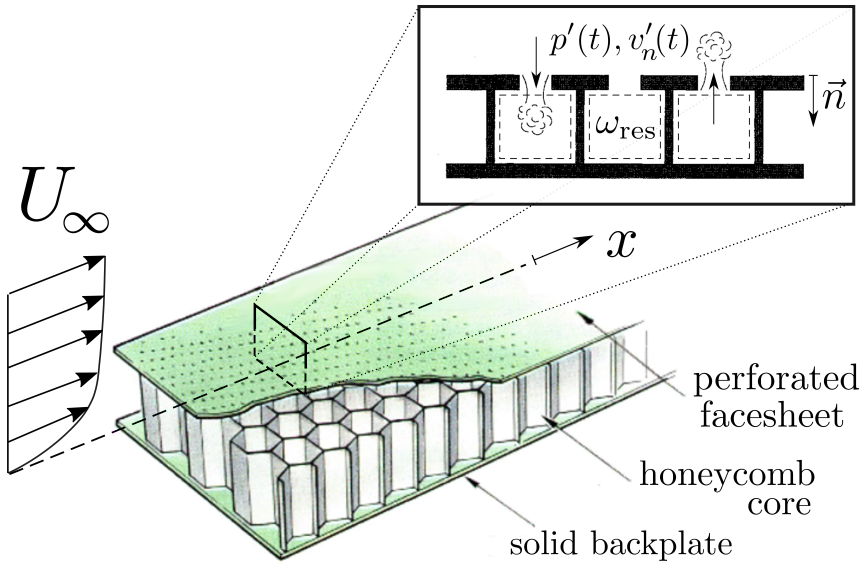
Impedance Boundary Conditions (IBC)

- Frequency response of porous surfaces is defined via acoustic impedance, $Z(\omega)$:

$$\hat{p} = \rho_0\, a_0 Z(\omega)\hat{v}_n, \quad Z(\omega) = \underbrace{R(\omega)}_{\text{resistance}} + i\underbrace{X(\omega)}_{\text{reactance}}, \quad (\text{hereafter:} \quad \rho_0\, a_0 = 1)$$

where $\hat{p}$ and $\hat{v}$ are the Fourier transforms of pressure and transpiration velocity





- Three-parameter model (Tam and Auriault, AIAA, 1996)

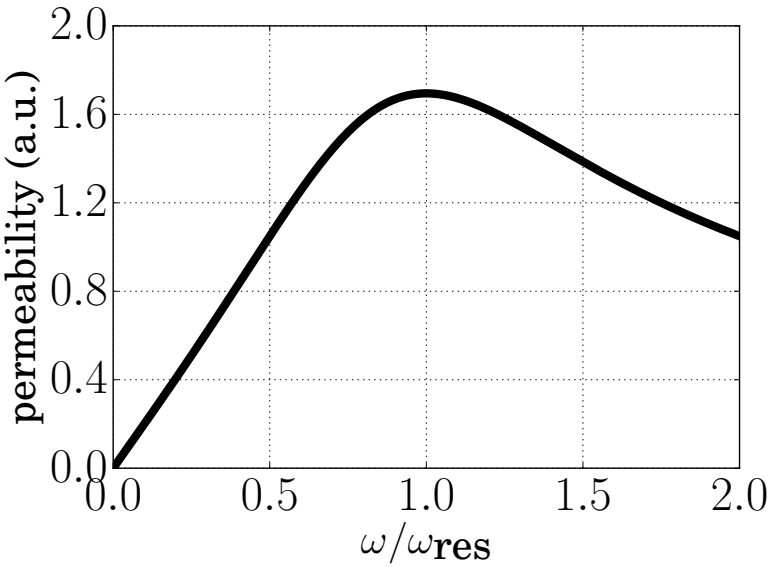
$$Z(\omega) = R - i\left(X_{(-1)}/\omega - X_{(+1)}\omega\right), \quad \text{where} \quad \omega_{\text{res}} = \sqrt{\frac{X_{(-1)}}{X_{(+1)}}}$$

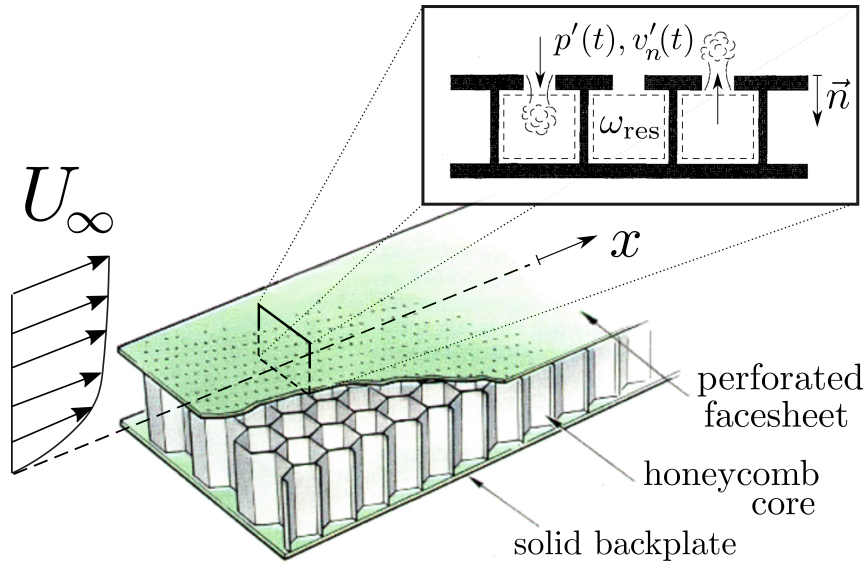
Impedance Boundary Conditions (IBC)

- Frequency response of porous surfaces is defined via acoustic impedance, $Z(\omega)$:

$$\hat{p} = \rho_0\, a_0 Z(\omega)\hat{v}_n, \quad Z(\omega) = \underbrace{R(\omega)}_{\text{resistance}} + i\underbrace{X(\omega)}_{\text{reactance}}, \quad \text{(hereafter:} \quad \rho_0\, a_0 = 1)$$

where $\hat{p}$ and $\hat{v}$ are the Fourier transforms of pressure and transpiration velocity





- Three-parameter model (Tam and Auriault, AIAA, 1996)

$$Z(\omega) = R - i\left(X_{(-1)}/\omega - X_{(+1)}\omega\right), \quad \text{where} \quad \omega_{\text{res}} = \sqrt{\frac{X_{(-1)}}{X_{(+1)}}}$$

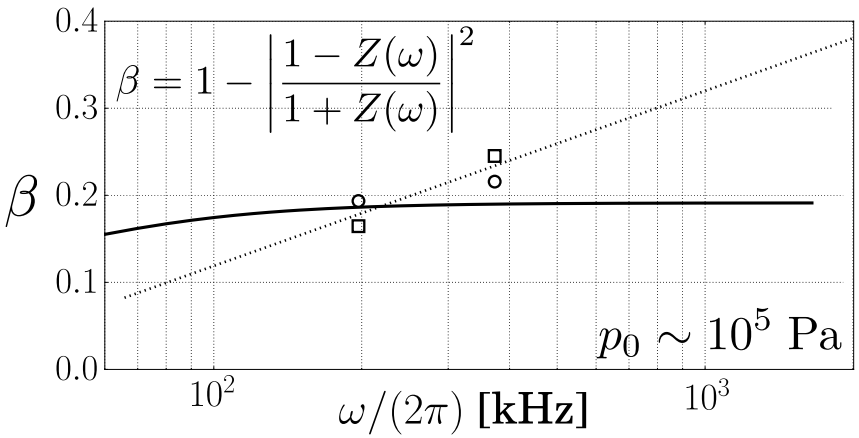
PURDUE UNIVERSITY

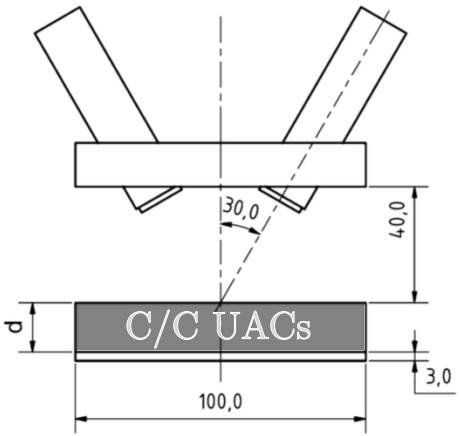
Impedance Boundary Conditions (IBC)

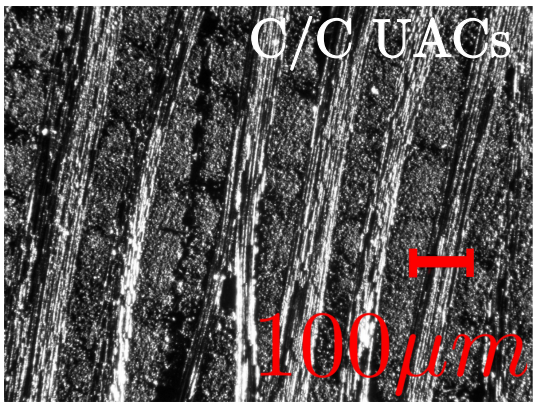
- Frequency response of porous surfaces is defined via acoustic impedance, $Z(\omega)$:

$$\hat{p} = \rho_0\, a_0 Z(\omega)\hat{v}_n, \quad Z(\omega) = \underbrace{R(\omega)}_{\text{resistance}} + i\underbrace{X(\omega)}_{\text{reactance}}, \quad \text{(hereafter:} \quad \rho_0\, a_0 = 1)$$

where $\hat{p}$ and $\hat{v}$ are the Fourier transforms of pressure and transpiration velocity







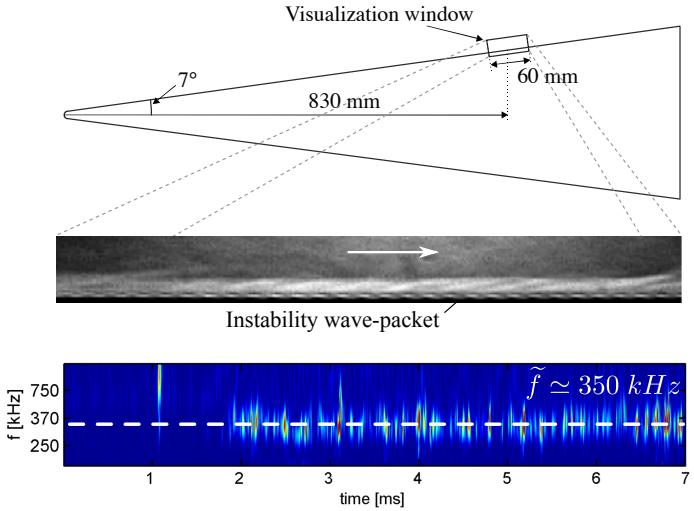
- C/C-UAC: Carbon-Carbon Ultrasonically Absorptive Coatings (see Wagner *et al.* [14, 12])

$$Z(\omega) = \rho_0\, c_0 \frac{\sqrt{k}}{\sigma}\sqrt{1 - j\frac{\omega_k}{\omega}}\frac{1 + e^{-j\,2\,k_a\,d}}{1 - e^{-j\,2\,k_a\,d}} \quad \text{absorber theory (solid line)}$$

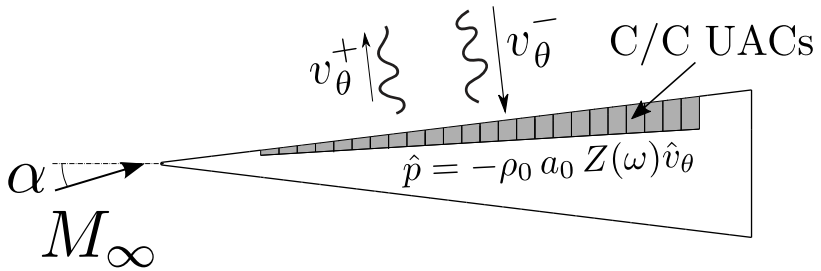
Motivation

Challenges/Questions in Hypersonics

(1) Can impedance boundary conditions be used in Direct Numerical Simulations?



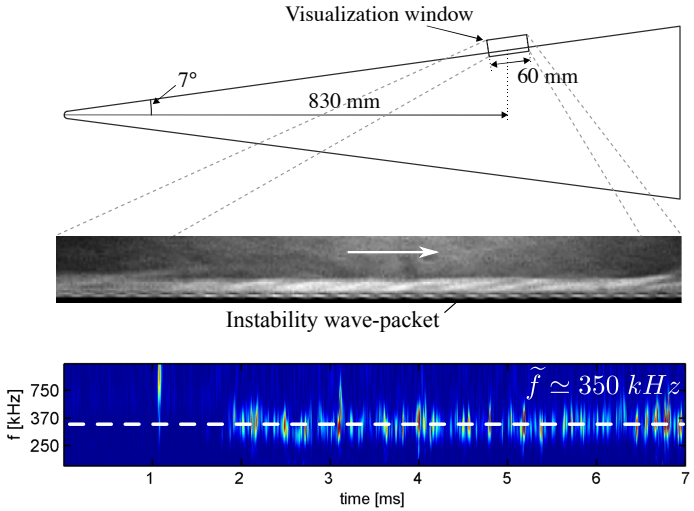


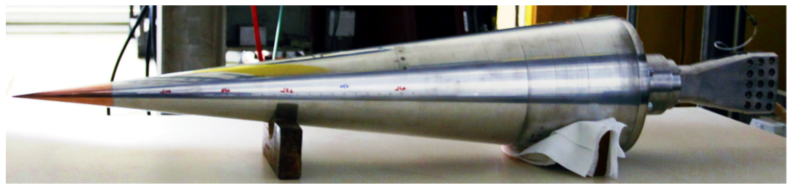


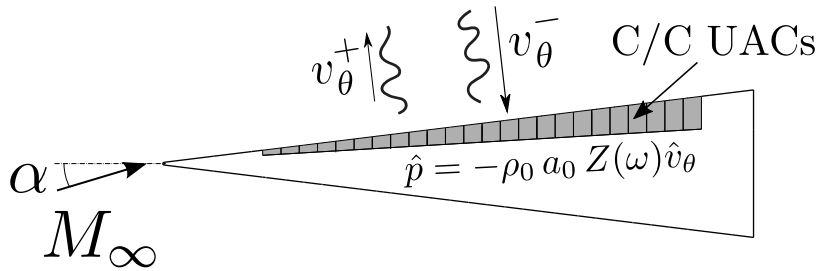
Motivation

Challenges/Questions in Hypersonics

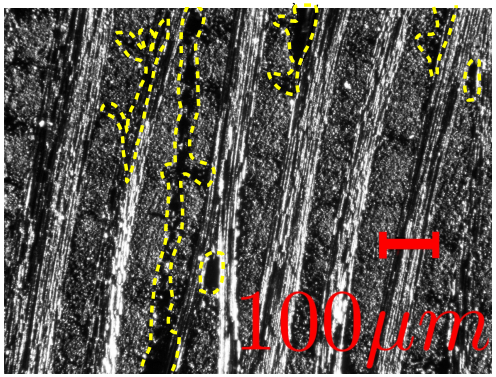
(1) Can impedance boundary conditions be used in Direct Numerical Simulations?

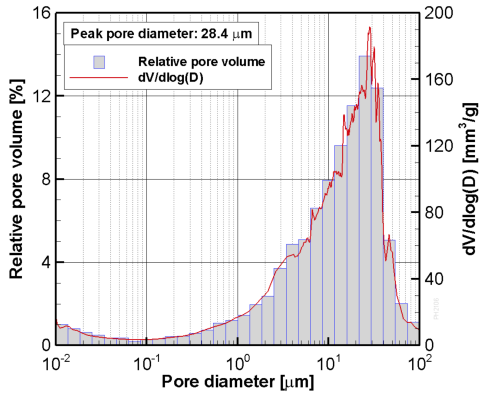






(2) Can the surface impedance of realistic UAC be accurately characterized?





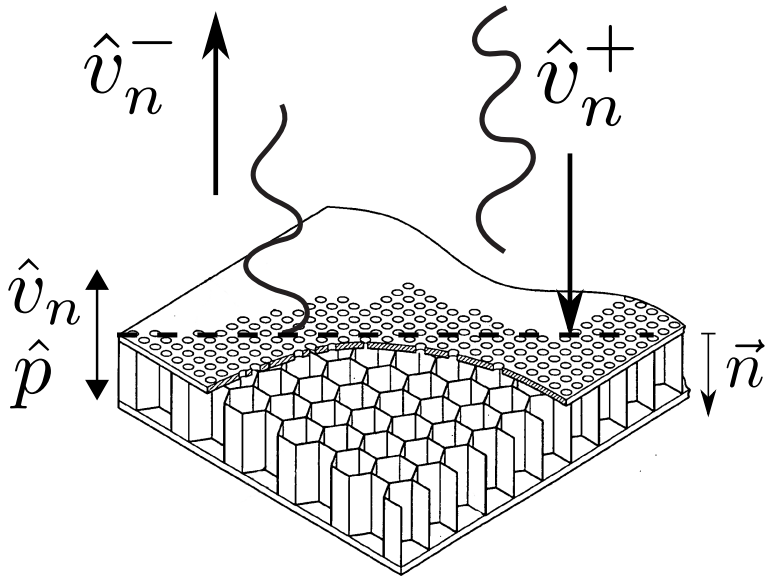
Time-Domain Impedance BCs

PURDUE UNIVERSITY

Is any impedance $Z(\omega)$ physically realizable?

- One approach to implementing time-domain impedance boundary conditions is:

$$\hat{p} = Z(\omega)\hat{v}_n \quad \Rightarrow \quad p(t) = \int_{-\infty}^{\infty} \bar{Z}(\tau) v_n(t-\tau) d\tau$$



Time-Domain Impedance BCs

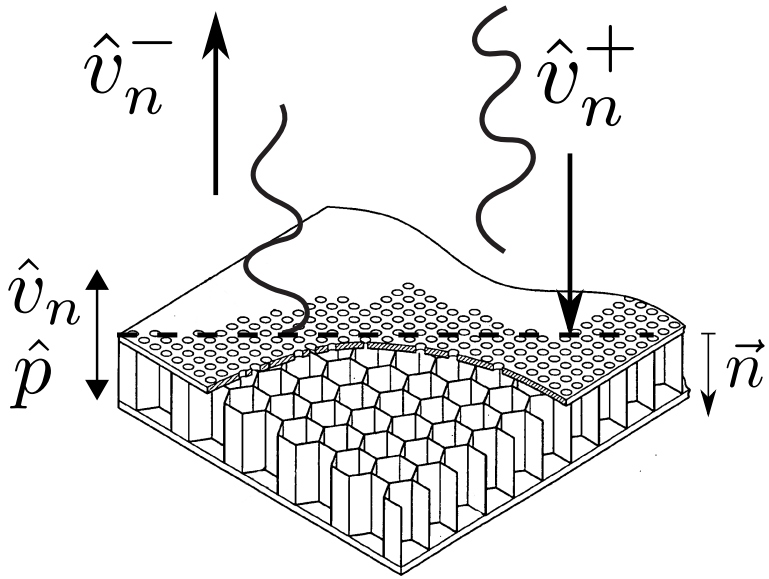
PURDUE UNIVERSITY

Is any impedance $Z(\omega)$ physically realizable?

- One approach to implementing time-domain impedance boundary conditions is:

$$\hat{p} = Z(\omega)\hat{v}_n \quad \Rightarrow \quad p(t) = \int_{-\infty}^{\infty} \bar{Z}(\tau) v_n(t-\tau) d\tau$$

- Physical realizability requires causality, i.e. current values of pressure cannot depend on future values of velocity



Time-Domain Impedance BCs

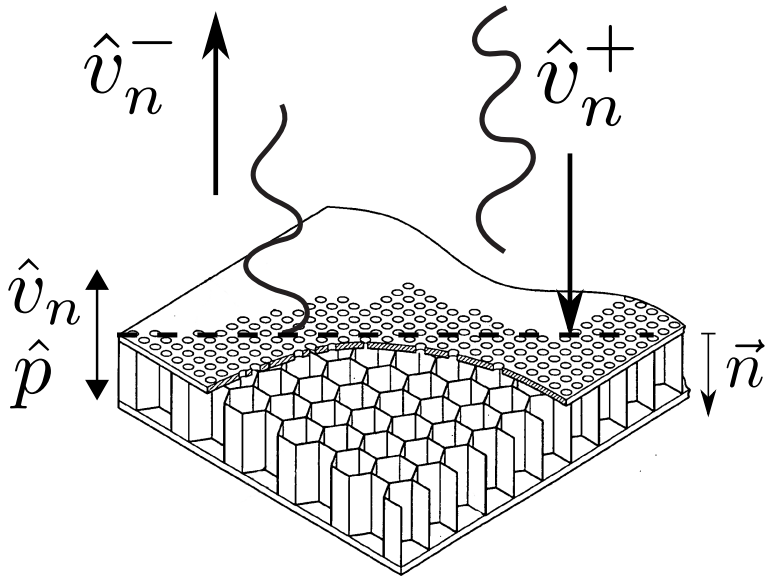
PURDUE UNIVERSITY

Is any impedance $Z(\omega)$ physically realizable?

- One approach to implementing time-domain impedance boundary conditions is:

$$\hat{p} = Z(\omega)\hat{v}_n \quad \Rightarrow \quad p(t) = \int_{-\infty}^{\infty} \bar{Z}(\tau) v_n(t-\tau) d\tau$$

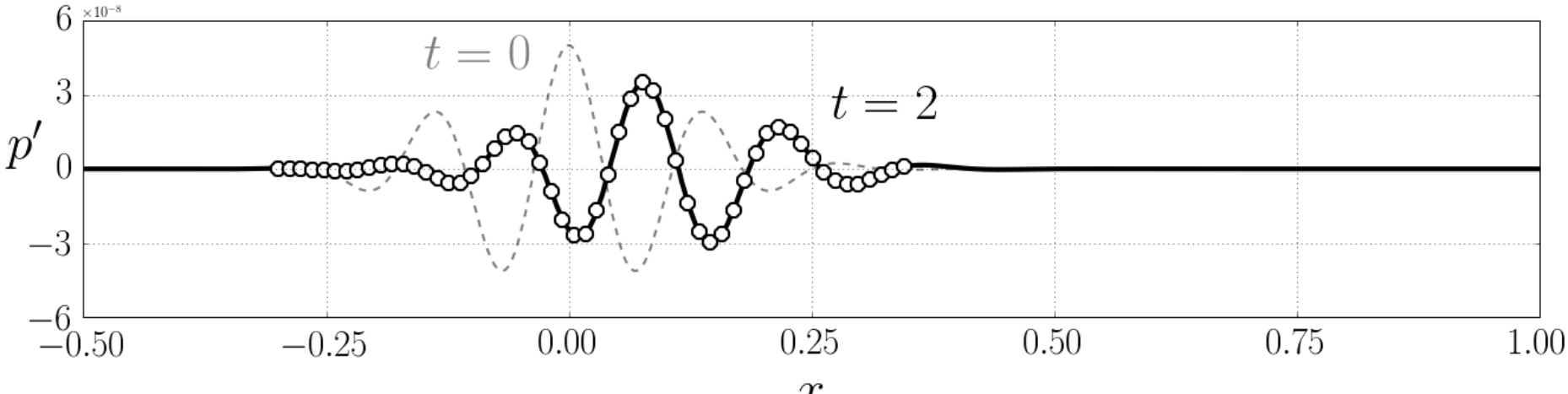
- Physical realizability requires causality, i.e. current values of pressure cannot depend on future values of velocity
- The inverse-transform of the complex impedance needs to satisfy: $\bar{Z}(\tau) = 0 \quad \forall \tau < 0$



Time-Domain Impedance Boundary Conditions (TDIBC)

- Exact imposition of IBCs in Navier-Stokes solver (Fung & Ju [2, 3], Scalo *et al.* [10, 6])
- Impedance Tube: test case with $Z(\omega) = R - i\left[X_{(-1)}\omega^{-1} - X_{(+1)}\omega\right]$ located at $x = 1$
- Navier-Stokes solver: high-order compact finite difference scheme (CFDSU)
  - right-traveling broadband pulse at $t = 0$:

$$p' = \frac{1}{2} A e^{-\alpha\, k^2\, x^2} \cos\left[2\,\pi\, k\, x\right]$$
$$u' = p'$$



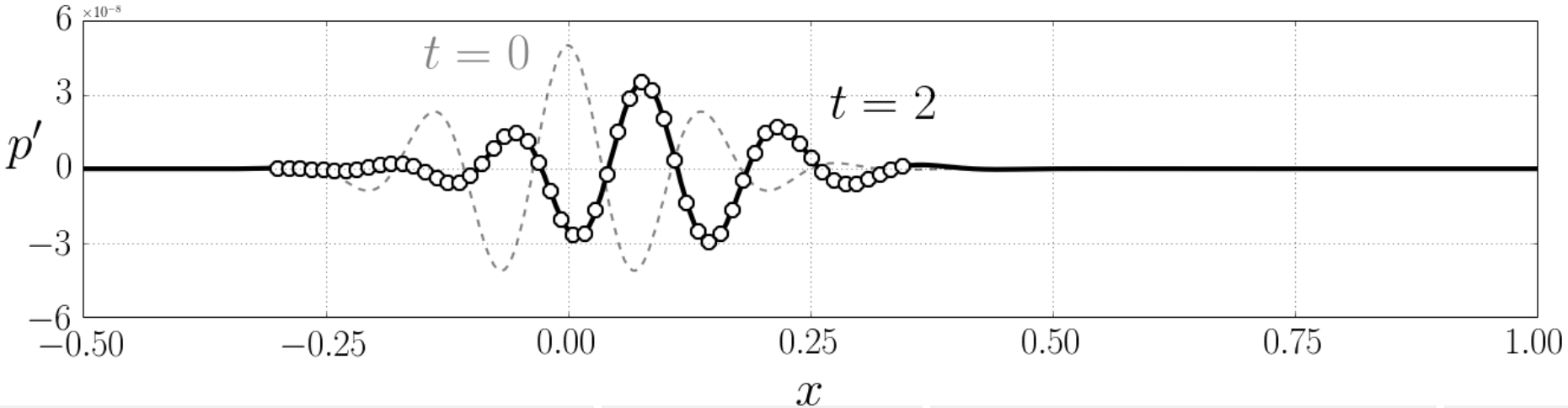
Time-Domain Impedance Boundary Conditions (TDIBC)

- Exact imposition of IBCs in Navier-Stokes solver (Fung & Ju [2, 3], Scalo *et al.* [10, 6])
- Impedance Tube: test case with $Z(\omega) = R - i\left[X_{(-1)}\omega^{-1} - X_{(+1)}\omega\right]$ located at $x = 1$
- Navier-Stokes solver: high-order compact finite difference scheme (CFDSU)
  - right-traveling broadband pulse at $t = 0$:

$$p' = \frac{1}{2} A e^{-\alpha\, k^2\, x^2} \cos\left[2\,\pi\, k\, x\right]$$
$$u' = p'$$

  - analytical solution for reflected wave at $t = 2$:

$$p'(x,t) = -\frac{A}{8\pi}\sqrt{\frac{\pi}{\alpha}} \int_{-\infty}^{+\infty} \frac{1 - Z(\omega)}{1 + Z(\omega)} e^{\mp \frac{(\omega/k \pm 2\pi)^2}{4\,\alpha}} e^{-i\omega\left[2-(x+t)\right]}\, d\omega$$



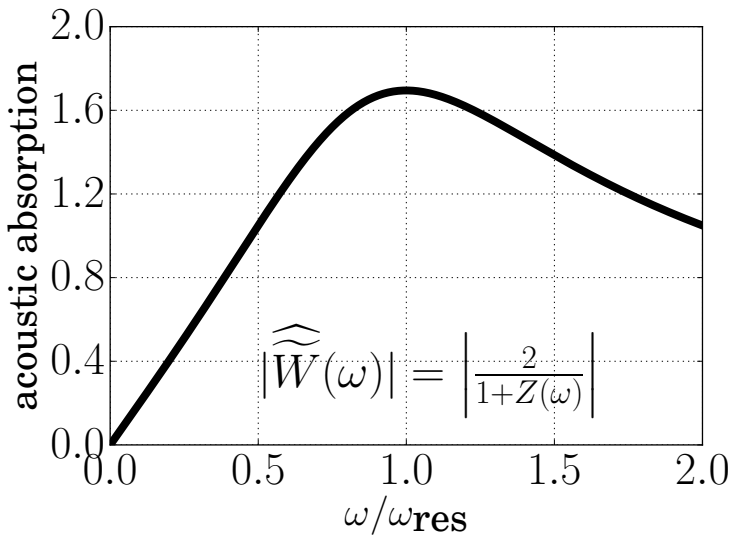
Time-Domain Impedance Boundary Conditions (TDIBC)

- Exact imposition of IBCs in Navier-Stokes solver (Fung & Ju [2, 3], Scalo *et al.* [10, 6])

Time-Domain Impedance Boundary Conditions (TDIBC)

- Exact imposition of IBCs in Navier-Stokes solver (Fung & Ju [2, 3], Scalo *et al.* [10, 6])
- Implementation based on complex absorption coefficient:

$$\widehat{\widetilde{W}}(\omega) = \frac{2}{1 + Z(\omega)}$$

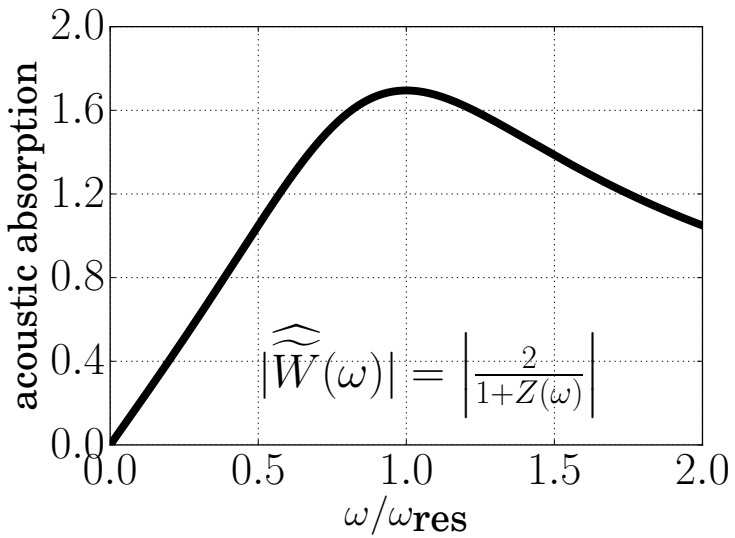


Time-Domain Impedance Boundary Conditions (TDIBC)

- Exact imposition of IBCs in Navier-Stokes solver (Fung & Ju [2, 3], Scalo *et al.* [10, 6])
- Implementation based on complex absorption coefficient:

$$\widehat{\widetilde{W}}(\omega) = \frac{2}{1 + Z(\omega)}$$

$$\underbrace{u^+(t) = u'(t) + p'(t)}_{\text{incoming wave at IB}}$$

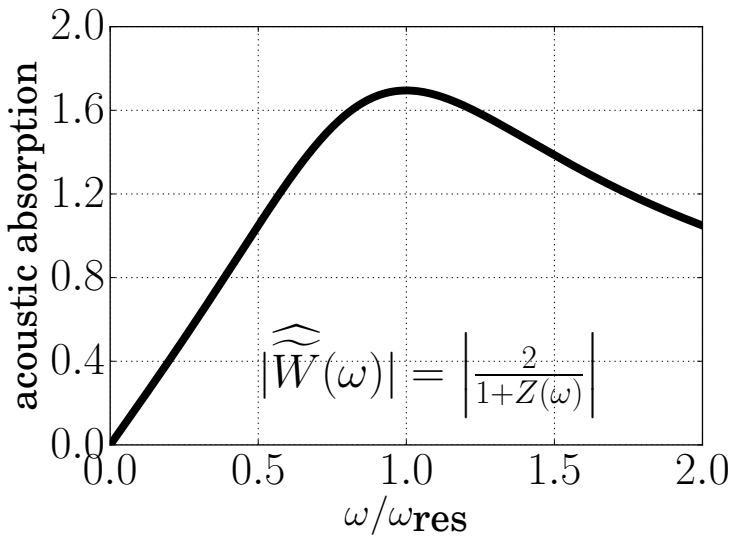


Time-Domain Impedance Boundary Conditions (TDIBC)

- Exact imposition of IBCs in Navier-Stokes solver (Fung & Ju [2, 3], Scalo *et al.* [10, 6])
- Implementation based on complex absorption coefficient:

$$\widehat{\widetilde{W}}(\omega) = \frac{2}{1 + Z(\omega)}$$

$$\underbrace{u^+(t) = u'(t) + p'(t)}_{\text{incoming wave at IB}} \quad \Rightarrow \quad \underbrace{\hat{u}^-(\omega) = -\hat{u}^+(\omega) + \widehat{\widetilde{W}}(\omega)\hat{u}^+(\omega)}_{\text{reflection/absorption}}$$

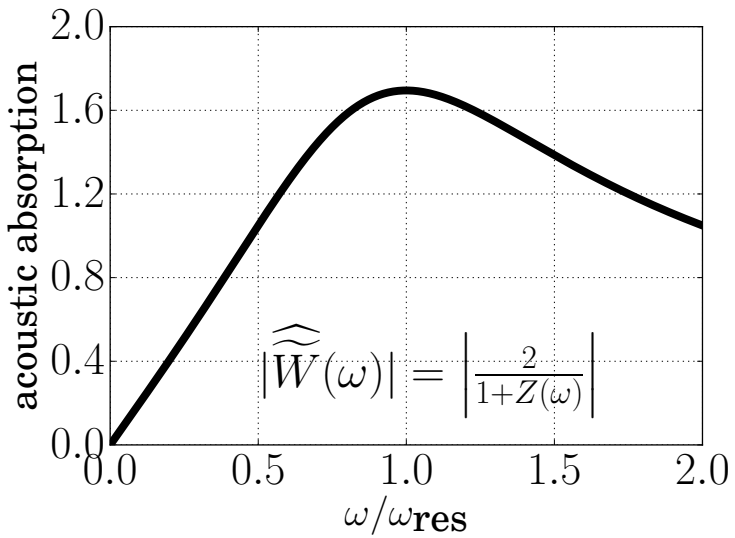


Time-Domain Impedance Boundary Conditions (TDIBC)

- Exact imposition of IBCs in Navier-Stokes solver (Fung & Ju [2, 3], Scalo *et al.* [10, 6])
- Implementation based on complex absorption coefficient:

$$\widehat{\widetilde{W}}(\omega) = \frac{2}{1 + Z(\omega)}$$

$$\underbrace{u^+(t) = u'(t) + p'(t)}_{\text{incoming wave at IB}} \quad \Rightarrow \quad \underbrace{\hat{u}^-(\omega) = -\hat{u}^+(\omega) + \widehat{\widetilde{W}}(\omega)\hat{u}^+(\omega)}_{\text{reflection/absorption}} \quad \Rightarrow \quad \underbrace{u^-(t) = u'(t) - p'(t)}_{\text{reflected wave at IB}}$$



Time-Domain Impedance Boundary Conditions (TDIBC)

- Exact imposition of IBCs in Navier-Stokes solver (Fung & Ju [2, 3], Scalo *et al.* [10, 6])
- Implementation based on complex absorption coefficient:

$$\widehat{\widetilde{W}}(\omega) = \frac{2}{1 + Z(\omega)}$$

$$\underbrace{u^+(t) = u'(t) + p'(t)}_{\text{incoming wave at IB}} \quad \Rightarrow \quad \underbrace{\hat{u}^-(\omega) = -\hat{u}^+(\omega) + \widehat{\widetilde{W}}(\omega)\hat{u}^+(\omega)}_{\text{reflection/absorption}} \quad \Rightarrow \quad \underbrace{u^-(t) = u'(t) - p'(t)}_{\text{reflected wave at IB}}$$

where the convolution operation in the time-domain reads:

$$u^-(t) \quad = \quad -u^+(t) + \int_{-\infty}^{\infty} \widetilde{W}(\tau)\, u^+(t-\tau)\, d\tau$$

Time-Domain Impedance Boundary Conditions (TDIBC)

- Exact imposition of IBCs in Navier-Stokes solver (Fung & Ju [2, 3], Scalo *et al.* [10, 6])
- Implementation based on complex absorption coefficient:

$$\widehat{\widetilde{W}}(\omega) = \frac{2}{1 + Z(\omega)}$$

$$\underbrace{u^+(t) = u'(t) + p'(t)}_{\text{incoming wave at IB}} \quad \Rightarrow \quad \underbrace{\hat{u}^-(\omega) = -\hat{u}^+(\omega) + \widehat{\widetilde{W}}(\omega)\hat{u}^+(\omega)}_{\text{reflection/absorption}} \quad \Rightarrow \quad \underbrace{u^-(t) = u'(t) - p'(t)}_{\text{reflected wave at IB}}$$

where the convolution operation in the time-domain reads:

$$u^-(t) \quad = \quad -u^+(t) + \int_0^\infty \widetilde{W}(\tau)\, u^+(t-\tau)\, d\tau$$

- Causality requirement on $\widehat{\widetilde{W}}(\omega)$ dictates that all its poles must be in the upper half ω-plane: $\widetilde{W}(\tau) = 0, \forall \tau < 0$: value of reflected wave cannot depend on future values of incoming wave!

Time-Domain Impedance Boundary Conditions (TDIBC)

- Exact imposition of IBCs in Navier-Stokes solver (Fung & Ju [2, 3], Scalo *et al.* [10, 6])
- Implementation based on complex absorption coefficient:

$$\widehat{\widetilde{W}}(\omega) = \frac{2}{1 + Z(\omega)}$$

$$\underbrace{u^+(t) = u'(t) + p'(t)}_{\text{incoming wave at IB}} \quad \Rightarrow \quad \underbrace{\hat{u}^-(\omega) = -\hat{u}^+(\omega) + \widehat{\widetilde{W}}(\omega)\hat{u}^+(\omega)}_{\text{reflection/absorption}} \quad \Rightarrow \quad \underbrace{u^-(t) = u'(t) - p'(t)}_{\text{reflected wave at IB}}$$

where the convolution operation in the time-domain reads:

$$u^-(t) \quad = \quad -u^+(t) + \int_0^\infty \widetilde{W}(\tau)\, u^+(t-\tau)\, d\tau$$

- Causality requirement on $\widehat{\widetilde{W}}(\omega)$ dictates that all its poles must be in the upper half ω-plane: $\widetilde{W}(\tau) = 0, \forall \tau < 0$: value of reflected wave cannot depend on future values of incoming wave!
- Linear superposition of *causal* Helmholtz oscillators (Lin, Scalo, Hesselink, *JFM*, 2016 [6]):

$$\widehat{\widetilde{W}}(\omega) = \sum_k^n \widehat{\widetilde{W}}_k(\omega) = \sum_k^n \left[\frac{\mu_k}{s - \lambda_k} + \frac{\overline{\mu}_k}{s - \overline{\lambda}_k} \right] = \sum_k^n \frac{A_{2k-1}(i\omega) + A_{2k}}{(i\omega + \bar{\alpha}\omega_{0k})^2 + \omega_{0k}^2 (1 - \bar{\alpha}^2)}$$

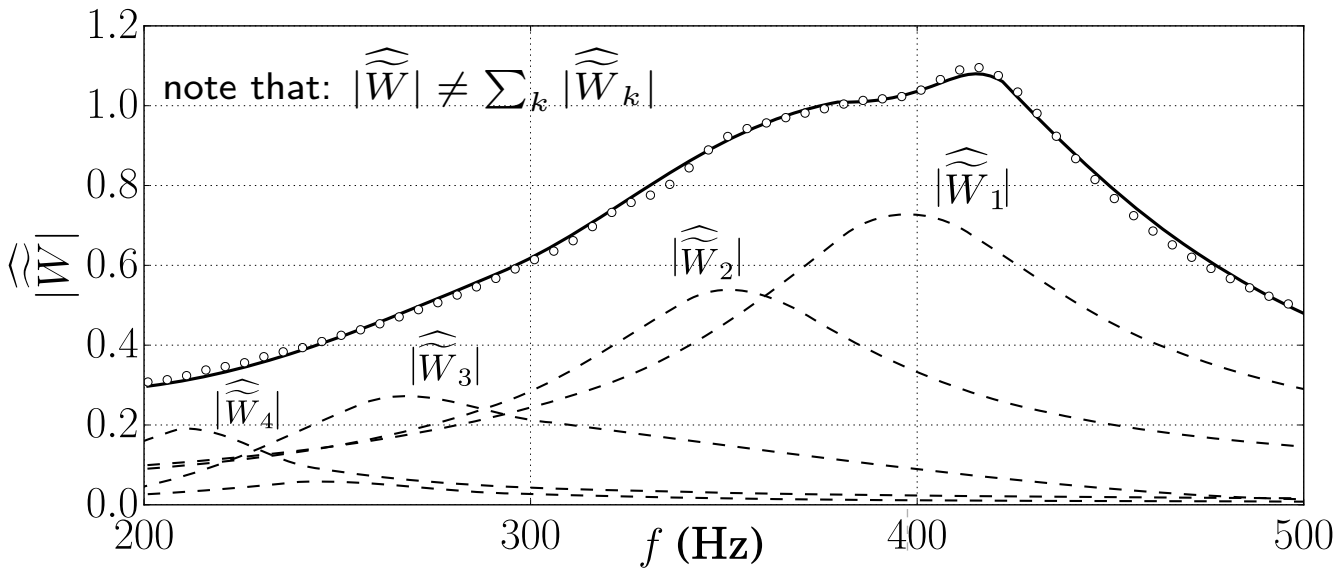
Time-Domain Impedance Boundary Conditions (TDIBC)

- Exact imposition of IBCs in Navier-Stokes solver (Fung & Ju [2, 3], Scalo *et al.* [10, 6])
- Implementation based on complex absorption coefficient:

$$\widehat{\widetilde{W}}(\omega) = \frac{2}{1 + Z(\omega)}$$

- Linear superposition of *causal* Helmholtz oscillators (Lin, Scalo, Hesselink, *JFM*, 2016 [6]):

$$\widehat{\widetilde{W}}(\omega) = \sum_k^n \widehat{\widetilde{W}}_k(\omega) = \sum_k^n \left[\frac{\mu_k}{s - \lambda_k} + \frac{\overline{\mu}_k}{s - \overline{\lambda}_k} \right] = \sum_k^n \frac{A_{2k-1}(i\omega) + A_{2k}}{(i\omega + \bar{\alpha}\omega_{0k})^2 + \omega_{0k}^2 (1 - \bar{\alpha}^2)}$$



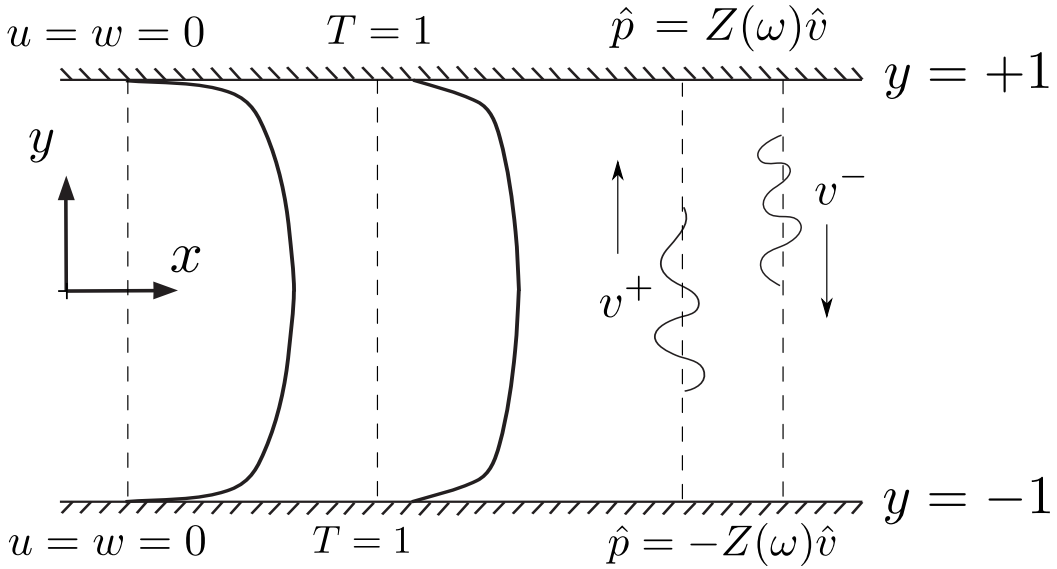
Compressible Turbulent Channel Flow over Impedance

(Bodart, Rahbari & Scalo, 2015 – 2017)

Previous Related Work

Turbulent Channel Flow with IBCs (Scalo et al., 2015 [10])

- Fixed bulk velocity, $Re_b = 6900$, and bulk Mach numbers: $M_b = \{0.05, 0.2, 0.5\}$
- No-slip isothermal BCs, transpiration by impedance: $Z(\omega) = R - i\left[X_{(-1)}\omega^{-1} - X_{(+1)}\omega\right]$
- For each M_b the impedance resistance was varied in the range: $R = \{1, 0.1, 0.01\}$



normalization based on:
- *channel semi-height*
- *speed of sound at the wall*
- *temperature at the wall*

IBC tuning condition:

$$\boxed{f_{res} = M_b}$$

Computational Tools

- Three-dimensional unstructured finite-volume Navier-Stokes solver (CharLES^X)
- Discretization: 2^{nd} – 4^{th} order in space, 3^{rd} order in time

Previous Related Work

Instantaneous Flow Visualization

- Transient flow response to tuned wall-impedance

Entry #: V0036

Near wall turbulence structures
under the effect of tuned wall-impedance

Julien Bodart, Carlo Scalo, Sanjiva K. Lele

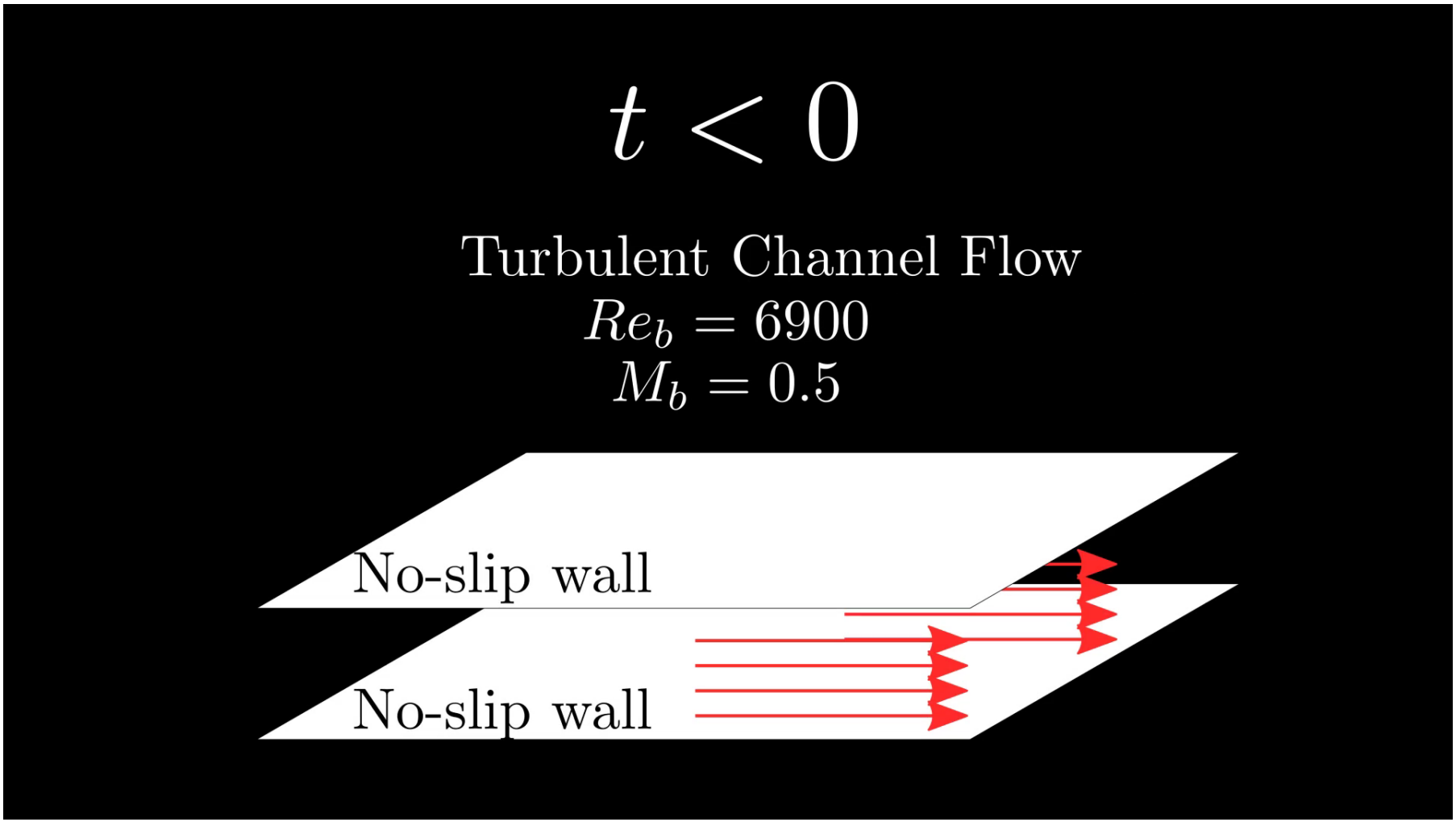
[1] DAEP, Université de Toulouse, ISAE, France
[2] Dept. of Mechanical Eng. Purdue University, IN, USA
[3] Dept. of Aeronautics and Astronautics & Center for Turbulence Research, Stanford University, CA, USA

Previous Related Work

PURDUE UNIVERSITY

Instantaneous Flow Visualization

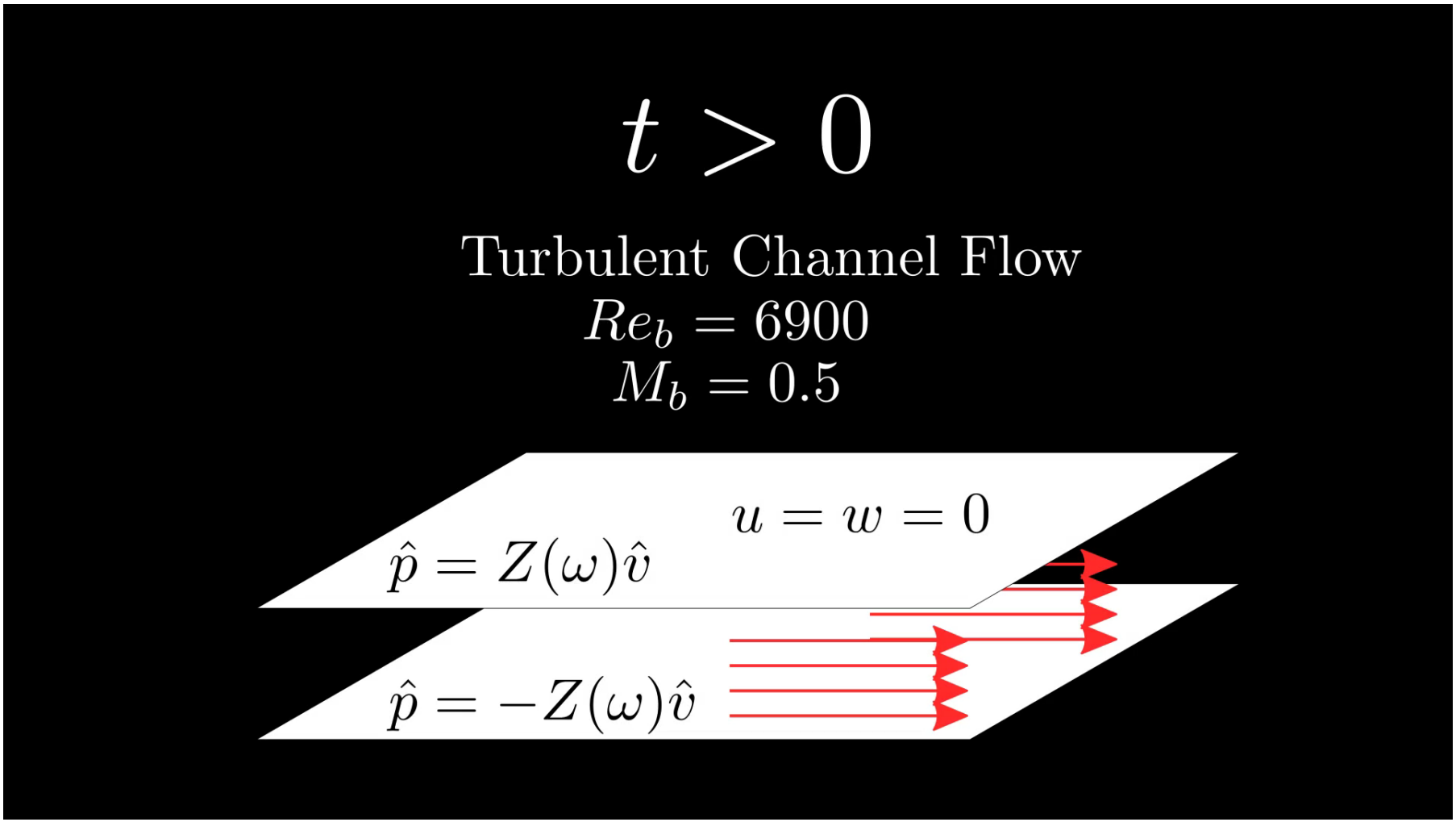
- Transient flow response to tuned wall-impedance



PURDUE UNIVERSITY

Instantaneous Flow Visualization

- Transient flow response to tuned wall-impedance



Previous Related Work

PURDUE UNIVERSITY

Instantaneous Flow Visualization

- Transient flow response to tuned wall-impedance

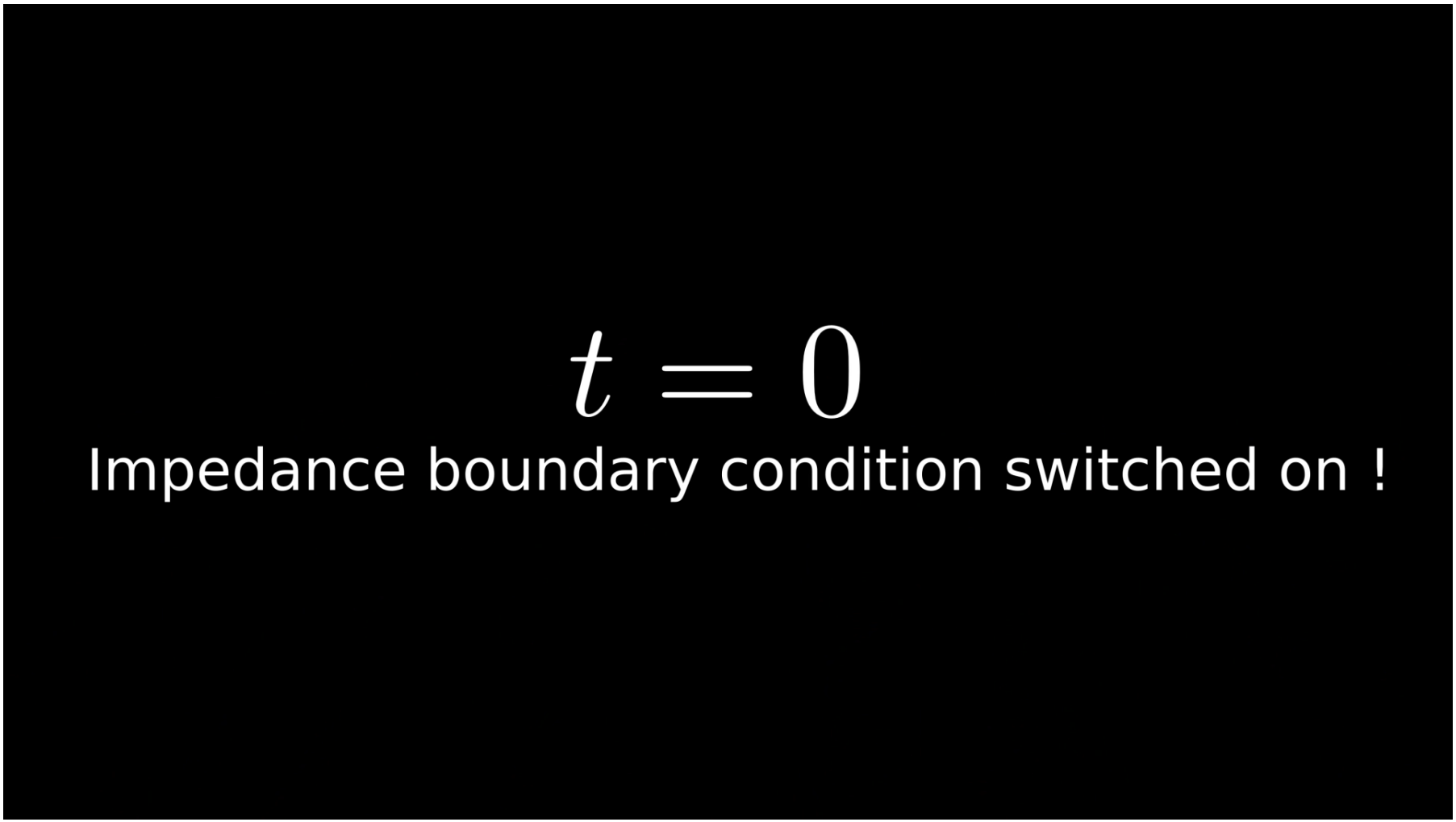


Previous Related Work

PURDUE UNIVERSITY

Instantaneous Flow Visualization

- Transient flow response to tuned wall-impedance

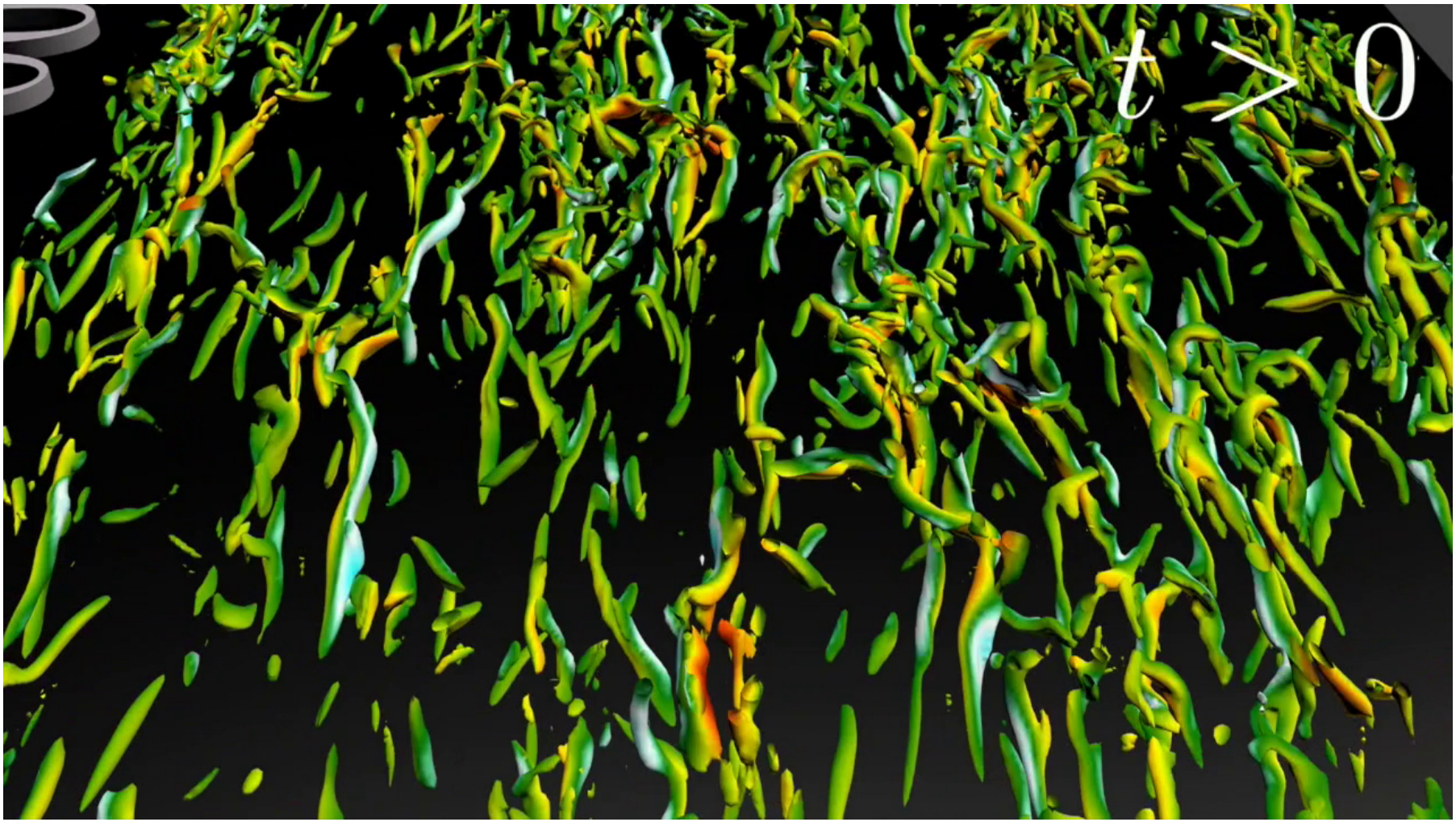


Previous Related Work

PURDUE UNIVERSITY

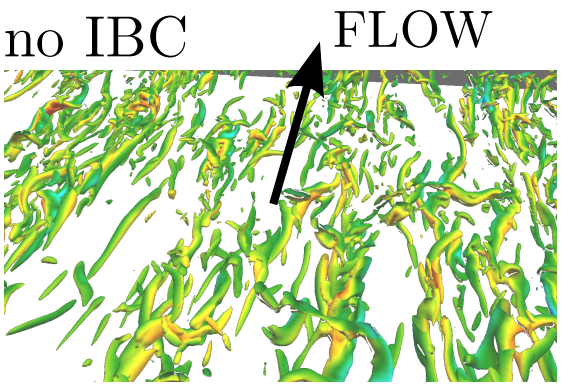
Instantaneous Flow Visualization

- Transient flow response to tuned wall-impedance



Instantaneous Flow Visualization

- Transient flow response to tuned wall-impedance

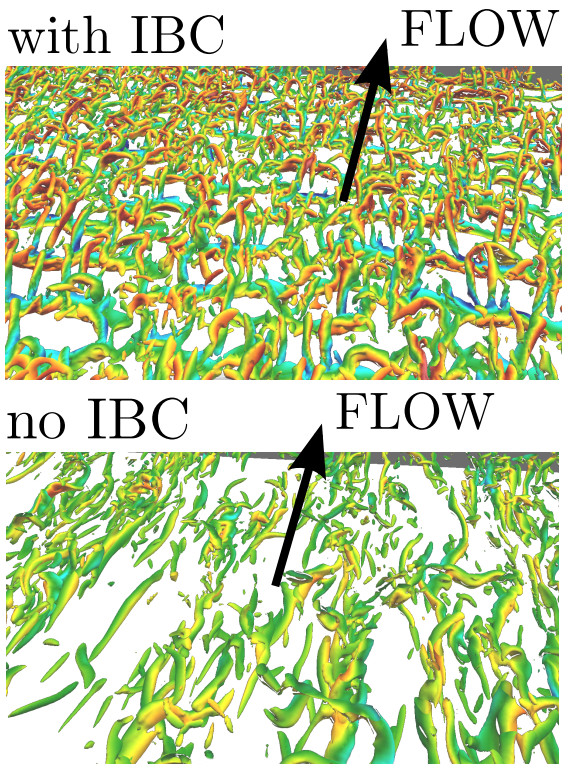


Recall Townsend (1976)'s conjecture on small/moderate roughness heights: buffer layer dynamics can be perturbed without altering the outer flow

Previous Related Work

Instantaneous Flow Visualization

- Transient flow response to tuned wall-impedance

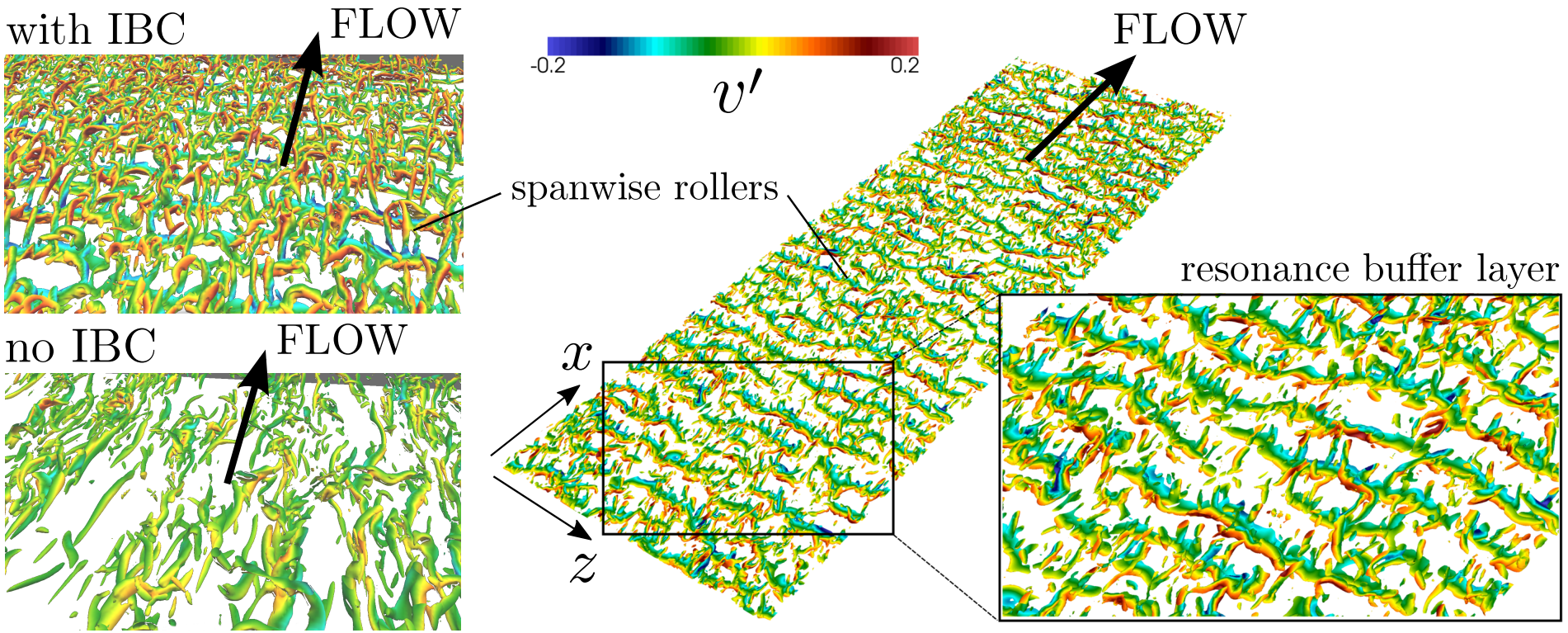


Recall Townsend (1976)'s conjecture on small/moderate roughness heights: buffer layer dynamics can be perturbed without altering the outer flow

Previous Related Work

Instantaneous Flow Visualization

- Transient flow response to tuned wall-impedance



Recall Townsend (1976)'s conjecture on small/moderate roughness heights: buffer layer dynamics can be perturbed without altering the outer flow

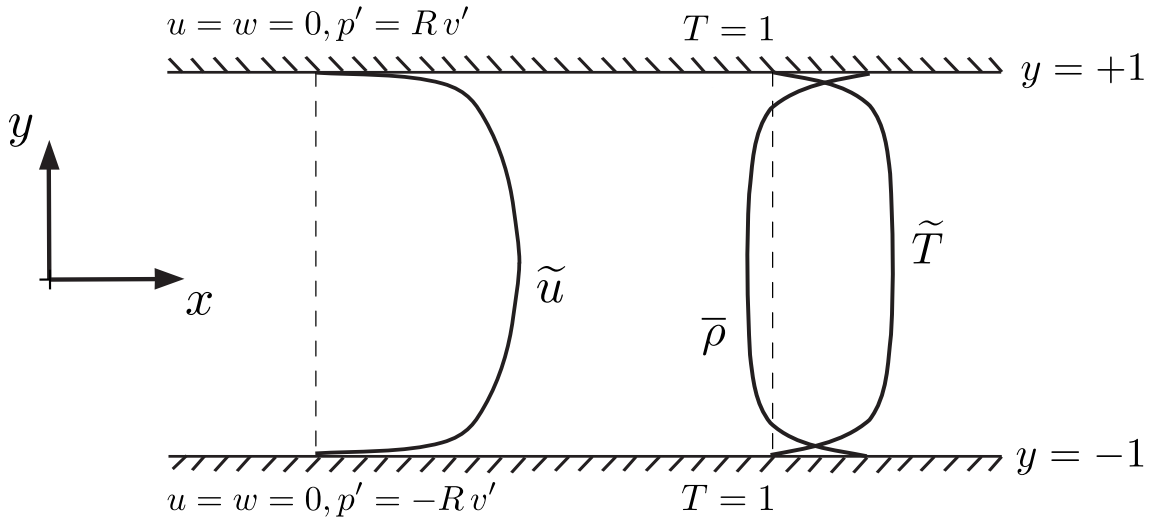
Previous Related Work

Analysis of hydro-acoustic instabilities by Rahbari & Scalo, 2016 [9]

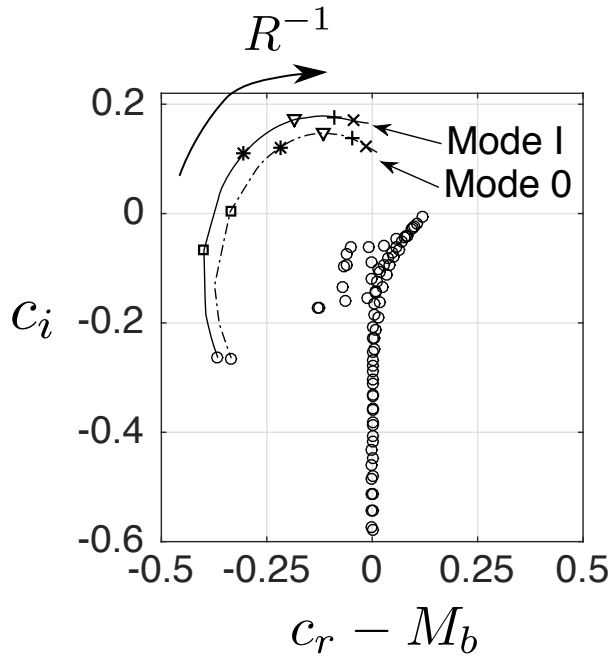
- Linear Stability Analysis assuming two-dimensional perturbation

$$\{u', v', p', T'\}^{tr} = \left\{\hat{u}, \hat{v}, \hat{p}, \hat{T}\right\}^{tr} e^{i\,k\,(x - c\,t)}$$

two unstable modes found for purely real impedance $Z(\omega) = R$, for increasing R^{-1}



channel flow with purely real impedance



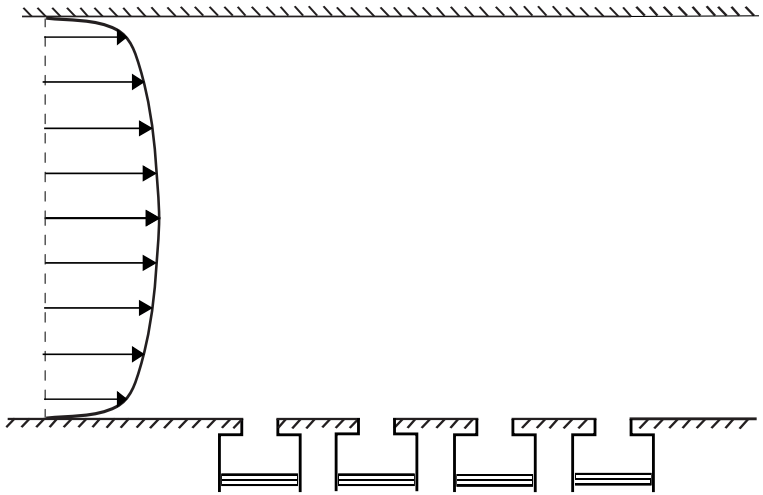
impermeable-wall eigenvalues ($\circ$)

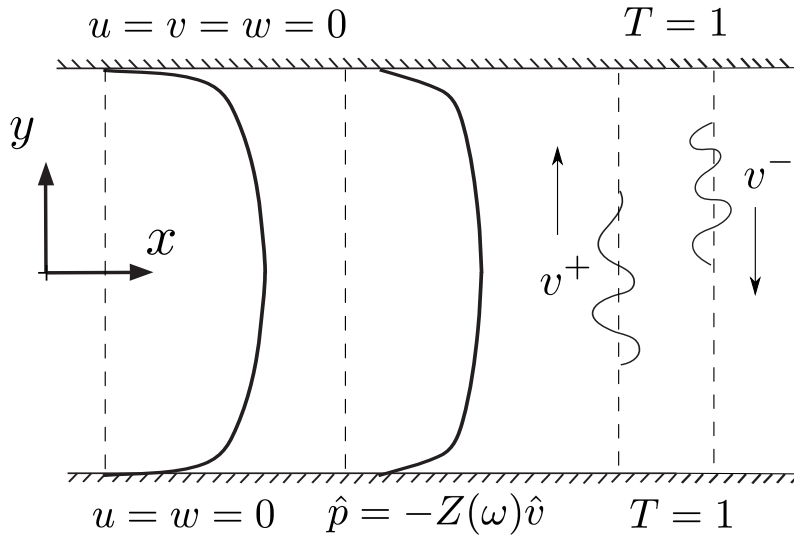
Turbulent Flow over IBCs (Rahbari & Scalo, AIAA, 2017 [8])

- Fixed bulk velocity, $Re_b = 6900$, and bulk Mach number $M_b = 0.85$
- No-slip isothermal BCs, transpiration by impedance: $Z(\omega) = R - i\left[X_{(-1)}\omega^{-1} - X_{(+1)}\omega\right]$
- Resonant frequency $f_{res} = \frac{\omega_{res}}{2\pi}$ is set in the range:

$$f_{res} = \{\frac{M_b}{200}, \frac{M_b}{20}, \frac{M_b}{2}\} \quad \text{, where} \quad \omega_{res} = \sqrt{\frac{X_{-1}}{X_{+1}}} \tag{1}$$

- For each M_b the impedance resistance was varied in the range: $R = \{1.0\}$



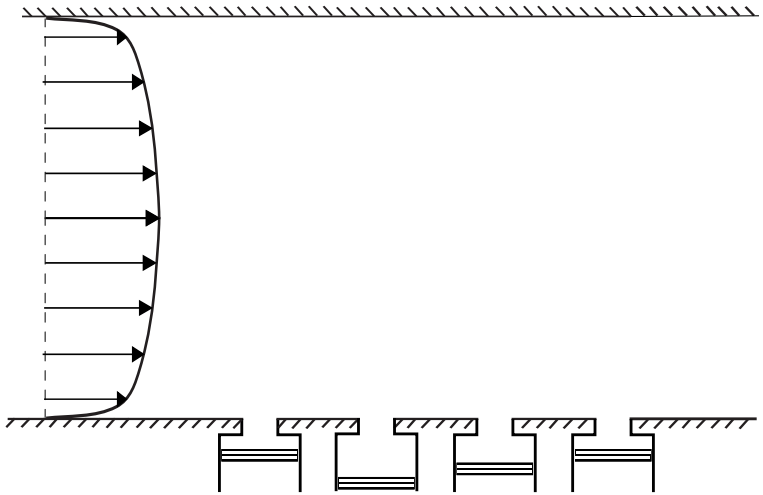


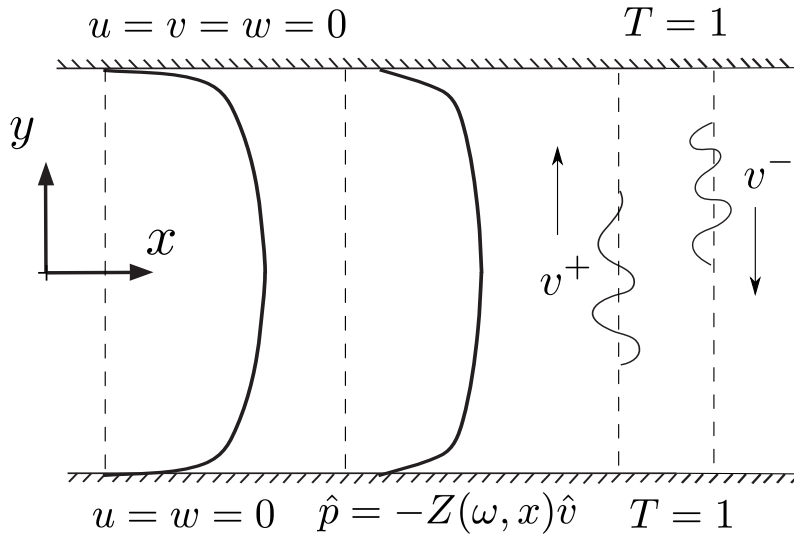
Turbulent Flow over IBCs (Rahbari & Scalo, AIAA, 2017 [8])

- Fixed bulk velocity, $Re_b = 6900$, and bulk Mach number $M_b = 0.85$
- No-slip isothermal BCs, transpiration by impedance: $Z(\omega) = R - i\left[X_{(-1)}\omega^{-1} - X_{(+1)}\omega\right]$
- Resonant frequency $f_{res} = \frac{\omega_{res}}{2\pi}$ is varying in x direction as

$$f_{res} = \frac{M_b}{20} \times \left(1 + 0.2 \times \sin\left(\frac{2\pi x}{L}\right)\right) \quad \text{, where} \quad \omega_{res} = \sqrt{\frac{X_{-1}}{X_{+1}}} \tag{2}$$

- Impedance resistance is considered constant $R = \{1.0\}$

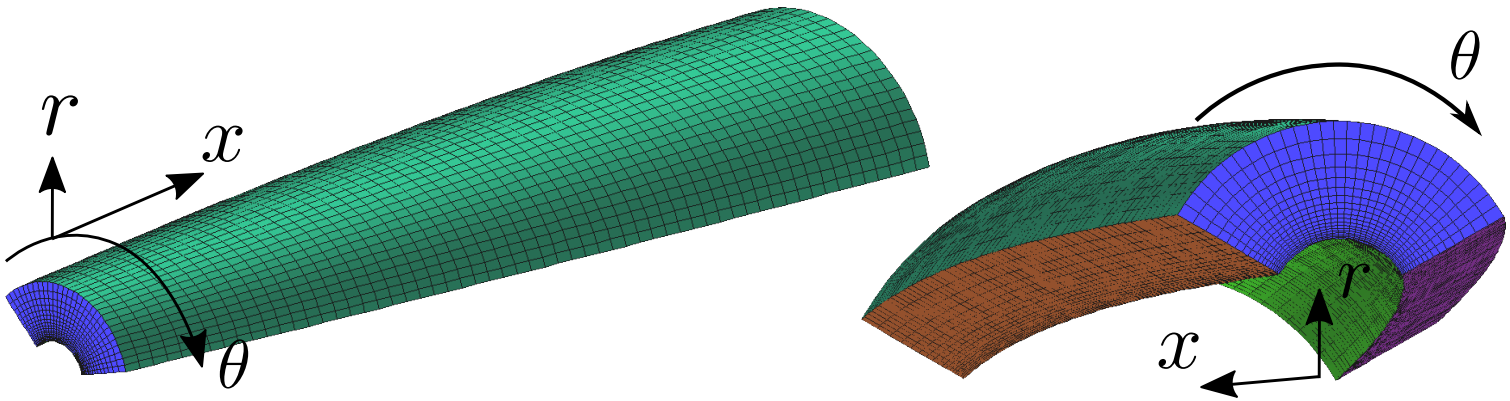




PURDUE UNIVERSITY

DNS Solver: CFDSU

- 6th-order compact FD scheme with 3rd-order Runge-Kutta
- Mildly complex geometries via generalized curvilinear coordinate
- Staggered arrangement for conservative variables (Nagarajan and Lele, 2003 [7])
- Explicitly filtered LES capabilities (Chapelier & Scalo, 2017 [1])

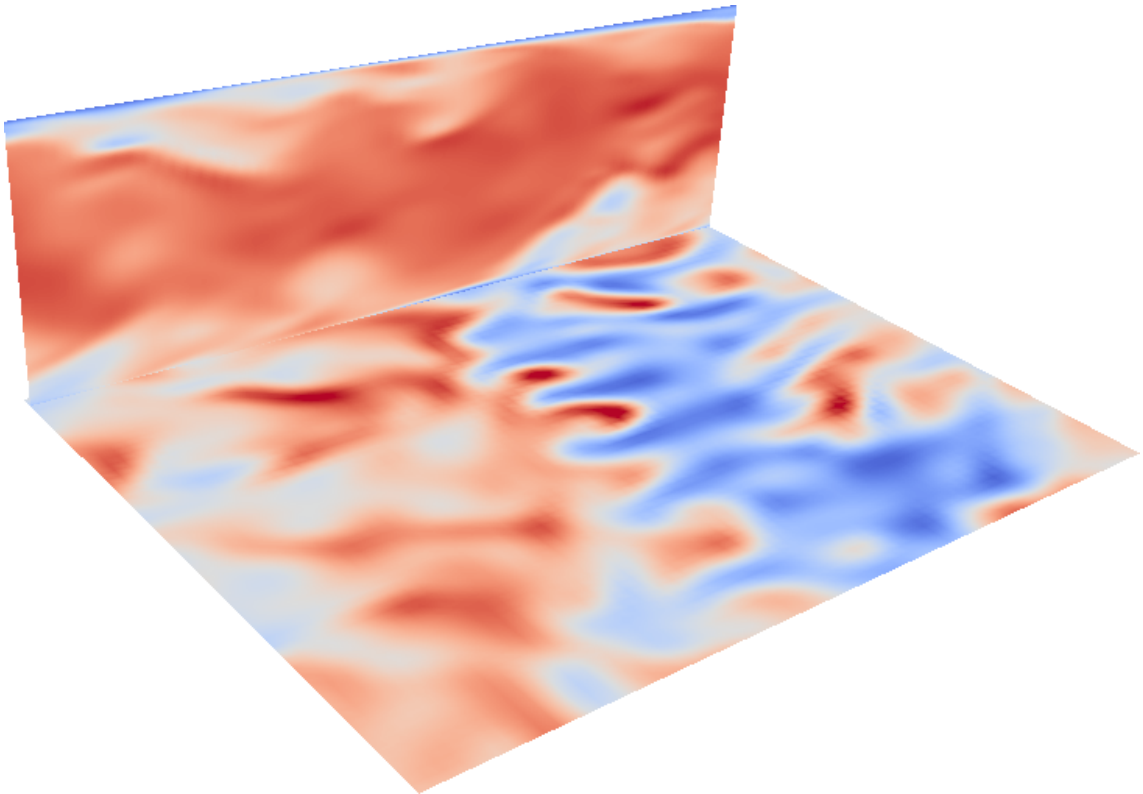


$$\frac{\partial \sqrt{g}\rho}{\partial t} + \frac{\partial}{\partial x^k}\left(\sqrt{g}\rho v^k\right) = 0$$

$$\frac{\partial \sqrt{g}\rho v^i}{\partial t} + \frac{\partial}{\partial x^j}\left(\sqrt{g}\rho v^i v^j\right) + \Gamma^i_{qj}\sqrt{g}\rho v^q v^j = \frac{\partial}{\partial x^k}\sqrt{g}\left[g^{ij}\left(p + \frac{2}{3}\mu v^k_{,k}\right) + \tau^{ij}\right] + \Gamma^i_{qj}\sqrt{g}\left[g^{ij}\left(p + \frac{2}{3}\mu v^k_{,k}\right) + \tau^{ij}\right]$$

Results of Navier-Stokes Calculation

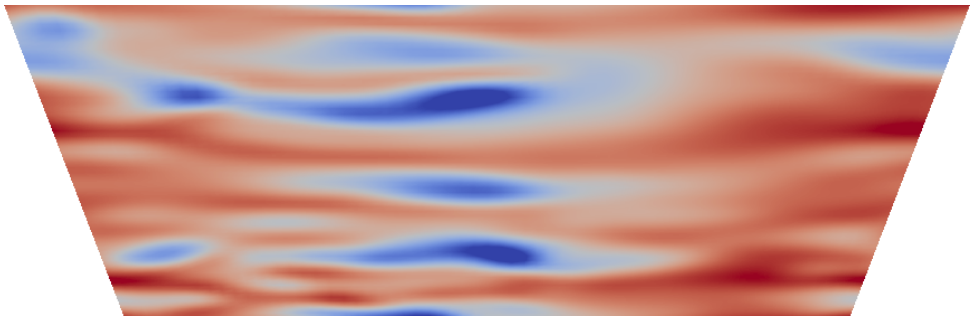
- $\mathrm{M}_b = 0.85$, $\mathrm{Re}_b = 6900$
- Impedance Properties: $\omega_{res} = 2\pi \times 0.0425$ and $R = 1.0$
- $L_x \times L_y \times L_z = 2\pi \times 2 \times 1.5\pi$ and $N_x \times N_y \times N_y = 128 \times 128 \times 64$



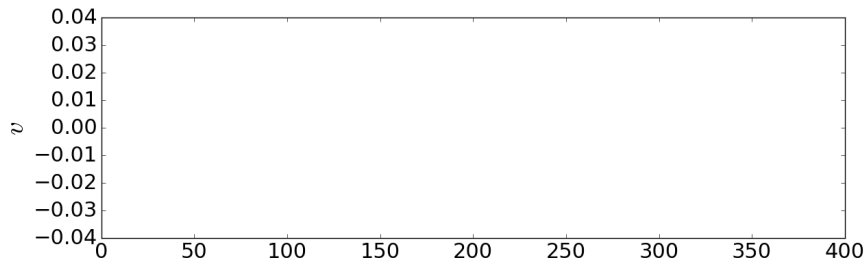
- **Vertical**: streamwise velocity at one cross section
- **Horizontal**: Wall normal derivative of streamwise velocity
- A very big coherent structure at the bottom of channel is observed

Results of Navier-Stokes Calculation

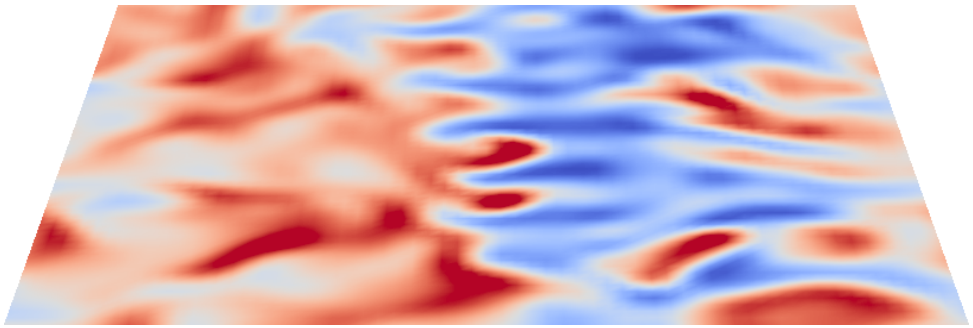
- $\mathrm{M}_b = 0.85$, $\mathrm{Re}_b = 6900$
- Impedance Properties: $\omega_{res} = 2\pi \times 0.0425$ and $R = 1.0$
- $L_x \times L_y \times L_z = 2\pi \times 2 \times 1.5\pi$ and $N_x \times N_y \times N_y = 128 \times 128 \times 64$



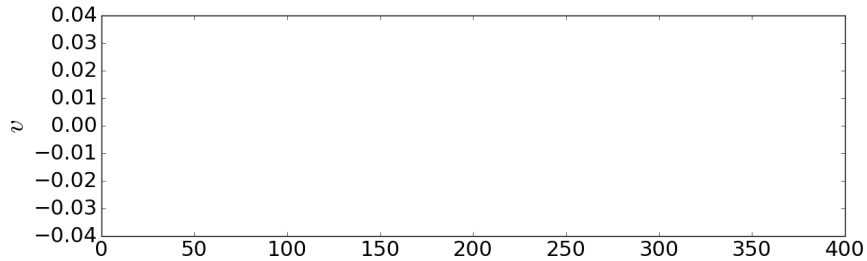
du/dy at the top wall



v on the top wall $(3.14, 3.14)$



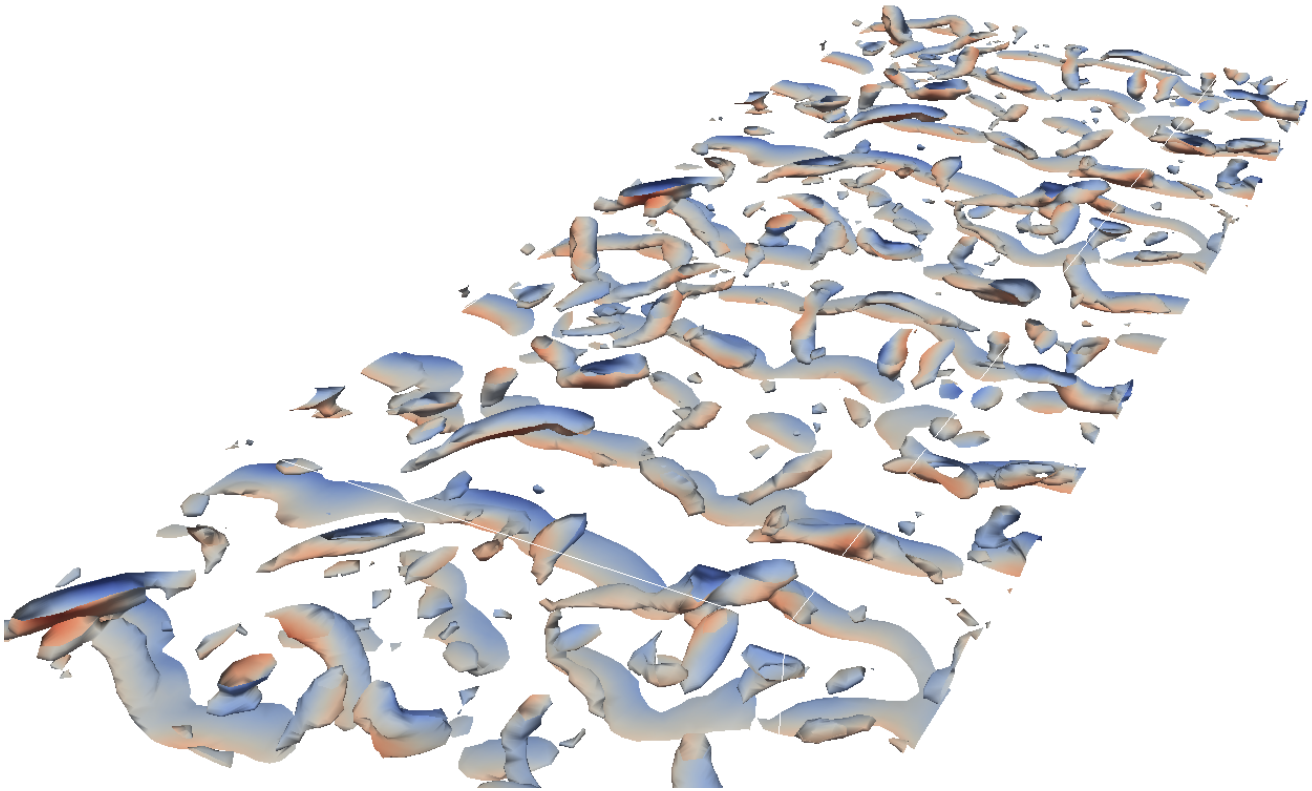
du/dy at the bottom wall



v on the bottom wall $(3.14, 3.14)$

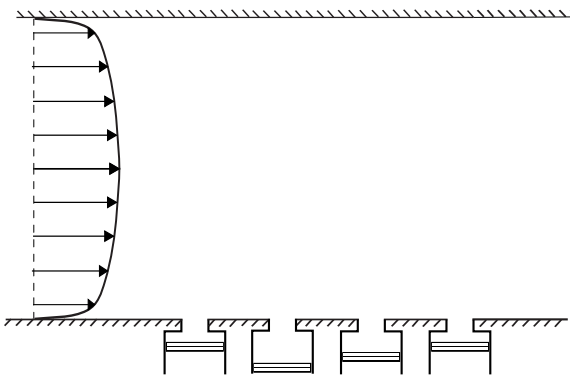
"Resonance Buffer Layer" Turbulence

- When resonance frequency is increased, structure size is reduced



Linear Stability Analysis

- Substituting the following forms of perturbation into the compressible Navier-Stokes equations.



Impedance Boundary Condition:
Z depends on x and ω, so we can only assume homogeneous form for perturbation in z-directions

- **Local Stability Analysis:**
  - For parallel flows
  - Homogeneous perturbations in two directions

$$a'(x,y,z,t) = \hat{a}(y)e^{i(\alpha x+\beta z-\omega t)}$$

- **Global Stability Analysis**
  - For two or three- dimensional flows
  - Homogeneous perturbation in one direction for *Bi*-global analysis

$$a'(x,y,z,t) = \hat{a}(x,y)e^{i(\beta z-\omega t)}$$

- No homogeneity assumption in *Tri*-global analysis

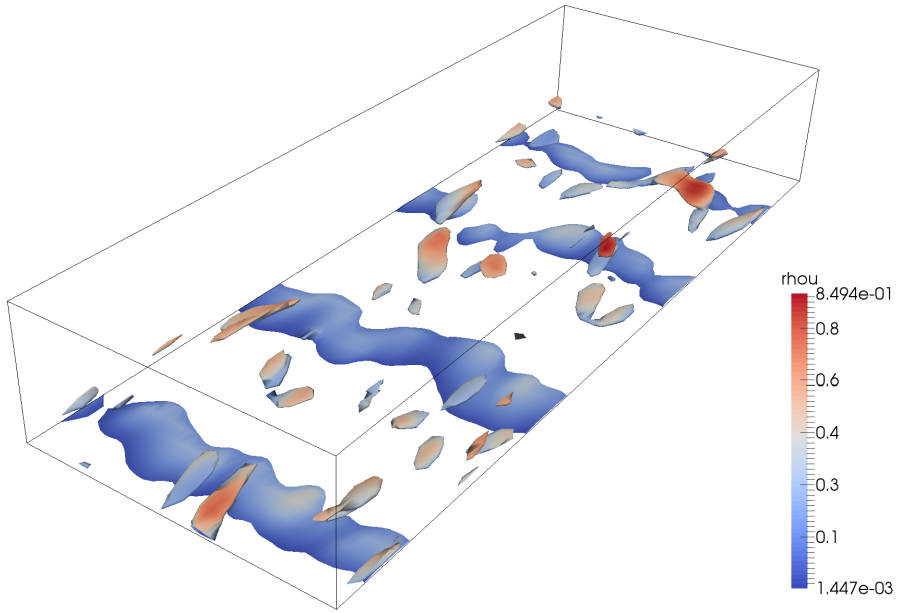
$$a'(x,y,z,t) = \hat{a}(x,y,z)e^{i(-\omega t)}$$

Global Linear Stability Analysis Solver (Rahbari & Scalo, AIAA, [8])

- Linearized Navier-Stokes equations are found by substituting the perturbation of form:

$$a'(x, y, z, t) = \hat{a}(x, y)e^{i(\beta z - \omega t)}$$

- A **new, truly sparse, implementation of Padé derivatives** for spatial discretization
- A scalable multi-node sparse eigenvalue solver to solve the resulting eigenvalue problem
- Shift-invert algorithm Arnoldi algorithm using SLEPc
- SuperLU package is used as the direct solver for the linear system of equations



Global Linear Stability Analysis Solver (Rahbari & Scalo, AIAA, [8])

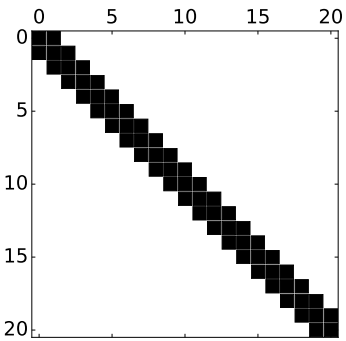
- Linearized Navier-Stokes Equations are discretized using a sixth-order fully-collocated Padé scheme. First derivative is written as:

$$\alpha f'_{i-1} + f'_i + \alpha f'_{i+1} = \frac{a}{2h}\left(f_{i+1} - f_{i-1}\right) + \frac{b}{4h}\left(f_{i+2} - f_{i-2}\right)$$

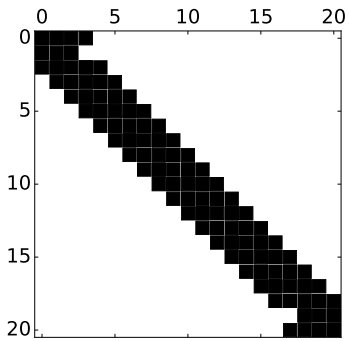
  in matrix notation:

$$[L]\left[f'\right] = [R]\,[f]$$

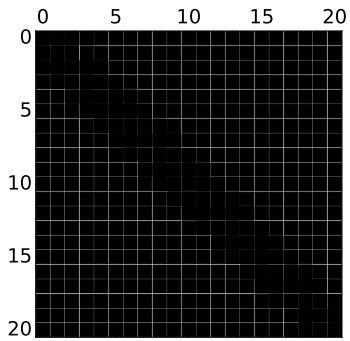
- Although L and R are banded matrices, their inverse will be a full matrix.



$[L]$



$[R]$



$[D] = [L]^{-1}[R]$

- In most of the global stability analysis available in the literature, D matrix is used to find the $[f']$, explicitly.

Global Linear Stability Analysis Solver (Rahbari & Scalo, AIAA, [8])

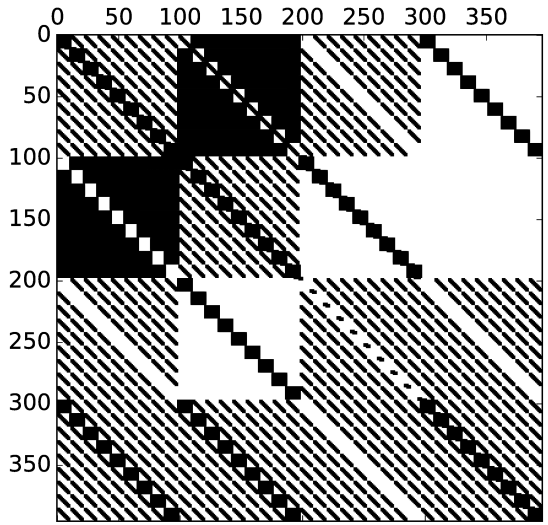
- Discretized Linearized Navier-Stokes Equations can be written in the form of a Generalized Eigenvalue Problem:

$$A\mathbf{\Psi} = \Lambda B\mathbf{\Psi}$$

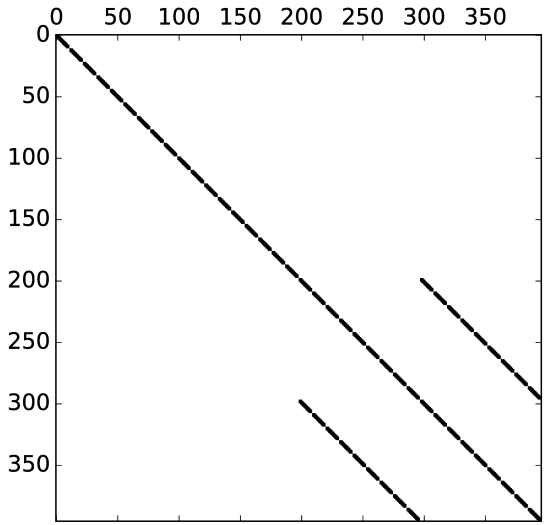
- In the literature, Ψ is mostly considered as:

$$\Psi = [\hat{u}, \hat{v}, \hat{w}, \hat{p}, \hat{T}]^{\mathrm{T}}$$

  - Explicit calculation of derivatives
  - Matrix A looks very "dense"
  - Computational cost $\sim$ O (spectral method)



$[A]$



$[B]$

Global Linear Stability Analysis Solver (Rahbari & Scalo, AIAA, [8])

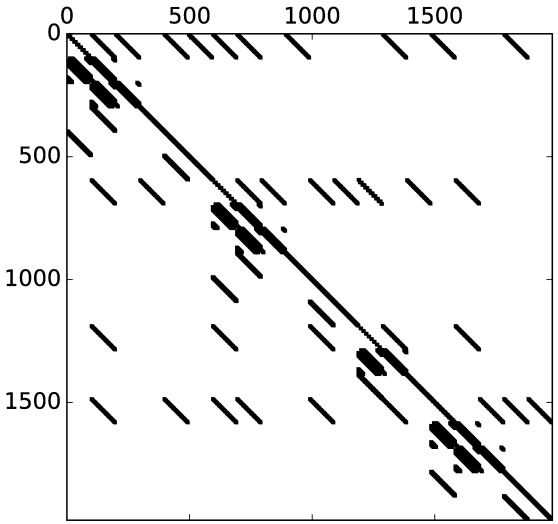
- Discretized Linearized Navier-Stokes Equations can be written in the form of a Generalized Eigenvalue Problem:

$$A\Psi = \Lambda B\Psi$$

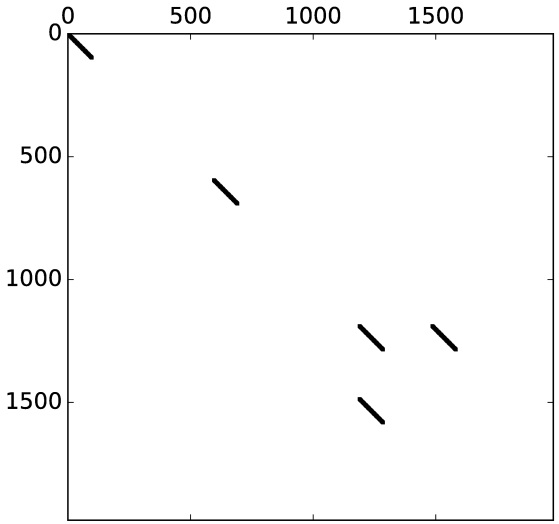
- To optimally exploit the sparsity of Padé scheme, Ψ is considered as:

$$\Psi = [\hat{u}, \hat{u}_x, \hat{u}_{xx}, \hat{u}_{xy}, \hat{u}_y, \hat{u}_{yy}, \hat{v}, \cdots, \hat{w}, \cdots, \hat{p}, \hat{p}_x, \hat{p}_y, \hat{T}, \cdots]^{\mathrm{T}}$$

  - Implicit calculation of derivatives
  - Number of variables is increased by a factor of 5
  - A and B matrices are very sparse



$[A]$



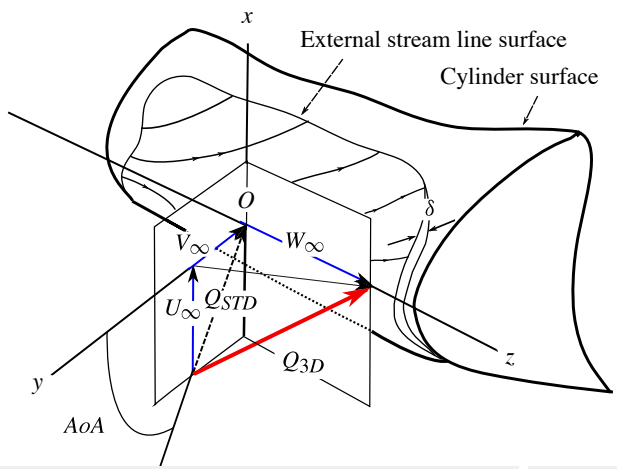
$[B]$

Validation of the Bi-global Solver

- Test case: "Biglobal Stability Analysis of Leading Edge Boundary Layer"
- $Re = 800$, $M = 0.02$, and $\beta = 0.255$
- Boundary Conditions:
  - at the wall: $\hat{u} = \hat{v} = \hat{w} = \hat{T} = 0$ and $\frac{\partial \hat{p}}{\partial y} = 0$
  - at the far-field: $\hat{u} = \hat{v} = \hat{w} = \hat{T} = \hat{p} = 0$
  - One-sided extrapolation at the chordwise direction ($\pm L_x$) for all quantities

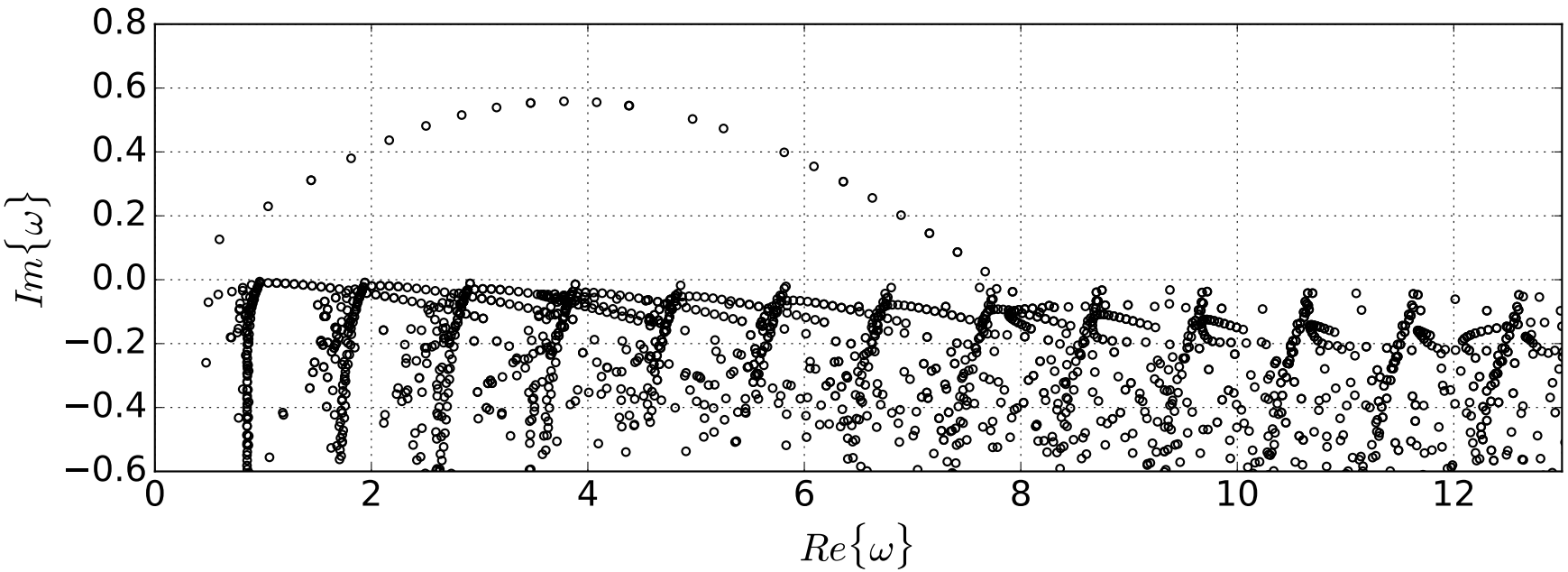
Grid: 48×48	$c_{r\,\mathrm{GH}}$	$c_{i\,\mathrm{GH}}$	$c_{r\,\mathrm{A1}}$	$c_{i\,\mathrm{A1}}$
Lin and Malik (1994)	0.35840982	0.00585325	0.35791970	0.00409887
Theofilis et al. (2003)	0.35844151	0.00585646	0.35793726	0.00401330
Current Study: Sparse	0.35844071	0.00585467	0.35795061	0.00410000
Current Study: Dense	0.35844457	0.00584620	0.35795353	0.00409183

- Görtler-Hämmerlin (GH): the most unstable mode
- A1: the second unstable mode
- c_r and c_i correspond $Re(\omega)/\beta$ and $Im(\omega)/\beta$.



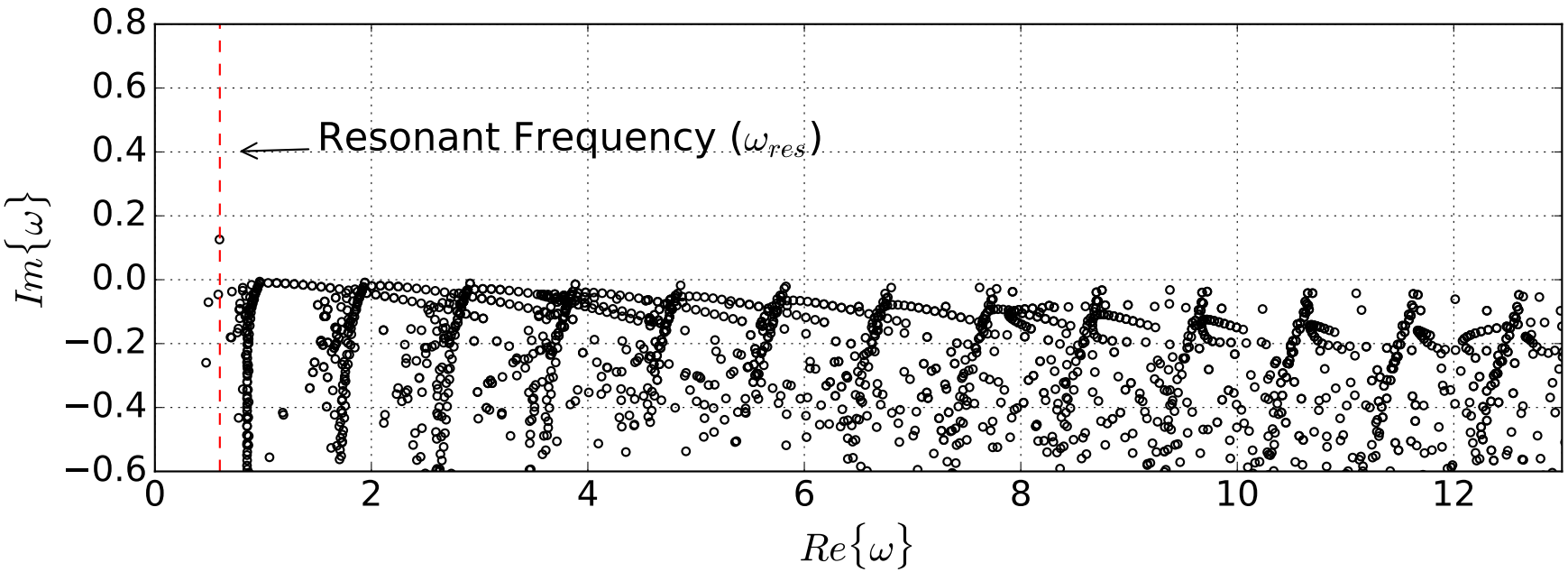
Finding the unstable modes

- $\mathrm{M}_b = 0.85$, $\mathrm{Re}_b = 6900$, and $R = 1.0$
- Eigenspectrum symmetric wrt the line $Re\{\omega\} = 0$.
- Discrete sets of eigenvalues are observed each corresponding to one streamwise wavenumber
- Only **one** unstable modes showed up for each set the rest are nearly untouched
- At constant permeability, $R = 1.0$, there is a critical wave number.
- Increasing the permeability, reducing the R, destabilizes the flow.



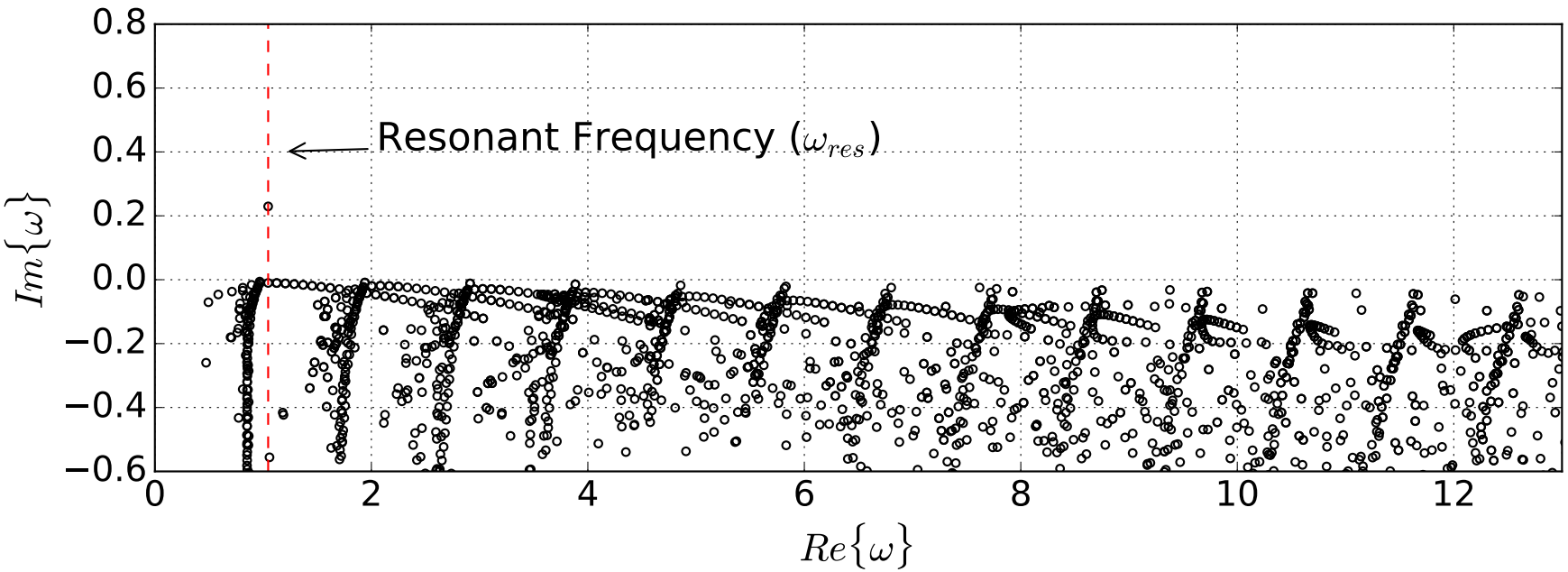
Finding the unstable modes

- $\mathrm{M}_b = 0.85$, $\mathrm{Re}_b = 6900$, and $R = 1.0$
- Eigenspectrum symmetric wrt the line $Re\{\omega\} = 0$.
- Discrete sets of eigenvalues are observed each corresponding to one streamwise wavenumber
- Only **one** unstable modes showed up for each set the rest are nearly untouched
- At constant permeability, $R = 1.0$, there is a critical wave number.
- Increasing the permeability, reducing the R, destabilizes the flow.



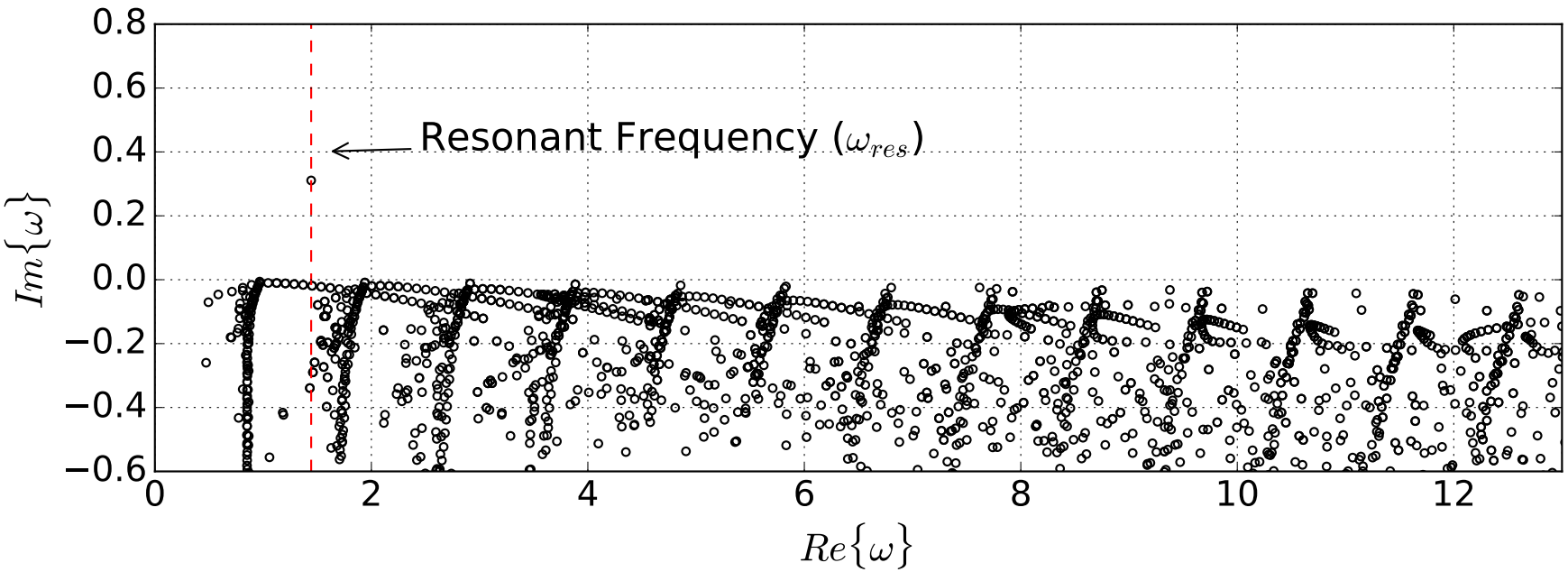
Finding the unstable modes

- $\mathrm{M}_b = 0.85$, $\mathrm{Re}_b = 6900$, and $R = 1.0$
- Eigenspectrum symmetric wrt the line $Re\{\omega\} = 0$.
- Discrete sets of eigenvalues are observed each corresponding to one streamwise wavenumber
- Only **one** unstable modes showed up for each set the rest are nearly untouched
- At constant permeability, $R = 1.0$, there is a critical wave number.
- Increasing the permeability, reducing the R, destabilizes the flow.



Finding the unstable modes

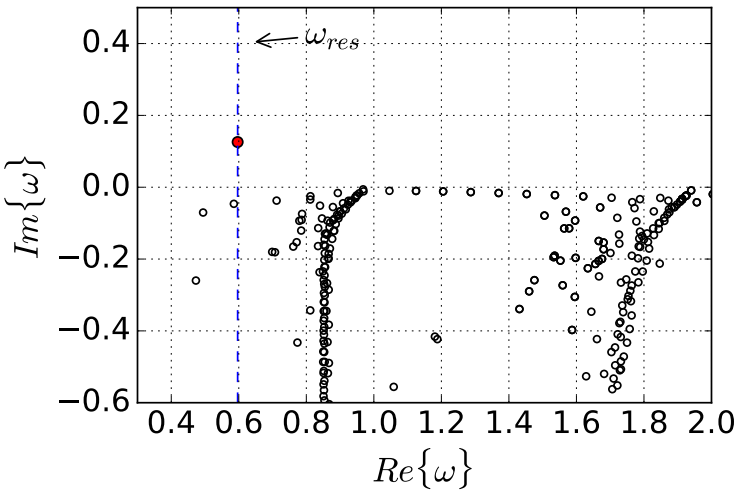
- $\mathrm{M}_b = 0.85$, $\mathrm{Re}_b = 6900$, and $R = 1.0$
- Eigenspectrum symmetric wrt the line $Re\{\omega\} = 0$.
- Discrete sets of eigenvalues are observed each corresponding to one streamwise wavenumber
- Only **one** unstable modes showed up for each set the rest are nearly untouched
- At constant permeability, $R = 1.0$, there is a critical wave number.
- Increasing the permeability, reducing the R, destabilizes the flow.



Results of GSA

Shape of eigenmodes

- Simulation at $\mathrm{M}_b = 0.85$, $\mathrm{Re}_b = 6900$, $\xi = 0.5$, and $R = 1.0$
- Grid $N_x \times N_y = 128 \times 128$



- Resonant frequency $\omega_{res} = 0.595$
- Only one unstable mode
- Streamwise wavenumber $k_x = 1$

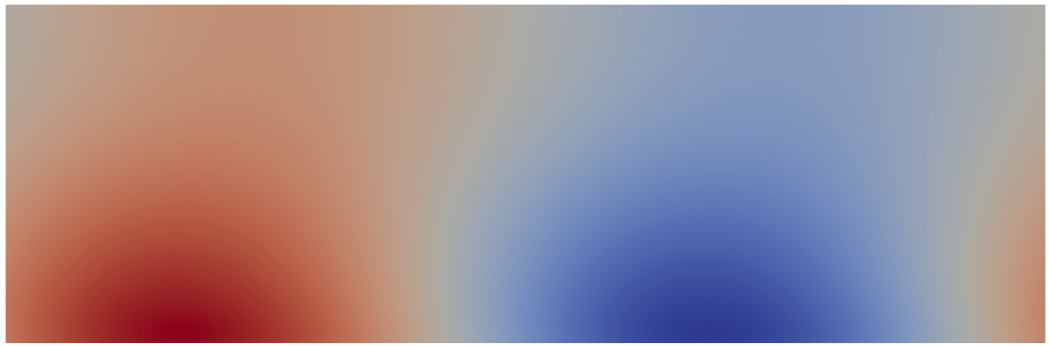


Figure: Pressure eigenfunction ($\hat{p}$)

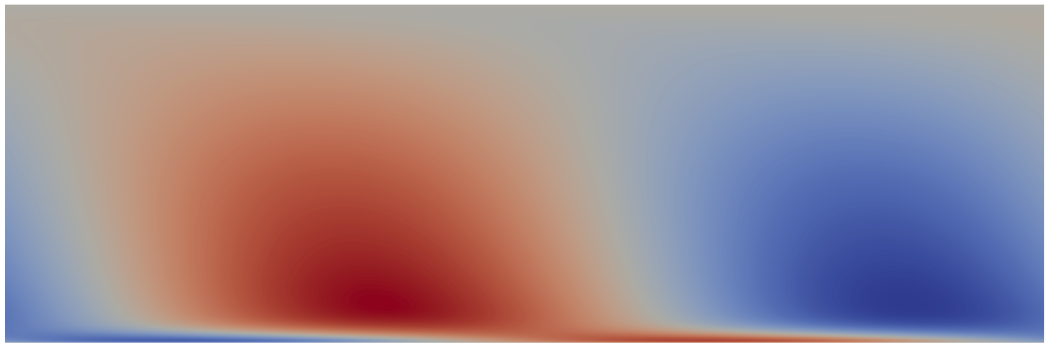
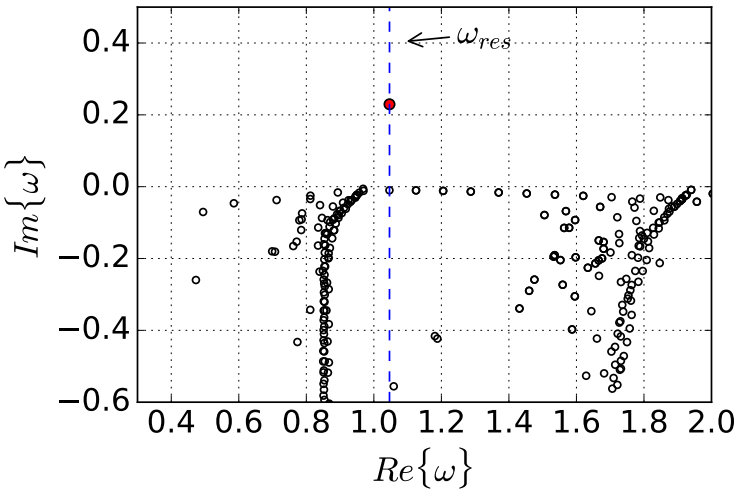


Figure: Wall normal velocity eigenfunction ($\hat{v}$)

Results of GSA

Shape of eigenmodes

- Simulation at $\mathrm{M}_b = 0.85$, $\mathrm{Re}_b = 6900$, $\xi = 0.5$, and $R = 1.0$
- Grid $N_x \times N_y = 128 \times 128$



- Resonant frequency $\omega_{res} = 1.046$
- Only one unstable mode
- Streamwise wavenumber $k_x = 2$

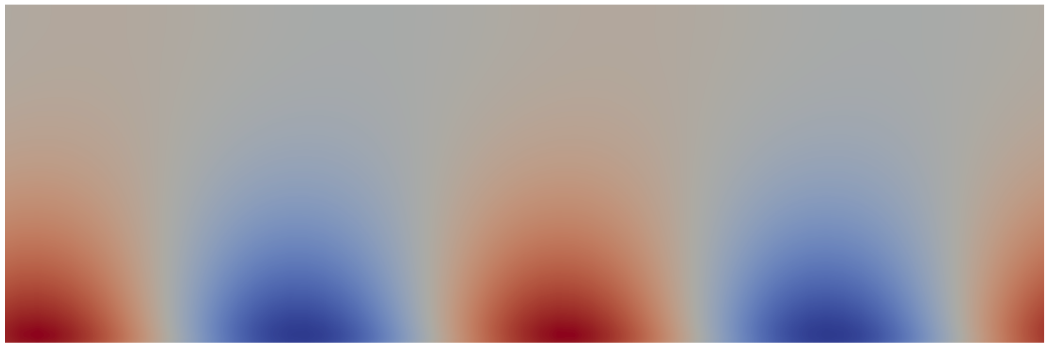


Figure: Pressure eigenfunction ($\hat{p}$)

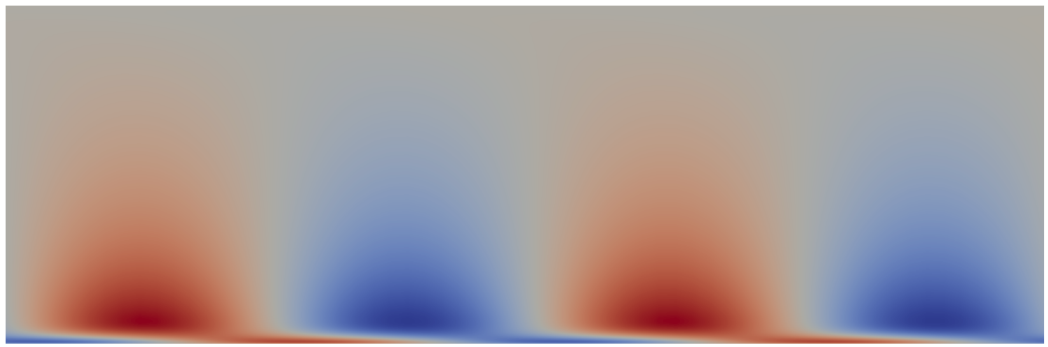
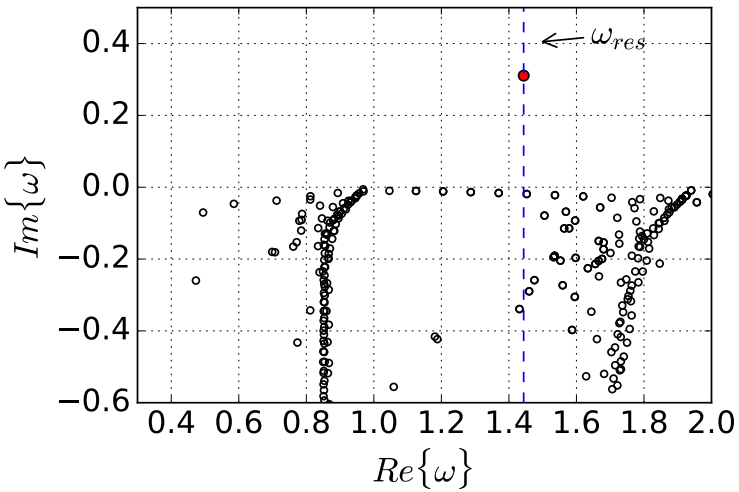


Figure: Wall normal velocity eigenfunction ($\hat{v}$)

Shape of eigenmodes

- Simulation at $\mathrm{M}_b = 0.85$, $\mathrm{Re}_b = 6900$, $\xi = 0.5$, and $R = 1.0$
- Grid $N_x \times N_y = 128 \times 128$



- Resonant frequency $\omega_{res} = 1.443$
- Only one unstable mode
- Streamwise wavenumber $k_x = 3$



Figure: Pressure eigenfunction ($\hat{p}$)

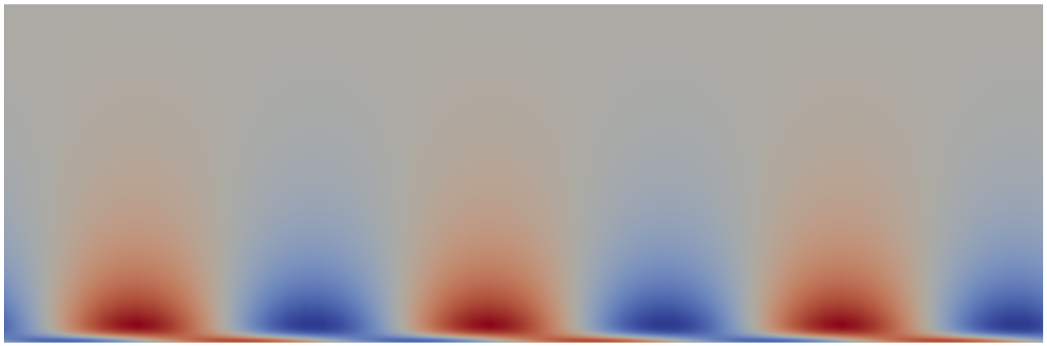
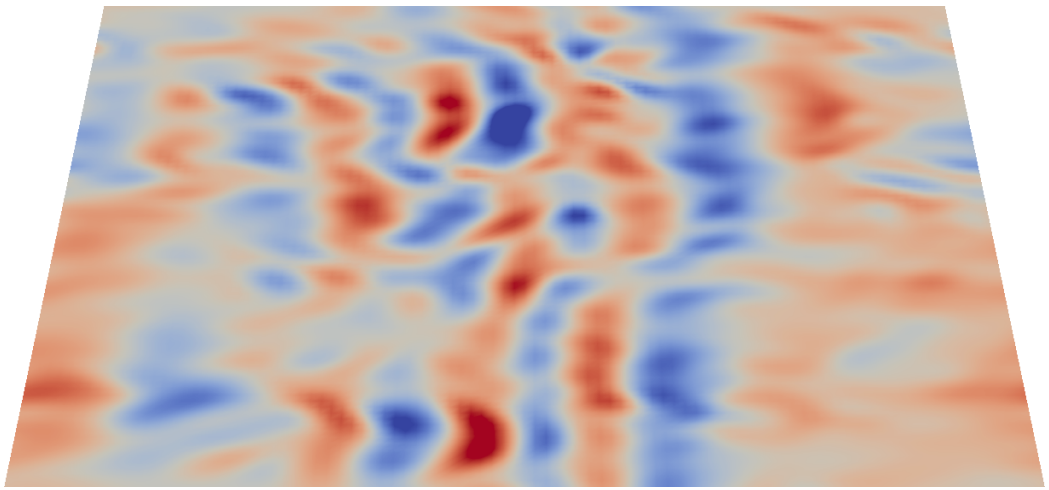
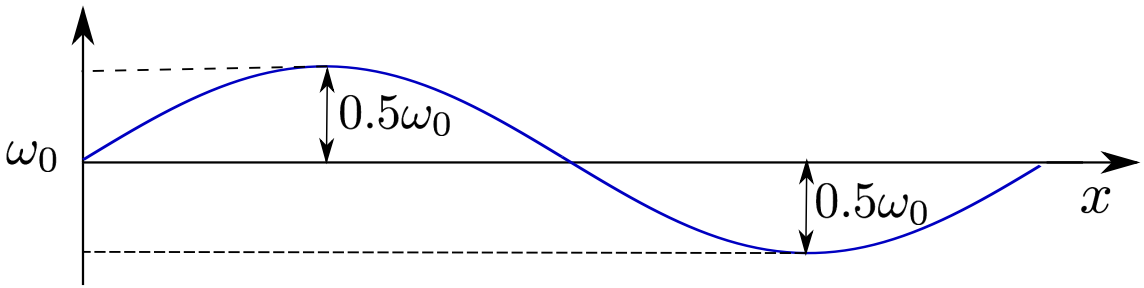


Figure: Wall normal velocity eigenfunction ($\hat{v}$)

Results for the Variable Resonant Frequency

- $\mathrm{M}_b = 0.85$, $\mathrm{Re}_b = 6900$
- Impedance Properties: $R = 1.0$,$\xi = 0.5$, $\omega_{res} = \omega_0 \times (1 + 0.5 \sin(x))$
- $L_x \times L_y \times L_z = 2\pi \times 2 \times 1.5\pi$ and $N_x \times N_y \times N_y = 96 \times 196 \times 96$





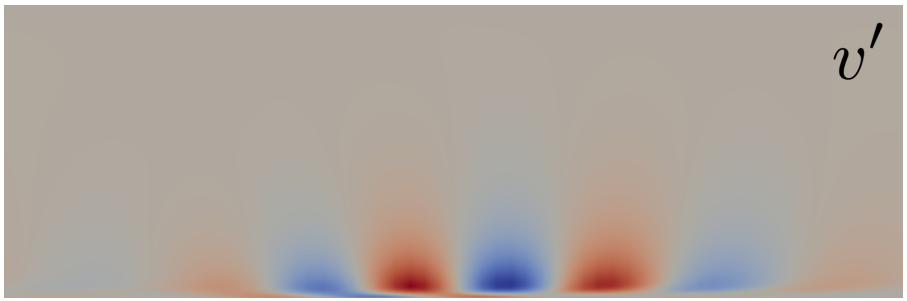
- We have chosen $\omega_0 = 1.443$ to cover a wide range of frequency in x-direction
- Rollers are very compressed in the middle and very elongated at the periodic boundaries
- Structures have different wave numbers (wave speed)

Results for the Variable Resonant Frequency

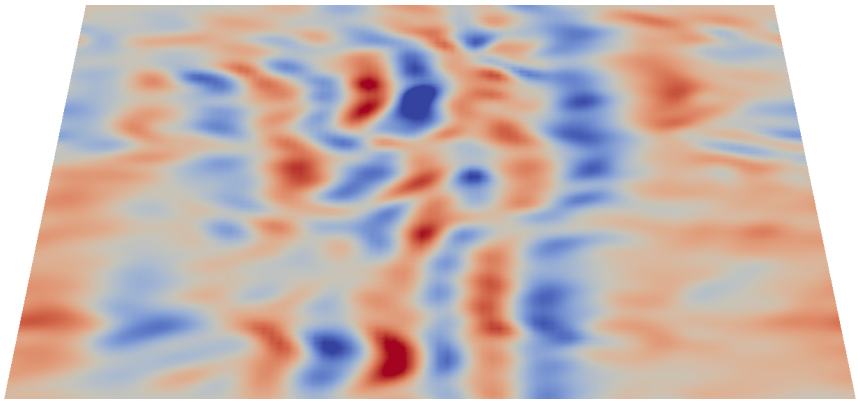
- Impedance Properties: $R = 1.0$,$\xi = 0.5$, $\omega_{res} = \omega_0 \times (1 + 0.5 \sin(x))$
- $L_x \times L_y \times L_z = 2\pi \times 2 \times 1.5\pi$ and $N_x \times N_y \times N_y = 96 \times 196 \times 96$

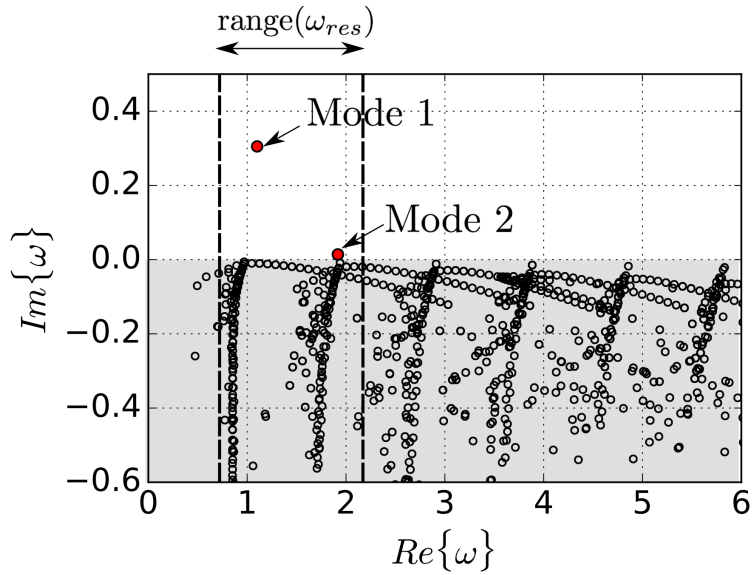


Mode 1: $\omega = 1.1005 + 0.3050j$



Mode 2: $\omega = 1.9174 + 0.0139j$





Results for the Variable Resonant Frequency

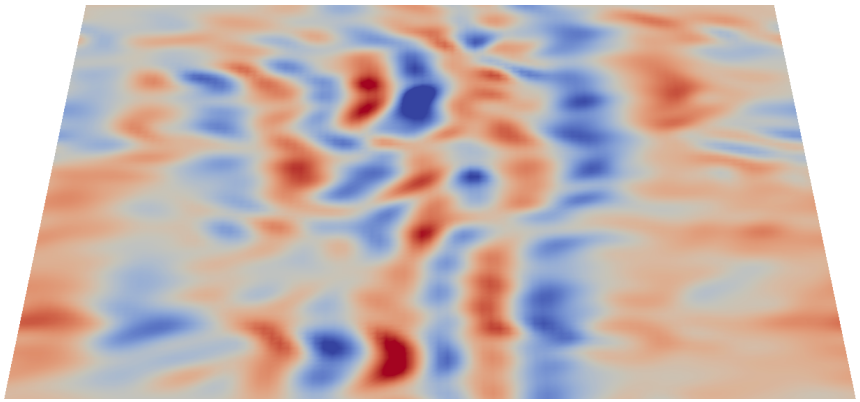
- Impedance Properties: $R = 1.0$,$\xi = 0.5$, $\omega_{res} = \omega_0 \times (1 + 0.5 \sin(x))$
- $L_x \times L_y \times L_z = 2\pi \times 2 \times 1.5\pi$ and $N_x \times N_y \times N_y = 96 \times 196 \times 96$

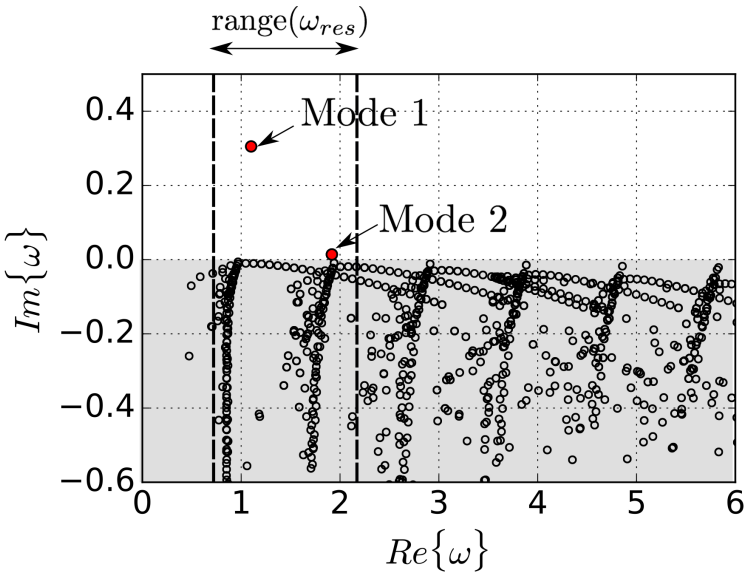


Mode 1: $\omega = 1.1005 + 0.3050j$



Mode 2: $\omega = 1.9174 + 0.0139j$



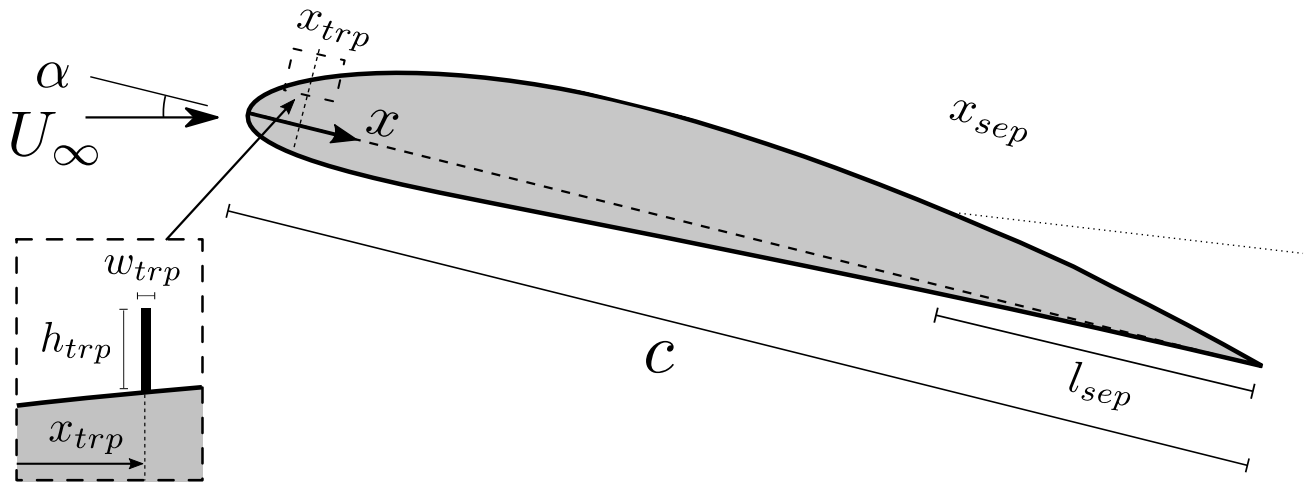


Turbulent Boundary Layer Separation over Impedance

(Bodart & Scalo, AIAA, 2017)

Turbulent Separation Control via Tuned IBCs

- pre-stalled NACA 4412: $M_\infty = 0.3$, $Re_c = 1.5 \times 10^6$, $\alpha = 14.5°$, $x_{sep}/c = 0.77$



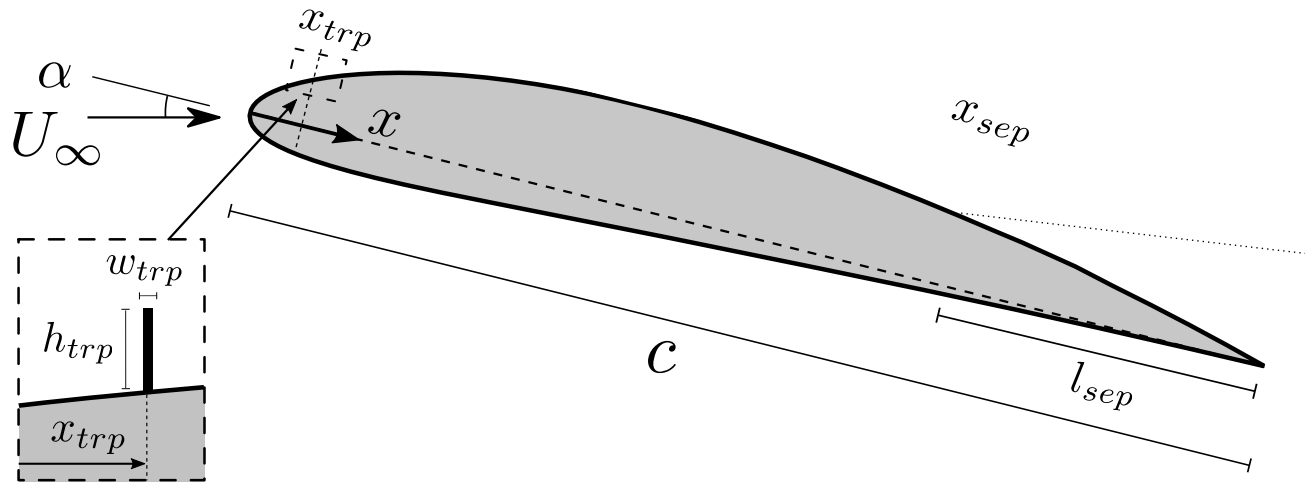
Computational Tools

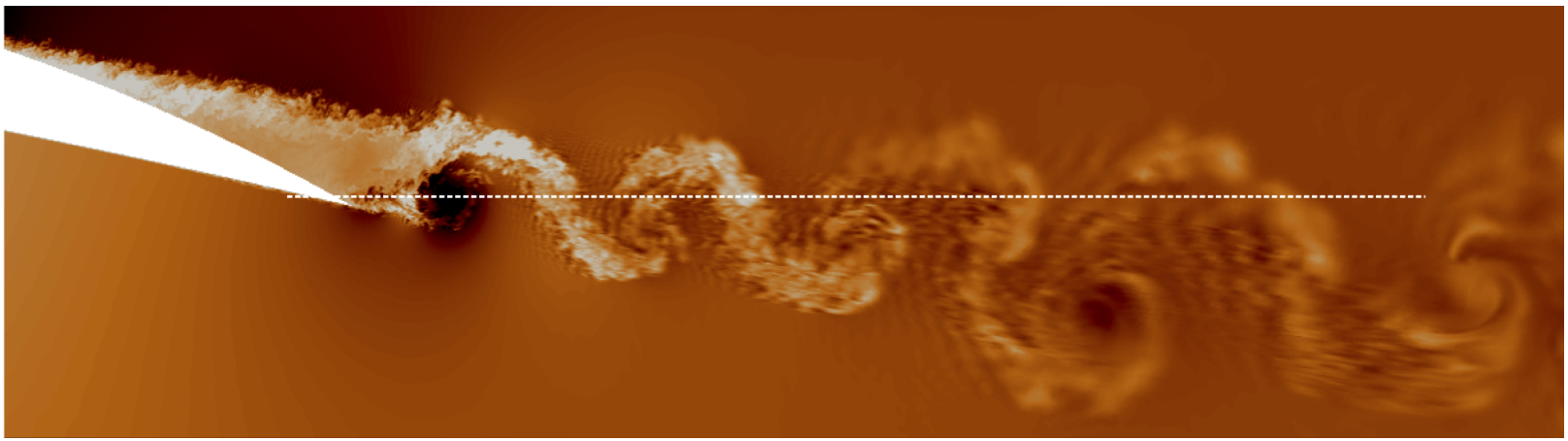
- Three-dimensional unstructured finite-volume Navier-Stokes solver (CharLES^X)
- Discretization: 2^{nd} – 4^{th} order in space, 3^{rd} order in time

PURDUE UNIVERSITY

Turbulent Separation Control via Tuned IBCs

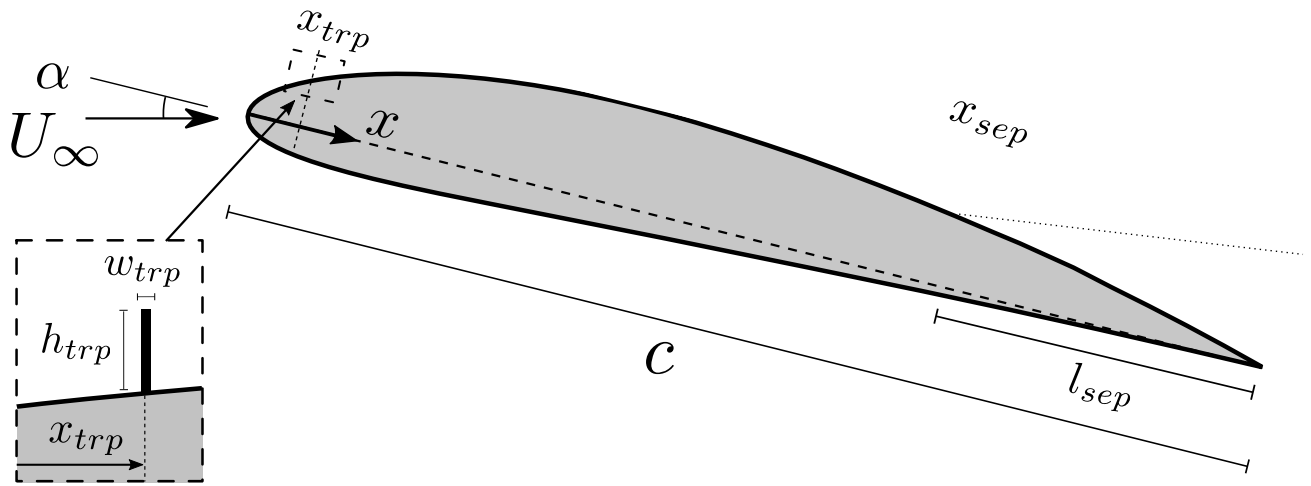
- pre-stalled NACA 4412: $M_\infty = 0.3$, $Re_c = 1.5 \times 10^6$, $\alpha = 14.5°$, $x_{sep}/c = 0.77$



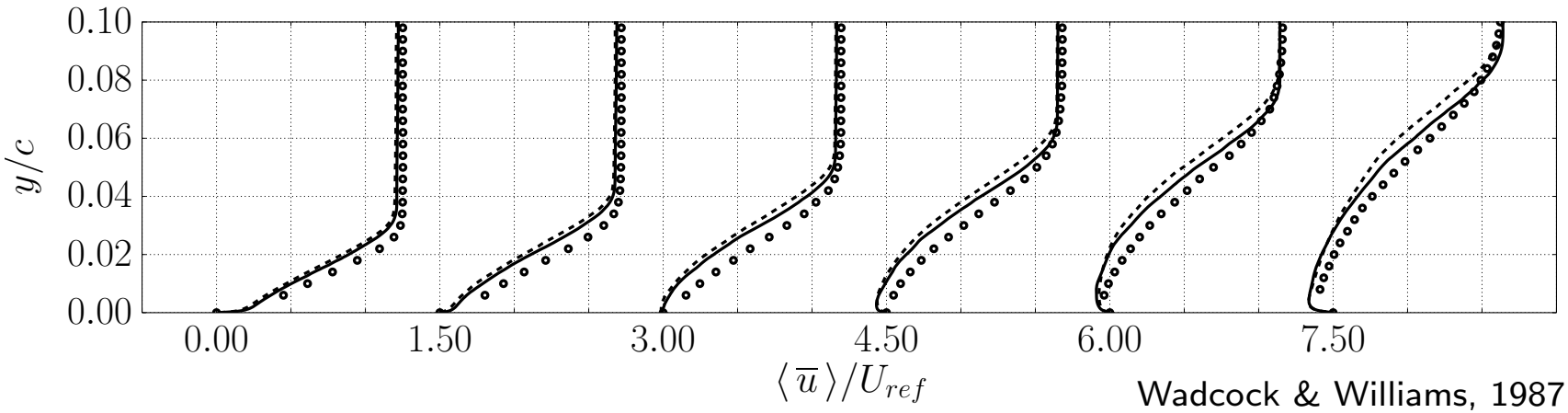


Turbulent Separation Control via Tuned IBCs

- pre-stalled NACA 4412: $M_\infty = 0.3$, $Re_c = 1.5 \times 10^6$, $\alpha = 14.5°$, $x_{sep}/c = 0.77$



- $L_z = 0.05\,c$, $N_{tot} = 34$M, $\Delta x^+ \times \Delta y^+ \times \Delta z^+ = 75 \times 6 \times 35$



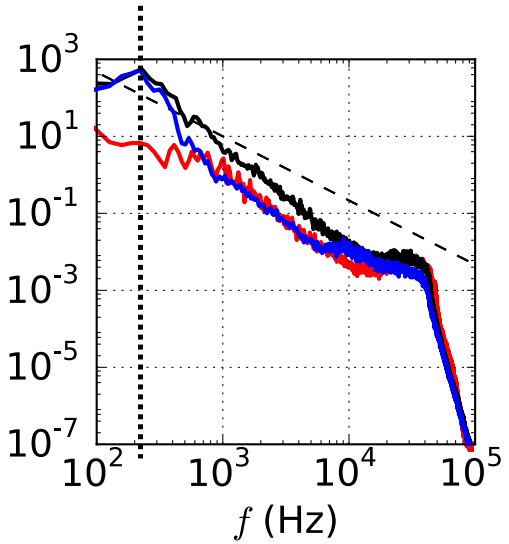
Wadcock & Williams, 1987 (○)

Time scale analysis: uncontrolled flow

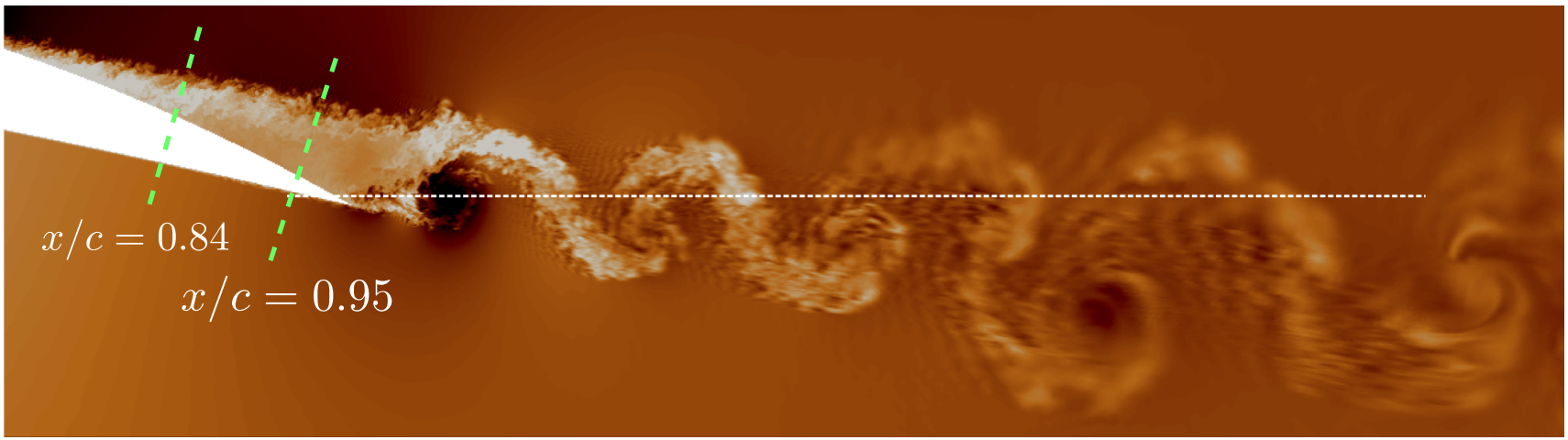
- Pressure spectrum extracted at $y \simeq \delta_{BL}$
- Spectrum peaks at $St_\theta^{sep} = 0.010$

$$St_\theta^{sep} = \frac{f\theta_{sep}}{U_\infty}$$

- frequency of shear layer convective instability

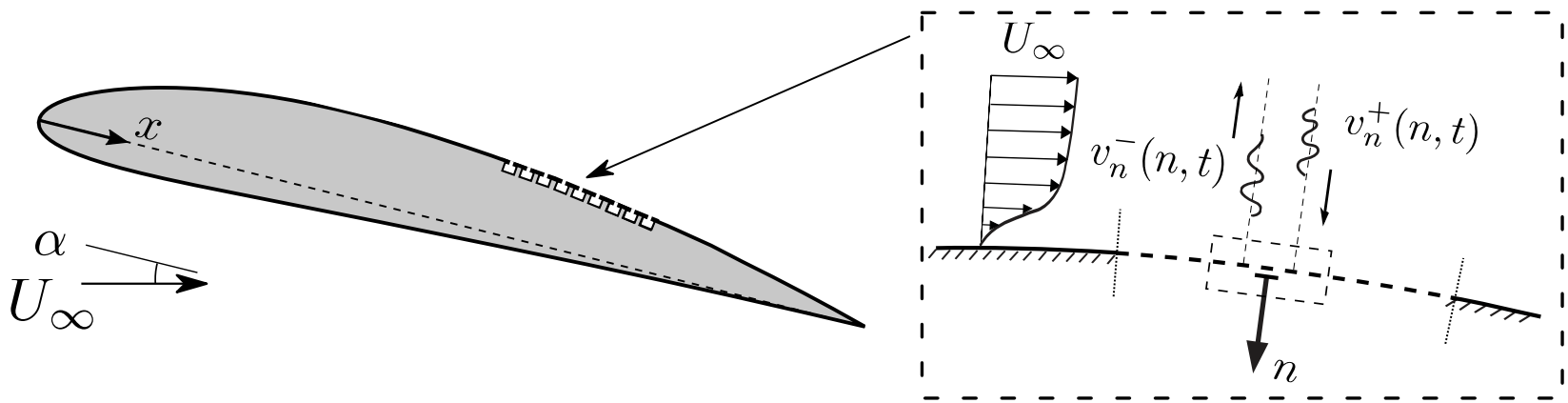


$x/c = 0.60$
$x/c = 0.84$
$x/c = 0.95$



Turbulent Separation Control via Tuned IBCs

- *Frequency-selective* passive flow separation control strategy



- Impedance panel settings:

impedance resistance R *resonating frequency,* f_{res}

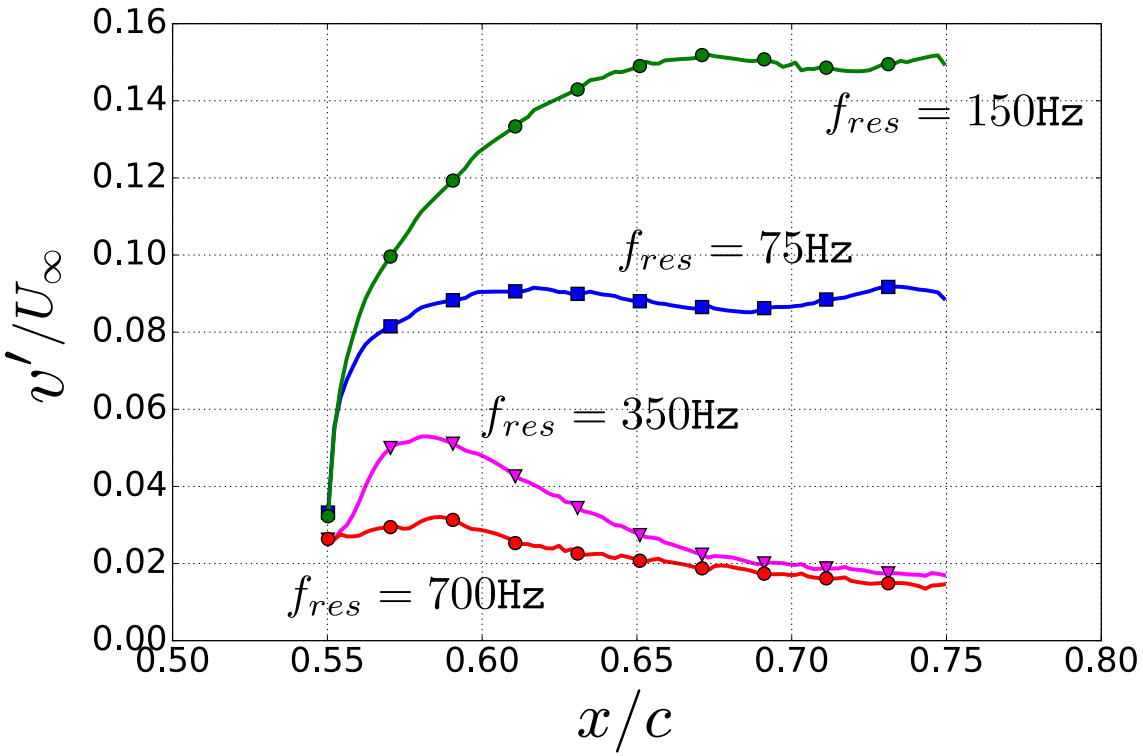
R					
0.1	f_{res}	75 Hz	150 Hz	300 Hz	700 Hz
0.2	St_θ^{res}	0.0041	0.0082	0.019	0.038
0.5					

PURDUE UNIVERSITY

Turbulent Separation Control via Tuned IBCs

- Panel response for resistance $R = 0.2$ at various frequencies
- Transpiration velocity intensity distribution along impedance panel
- Momentum coefficient:

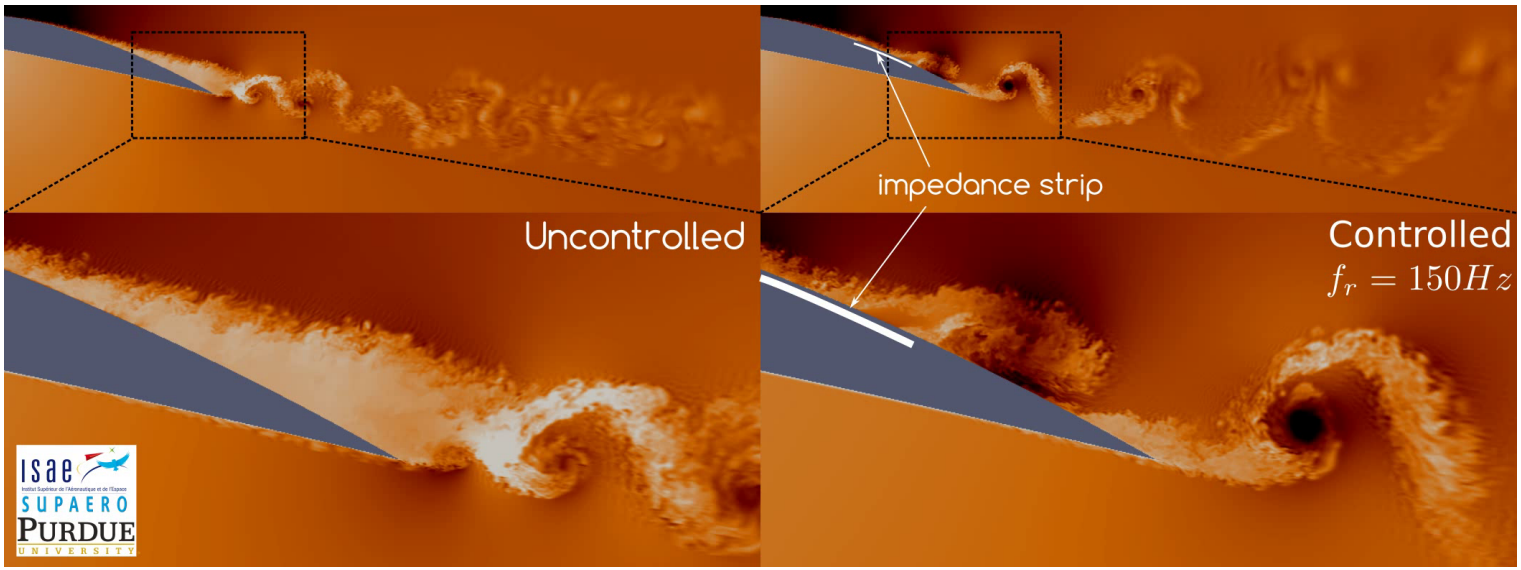
$$C_\mu = \frac{\int_{IBC} \rho v'^2}{1/2\, \rho_\infty\, U_\infty^2} \frac{\ell_{IBC}}{c}$$



f_{res}	C_μ
75	0.06%
150	0.15%
300	0.009%
700	0.004%

Turbulent Separation Control via Tuned IBCs

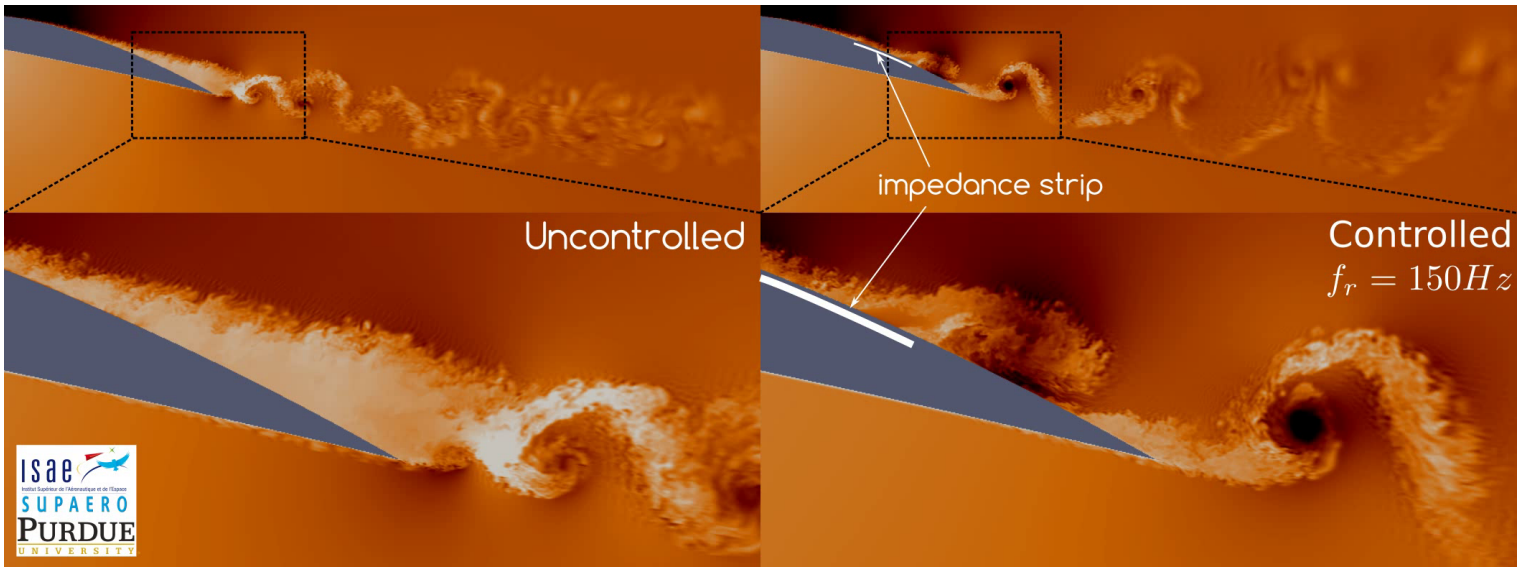
- Hydro-acoustic instabilities re-energize the (otherwise separated) compressible shear layer



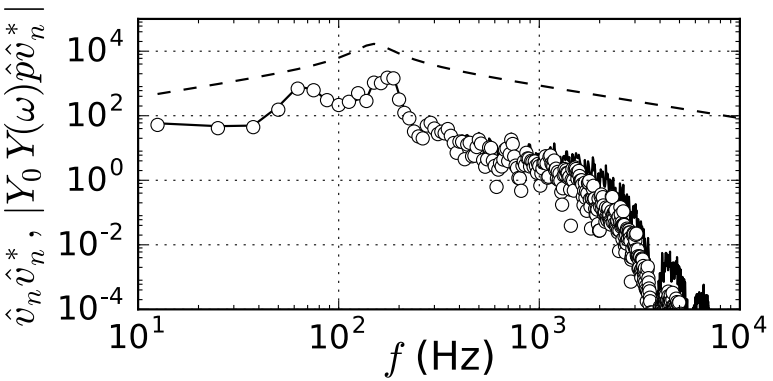
PURDUE UNIVERSITY

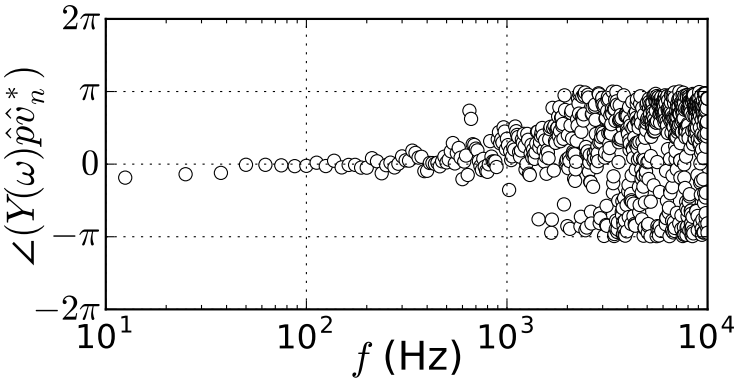
Turbulent Separation Control via Tuned IBCs

- Hydro-acoustic instabilities re-energize the (otherwise separated) compressible shear layer



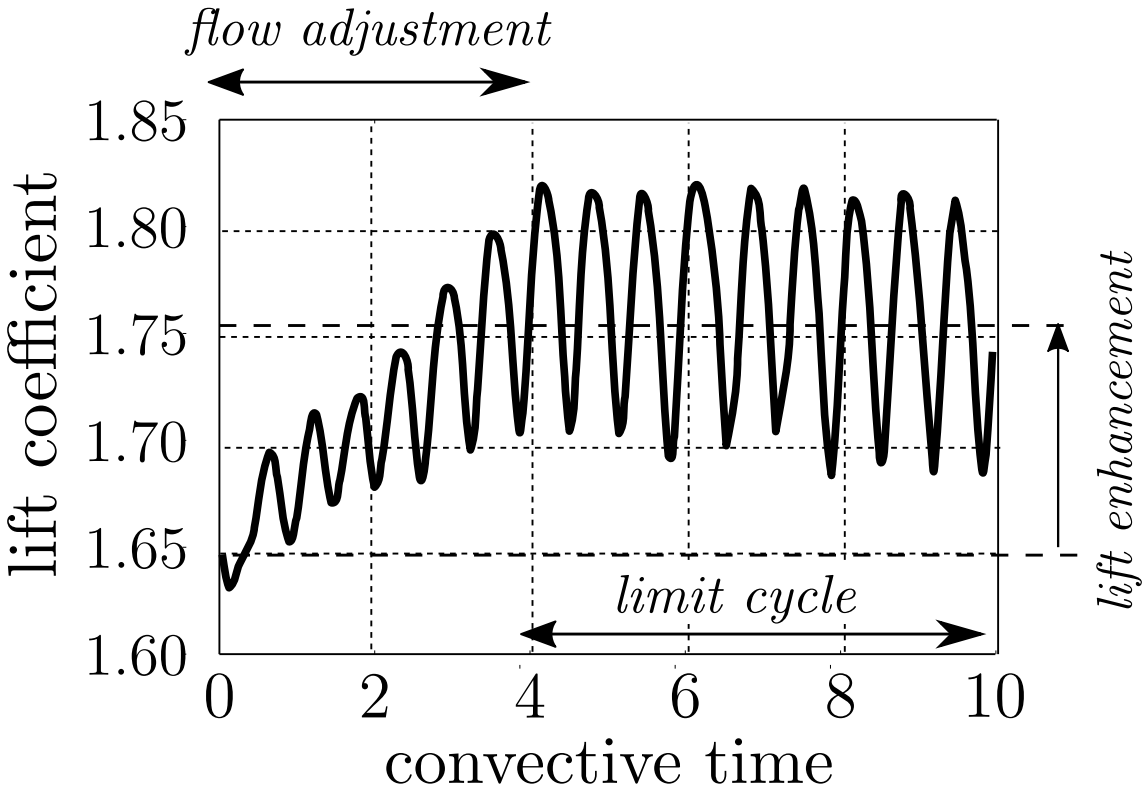
- IBC implementation verification: $\hat{p} = Z_0 Z(\omega)\hat{v}_n \Rightarrow \hat{v}_n = Y_0 Y(\omega)\hat{p} \Rightarrow \hat{v}_n \hat{v}_n^* = Y_0 Y(\omega)\hat{p}\hat{v}_n^*$



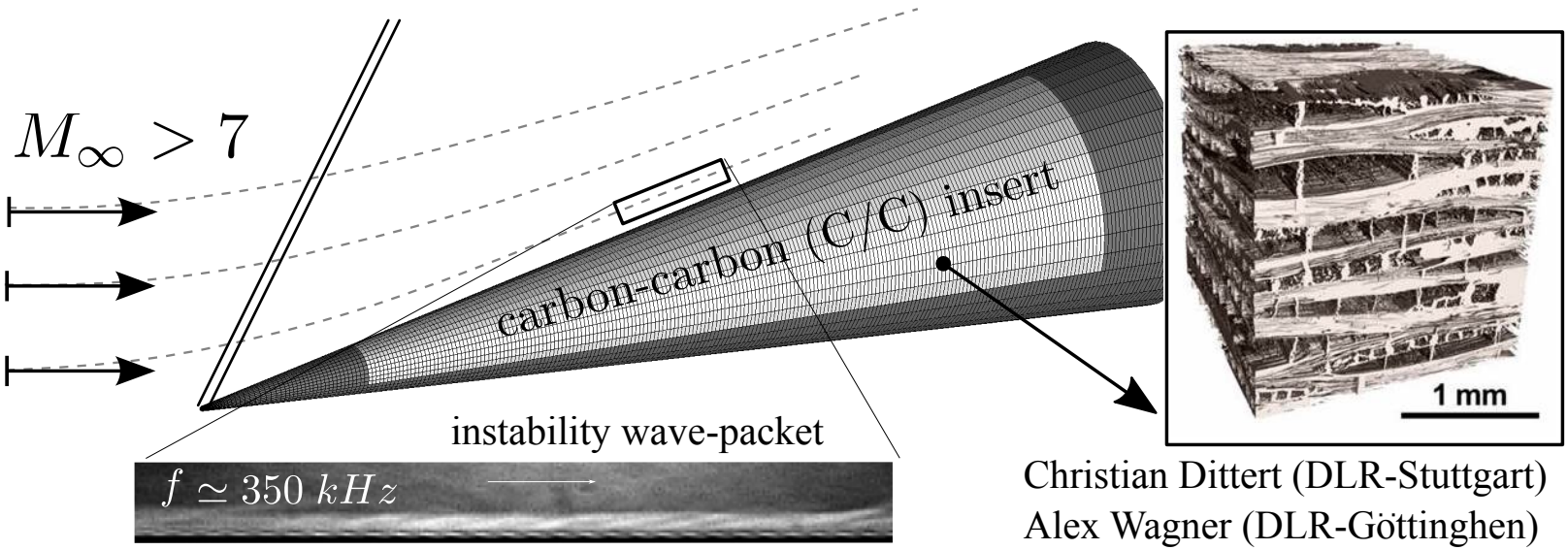


Turbulent Separation Control via Tuned IBCs

- Hydro-acoustic instabilities re-energize the (otherwise separated) compressible shear layer
- Lift is increased but is unsteady



Hypersonic Boundary Layer Control over Impedance

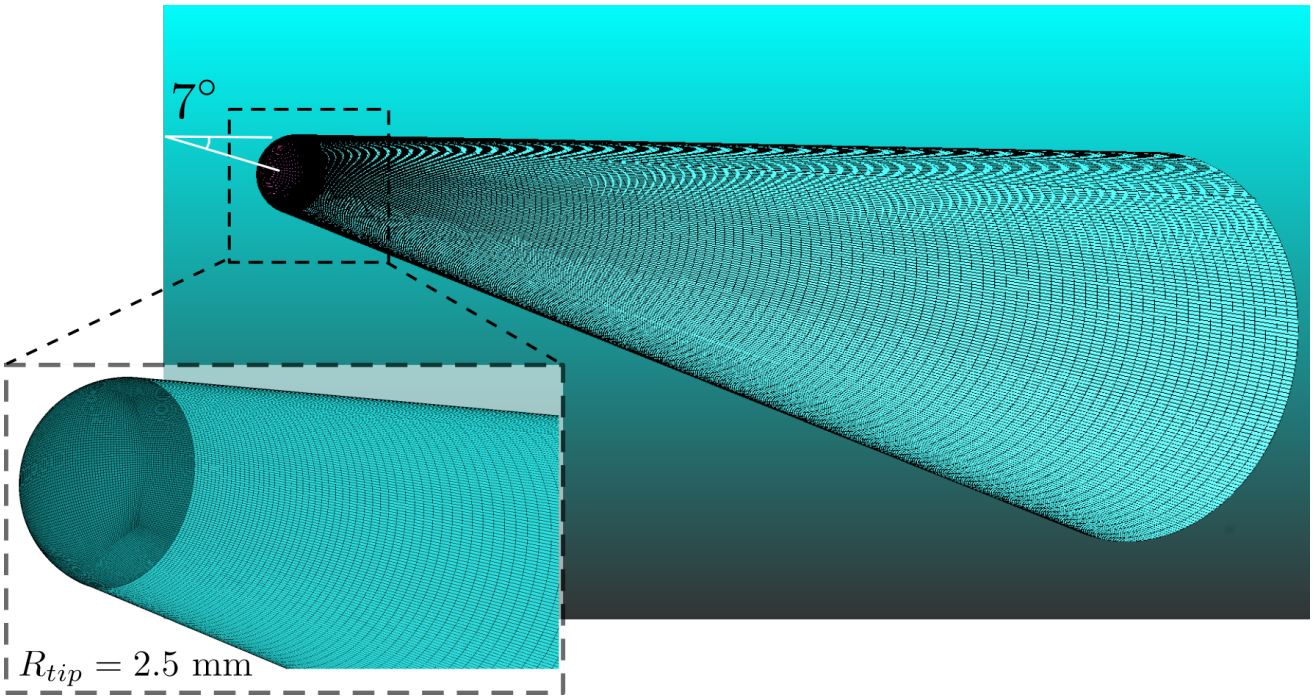


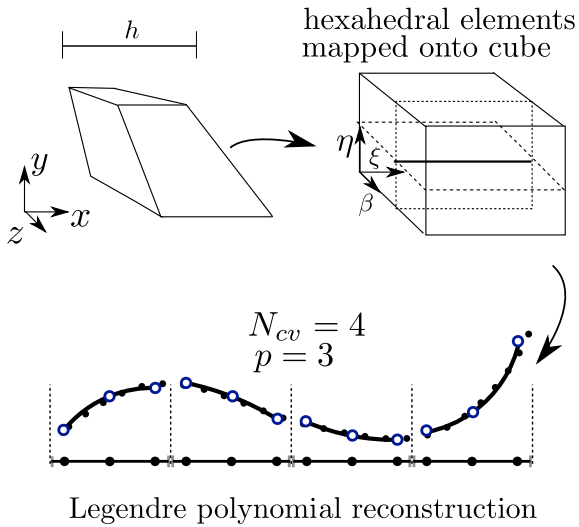
Christian Dittert (DLR-Stuttgart)
Alex Wagner (DLR-Göttinghen)

(Victor Sousa, Danish Patel, Jean B. Chapelier, Kuehl Joe, Carlo Scalo)

Block-spectral unstructured simulations: sd3DvisP

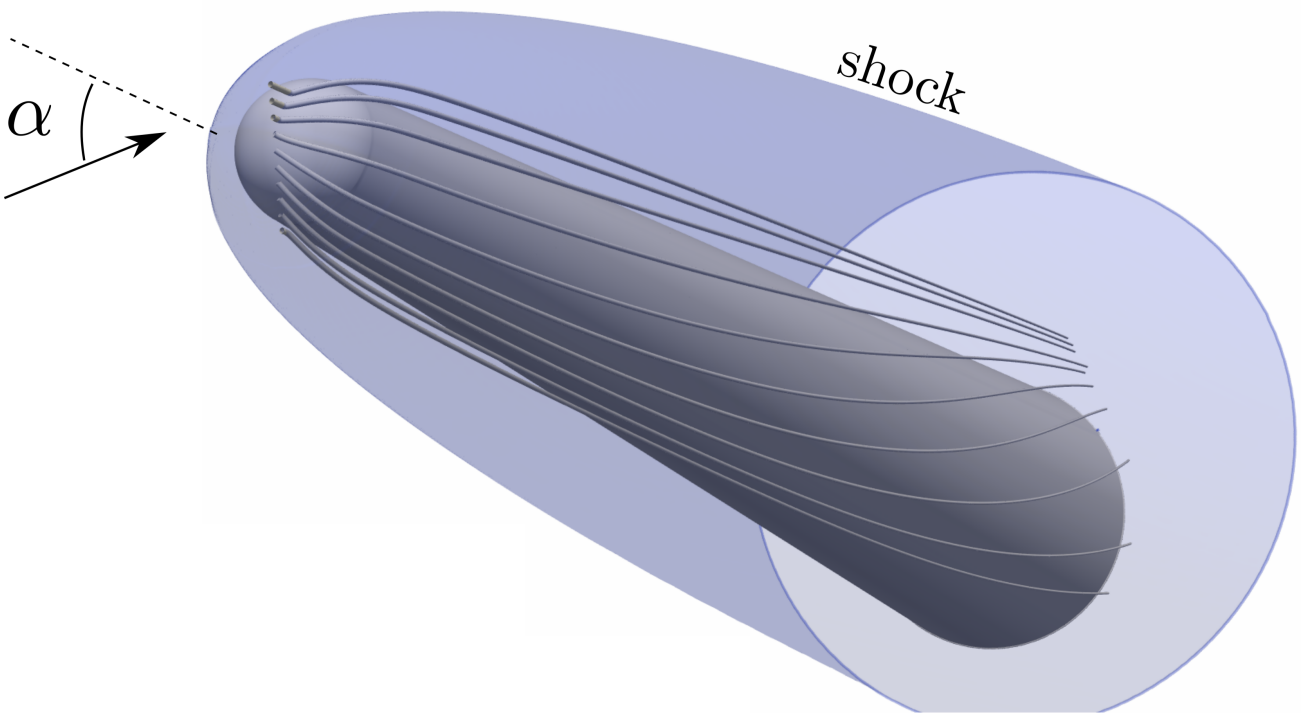
- Unstructured Spectral Difference scheme (Kopriva, Kolias, J.Comput.Phys., 1996)
- Subcell shock capturing via Laplacian artificial viscosity (Persson and Peraire, AIAA, 2006)

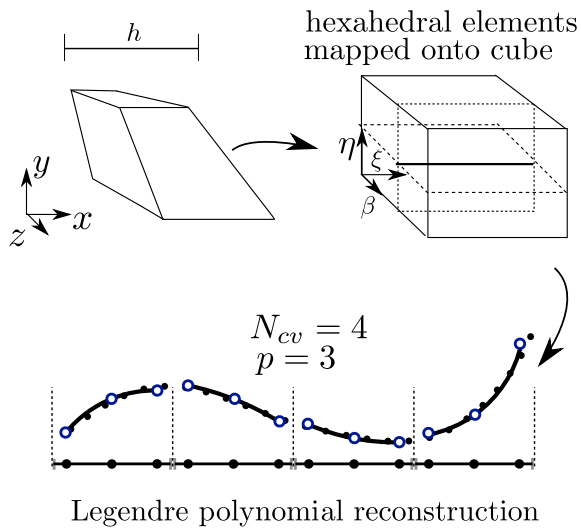




Block-spectral unstructured simulations: sd3DvisP

- Unstructured Spectral Difference scheme (Kopriva, Kolias, J.Comput.Phys., 1996)
- Subcell shock capturing via Laplacian artificial viscosity (Persson and Peraire, AIAA, 2006)

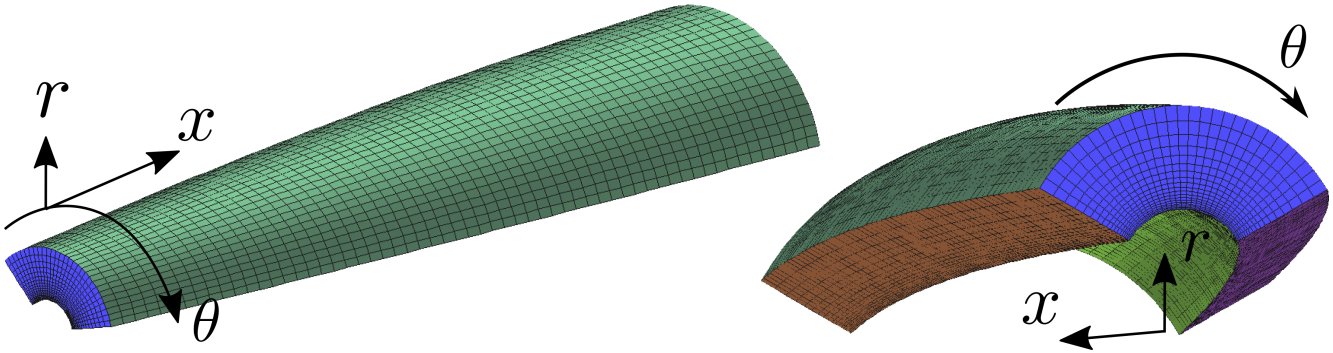




- **Work in progress:** achieving stable high-order ($p > 1$) cone-scale calculations

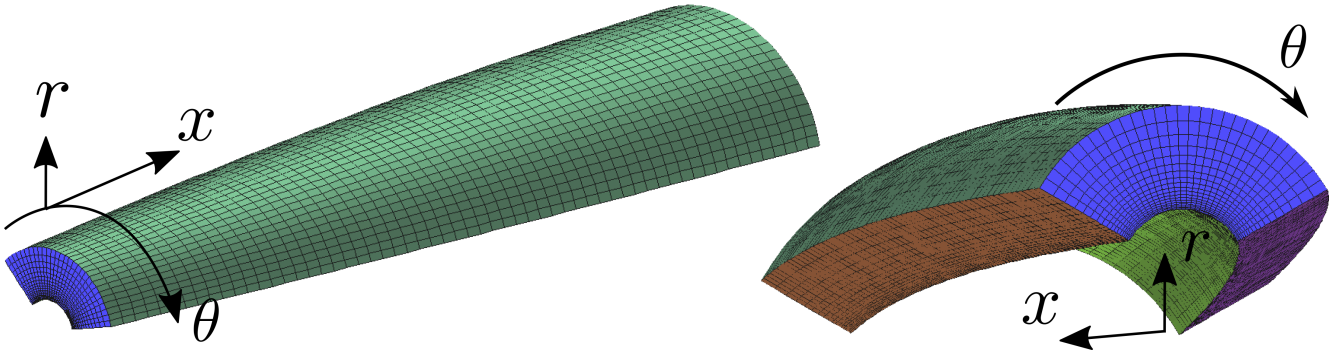
High-order structured simulations over wall impedance: CFDSU

- 6^{th}-order compact finite-difference on curvilinear grid [5]

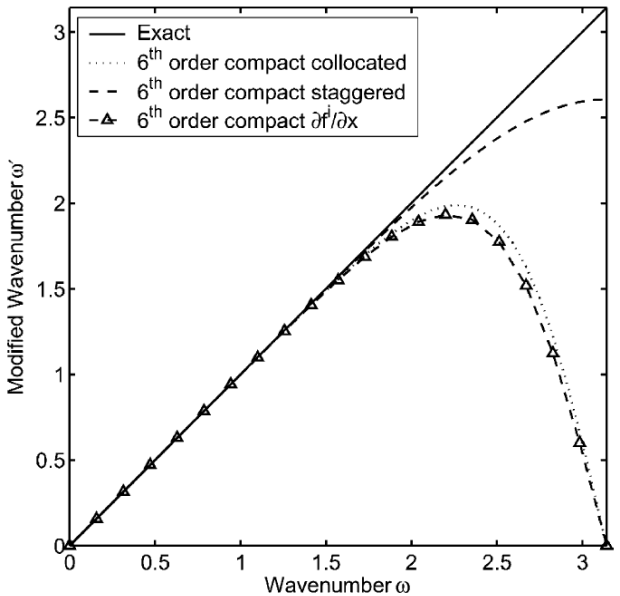


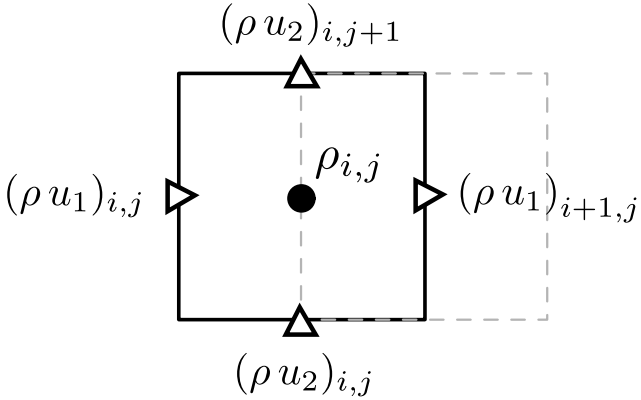
High-order structured simulations over wall impedance: CFDSU

- 6^{th}-order compact finite-difference on curvilinear grid [5]



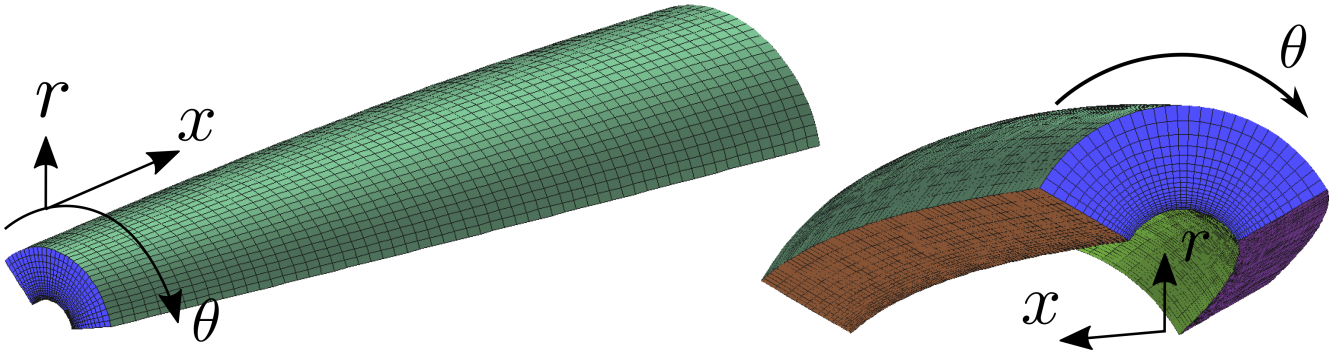
- Staggered grid improves modified wavenumber behavior [7]



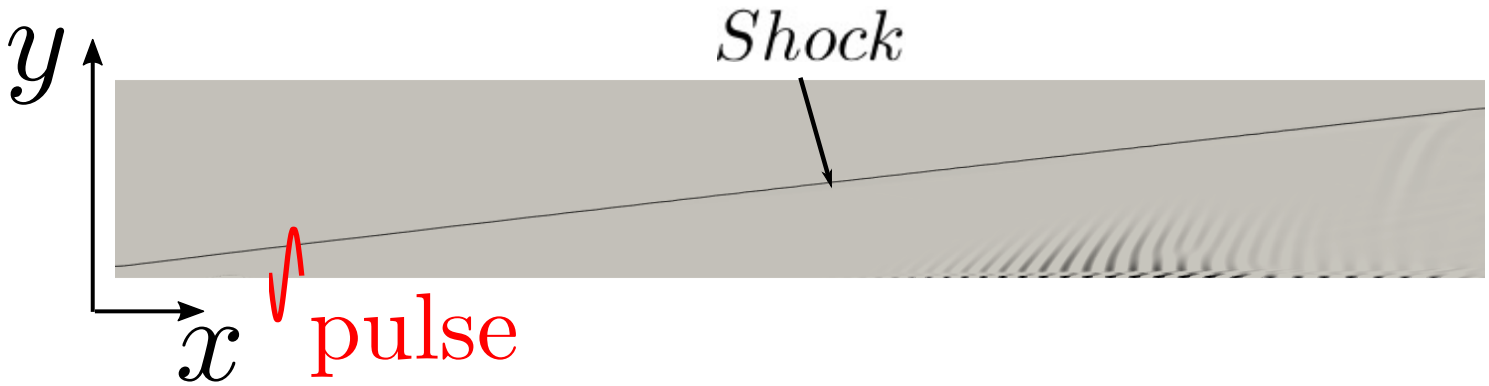


High-order structured simulations over wall impedance: CFDSU

- 6^{th}-order compact finite-difference on curvilinear grid [5]



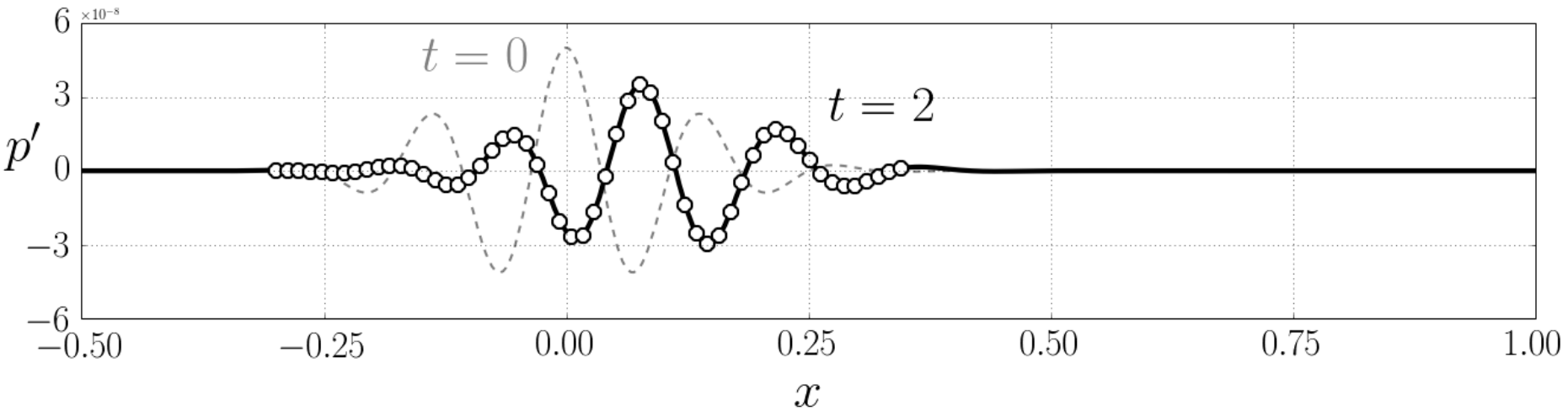
- Staggered grid improves modified wavenumber behavior [7], ideal for wave propagation



High-order structured simulations over wall impedance: CFDSU

- Exact imposition of IBCs in Navier-Stokes solver (Fung & Ju [2, 3], Scalo *et al.* [10, 6])
- Test case: impedance tube with Helmholtz oscillator $Z(\omega) = R - i\left[X_{(-1)}\omega^{-1} - X_{(+1)}\omega\right]$ located at $x = 1$
  - right-traveling broadband pulse at $t = 0$:

$$p' = \frac{1}{2} A e^{-\alpha\, k^2\, x^2} \cos\left[2\,\pi\, k\, x\right]$$
$$u' = p'$$



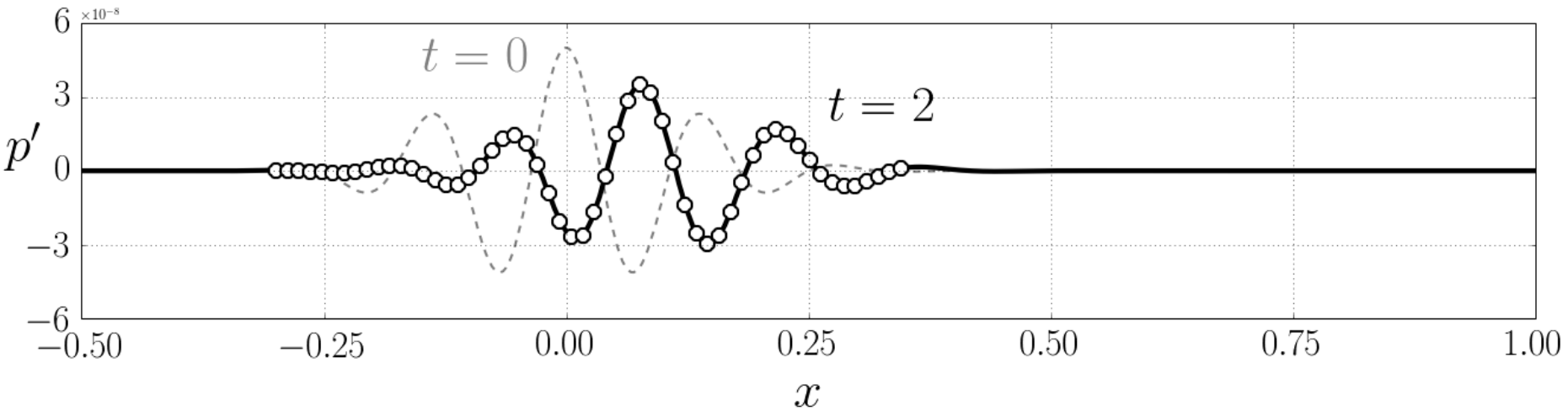
High-order structured simulations over wall impedance: CFDSU

- Exact imposition of IBCs in Navier-Stokes solver (Fung & Ju [2, 3], Scalo *et al.* [10, 6])
- Test case: impedance tube with Helmholtz oscillator $Z(\omega) = R - i\left[X_{(-1)}\omega^{-1} - X_{(+1)}\omega\right]$ located at $x = 1$
  - right-traveling broadband pulse at $t = 0$:

$$p' = \frac{1}{2} A e^{-\alpha\, k^2\, x^2} \cos\left[2\,\pi\, k\, x\right]$$
$$u' = p'$$

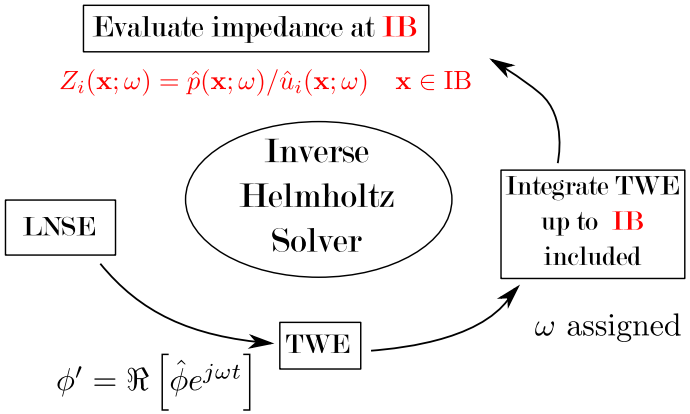
  - analytical solution for reflected wave at $t = 2$:

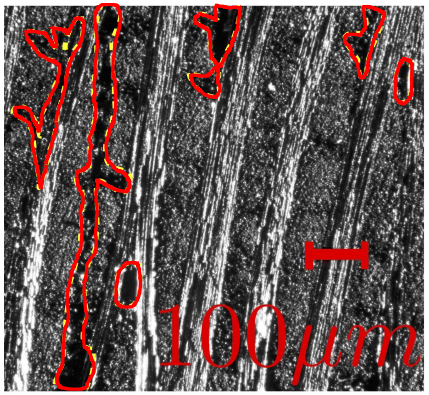
$$p'(x,t) = -\frac{A}{8\pi}\sqrt{\frac{\pi}{\alpha}} \int_{-\infty}^{+\infty} \frac{1 - Z(\omega)}{1 + Z(\omega)} e^{\mp \frac{(\omega/k \pm 2\pi)^2}{4\,\alpha}} e^{-i\omega\left[2-(x+t)\right]}\, d\omega$$

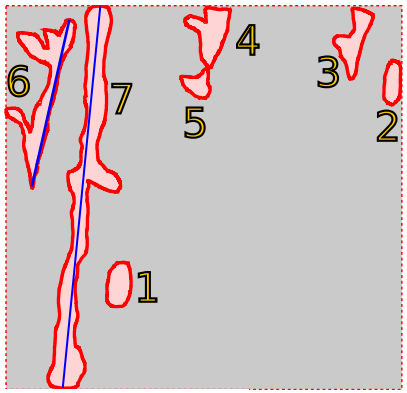


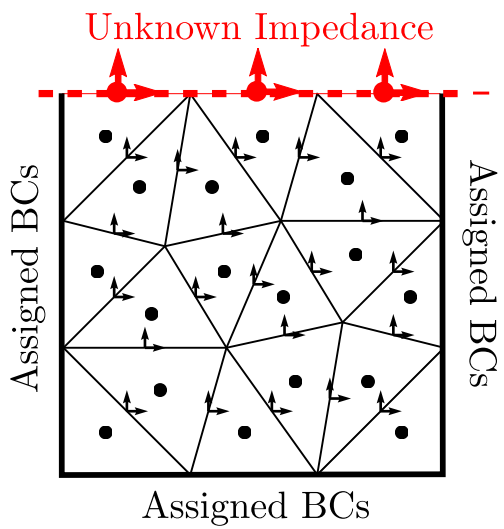
Inverse acoustic Helmholtz solver: iHS

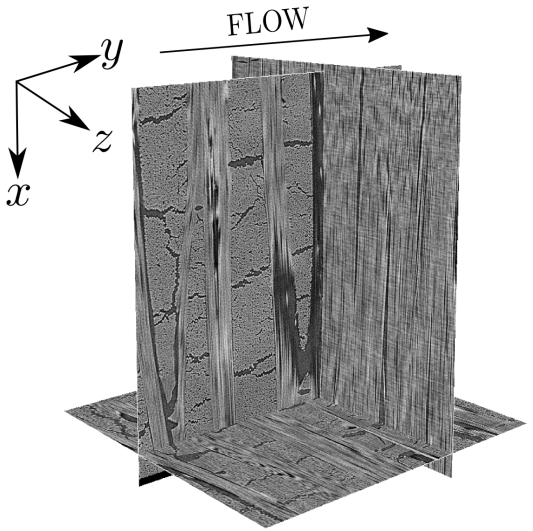
- Acoustic impedance reconstruction via iHS: Patel, Gupta, and Scalo, *JCP*, 2017 (submitted)
- iHS analysis applied to μCT scans of German C/C: Patel *et al. AIAA-SciTech*, 2017







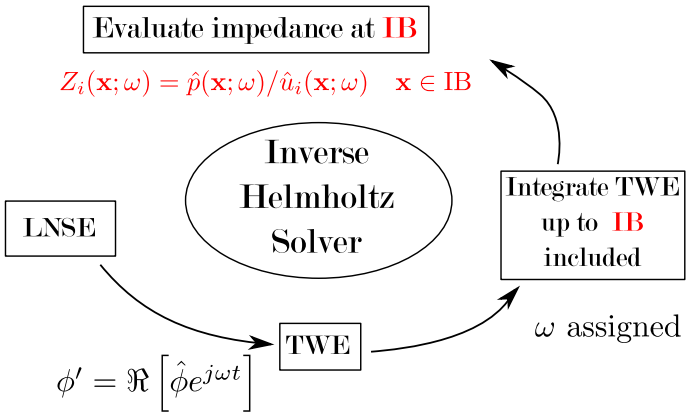


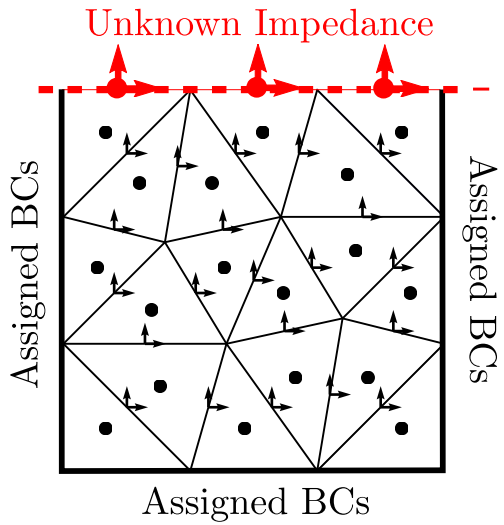


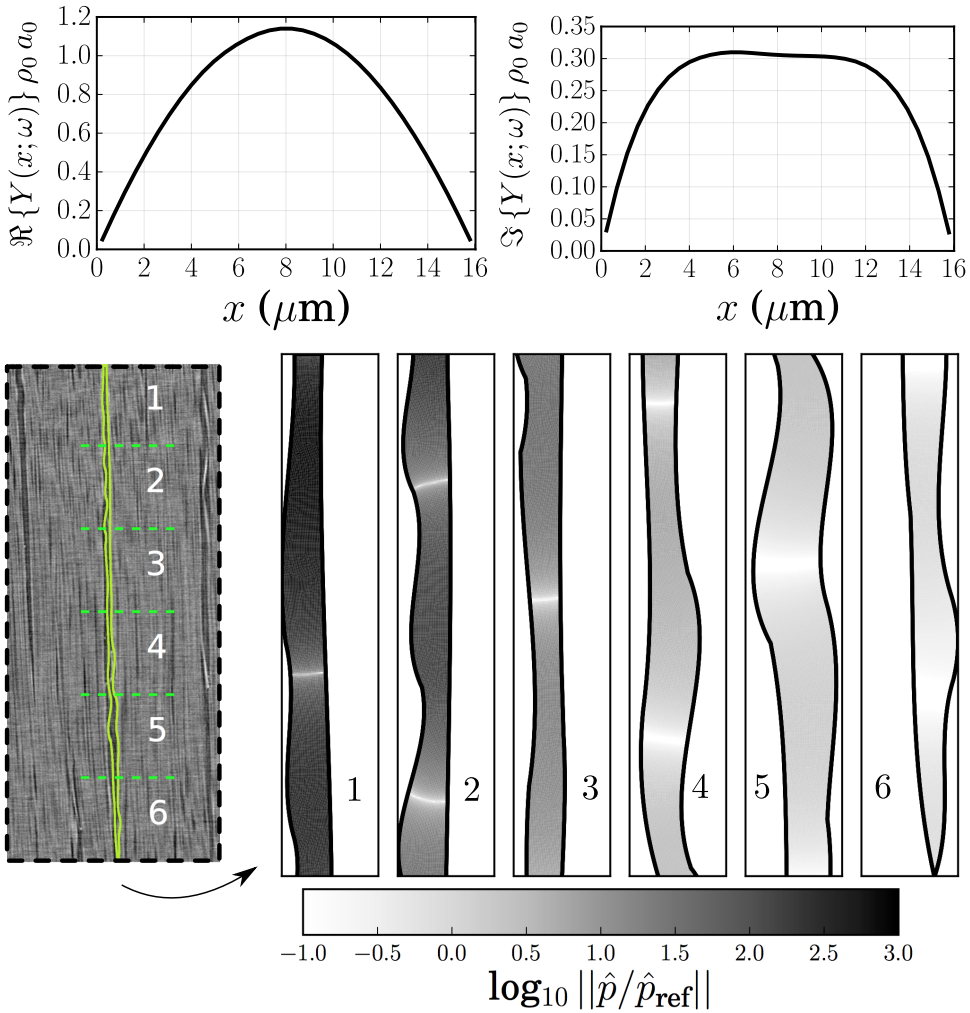
PURDUE UNIVERSITY

Inverse acoustic Helmholtz solver: iHS

- Acoustic impedance reconstruction via iHS: Patel, Gupta, and Scalo, *JCP*, 2017 (submitted)
- iHS analysis applied to μCT scans of German C/C: Patel *et al. AIAA-SciTech*, 2017

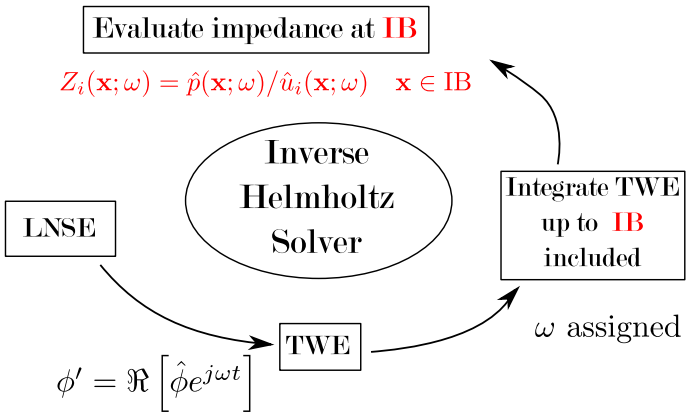


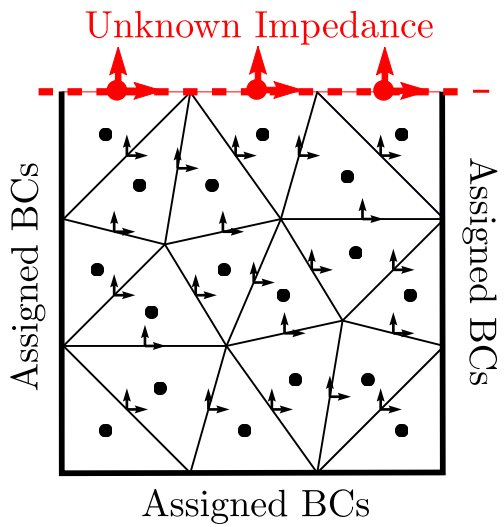




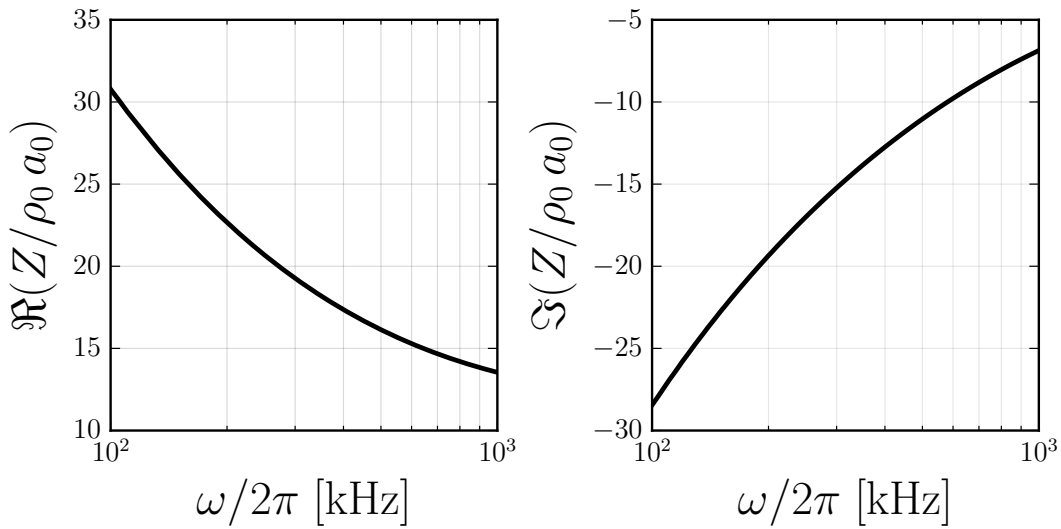
Inverse acoustic Helmholtz solver: iHS

- Acoustic impedance reconstruction via iHS: Patel, Gupta, and Scalo, *JCP*, 2017 (submitted)
- iHS analysis applied to μCT scans of German C/C: Patel *et al. AIAA-SciTech*, 2017





surface-averaged broadband impedance



$$Z(\omega) = \Re\left[Z(\omega)\right] + i\Im\left[Z(\omega)\right]$$

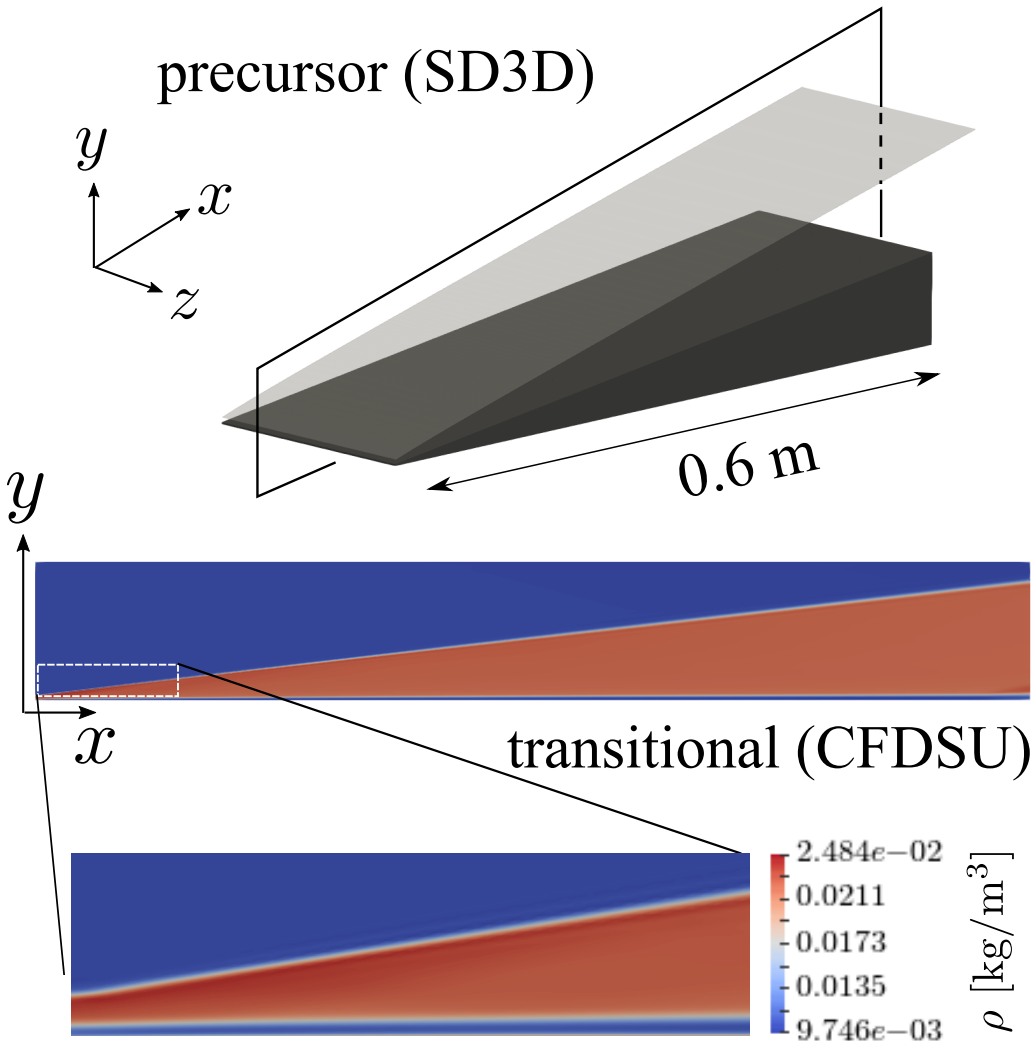
Proof of Concept: transition delay via assigned wall-impedance

- The flow conditions reported in Wagner et al. [12] experiments are used as the basis of this numerical study.

Table: *Freestream Values*

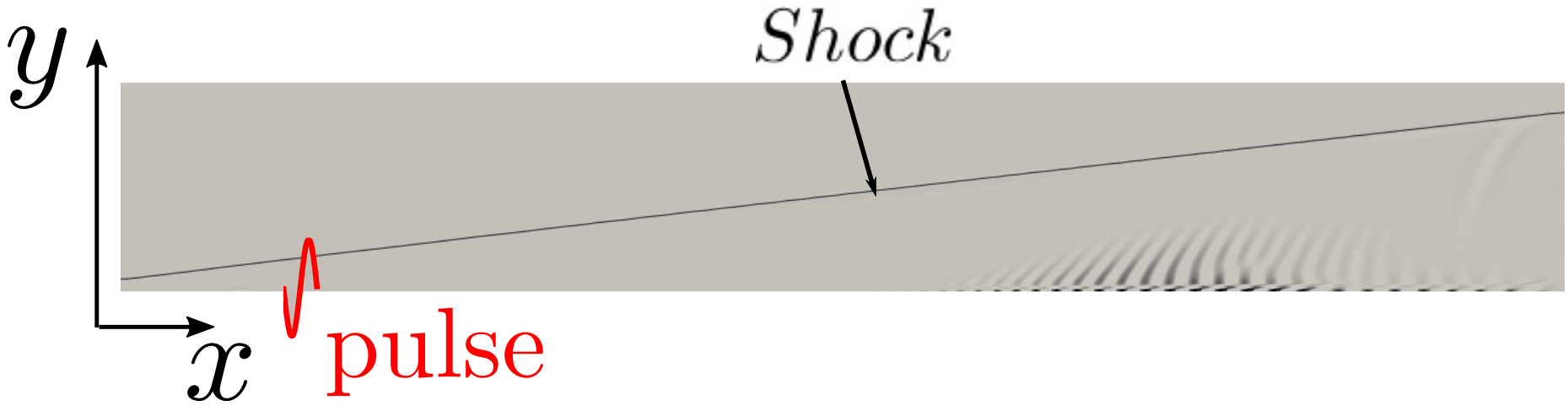
Re_m	$1.46 \cdot 10^6$
M_∞ $[-]$	7.3
p_∞ $[Pa]$	789
T_∞ $[K]$	267
ρ_∞ $[g/m^3]$	10.2
u_∞ $[m/s]$	2409

- Test Case: hypersonic boundary layer flow over a wedge
- Gradual introduction of shock into high-order computation



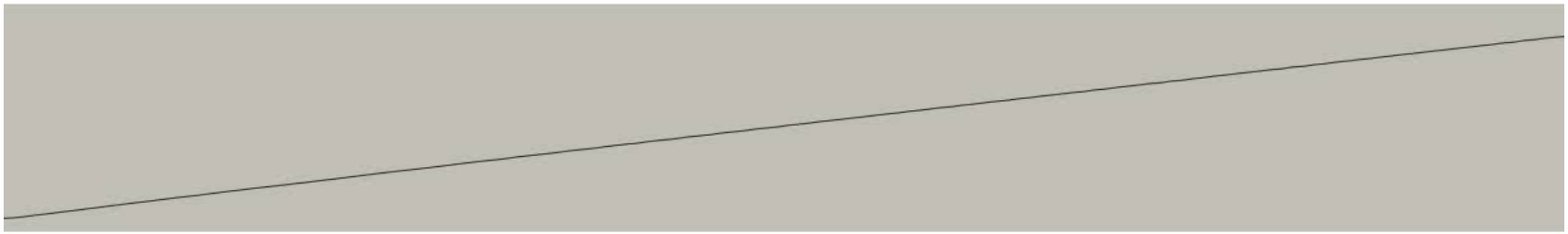
Pulse Excitation

- Broadband pulse excitation (Fasel *et al.* [4, 11]): finding most amplified frequency



Pulse Excitation

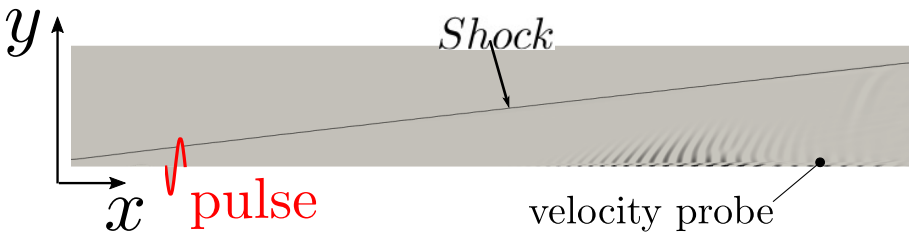
- Broadband pulse excitation (Fasel *et al.* [4, 11]): finding most amplified frequency

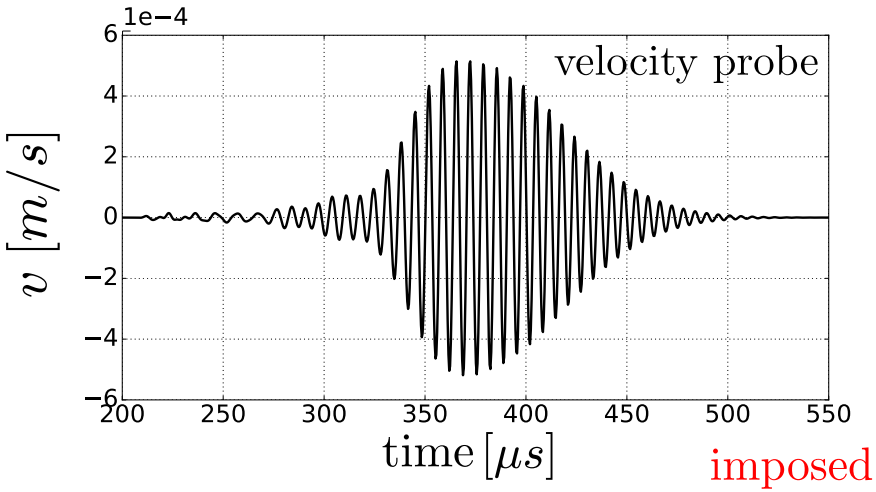


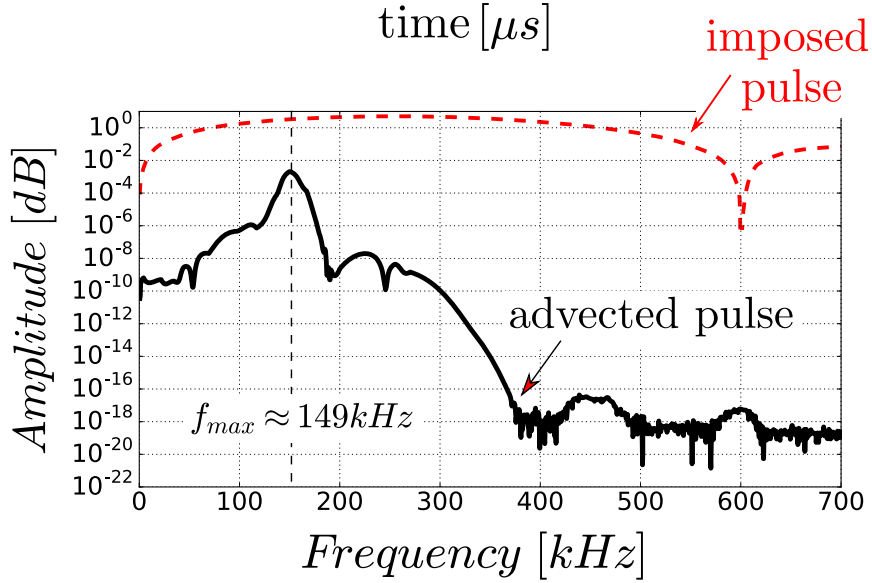
Results

Pulse Excitation

- Broadband nature of imposed pulse
- The advected perturbation is acquired at the end of the simulation domain
- The most unstable frequency for the studied case is captured
- Used for a harmonic excitation study over walls of different porosity (impedance)



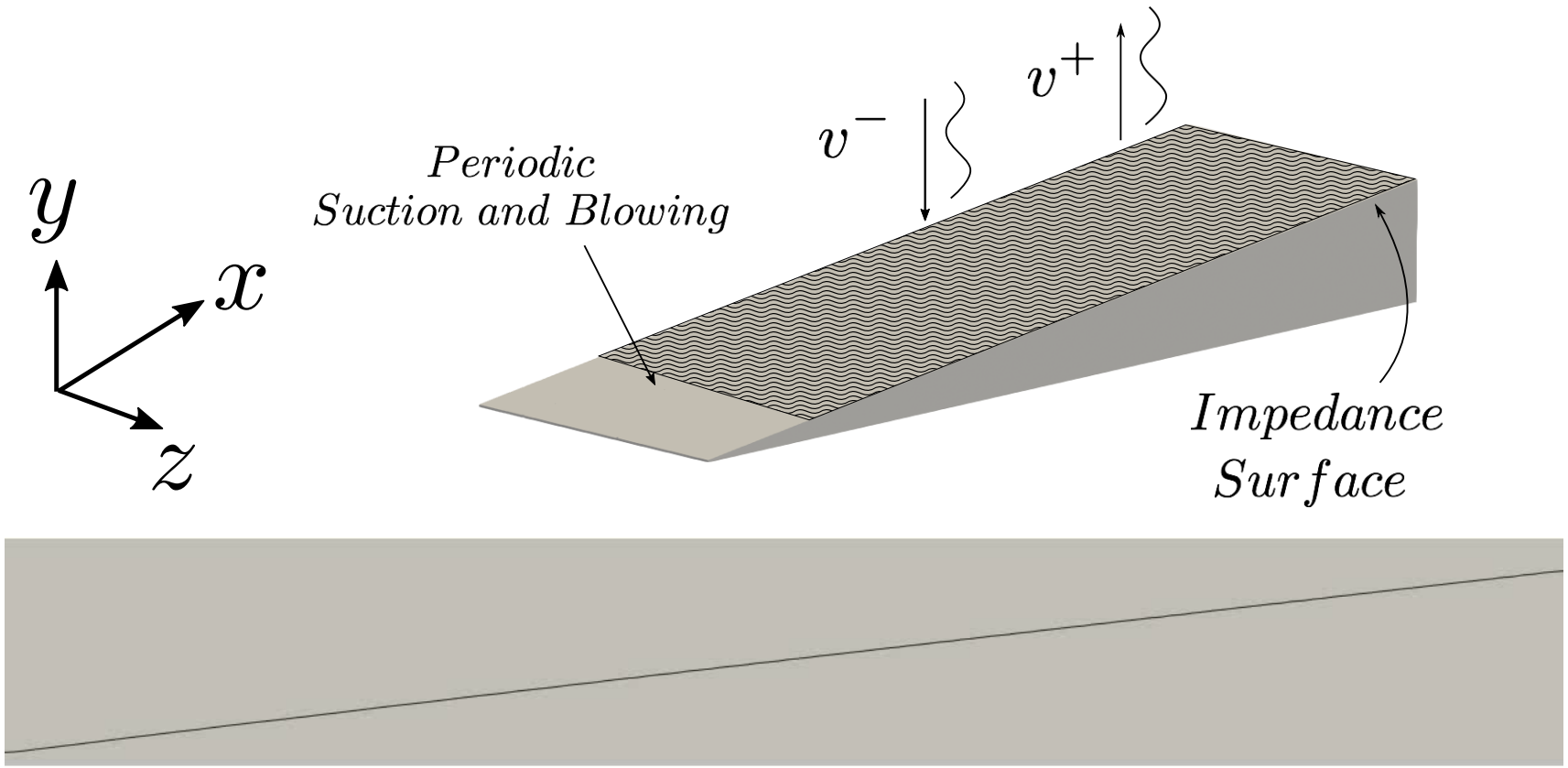




PURDUE UNIVERSITY

Harmonic Excitation

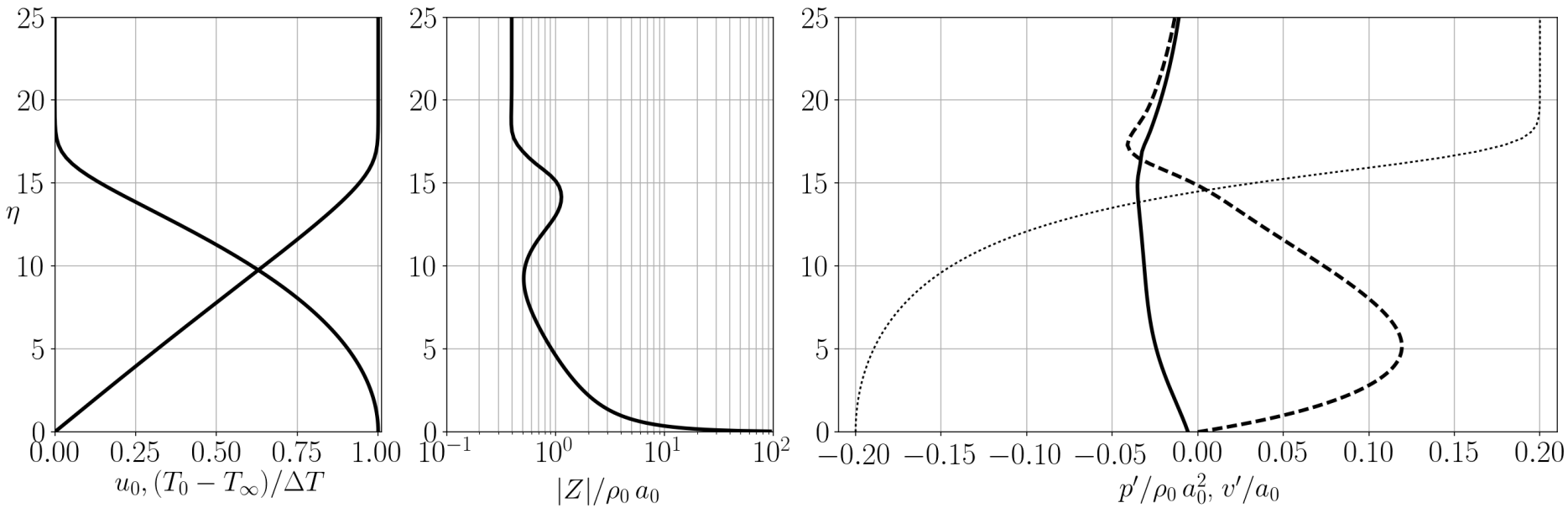
- Example of a harmonic excitation run over purely reflective walls $Z(\omega) \to \infty$ (hard wall)
- This case is run until a steady state is reached
  - The amplitudes are acquired for the different wall impedance cases



Flat Plate Hypersonic Boundary Layer (Kuehl & Scalo, 2017)

- Dimensional parameters: $u_\infty = 1100$ m/s, $a_\infty = 194$ m/s, $\omega/2\pi \simeq 156$kHz, $\delta_{99} \simeq 3.2$mm

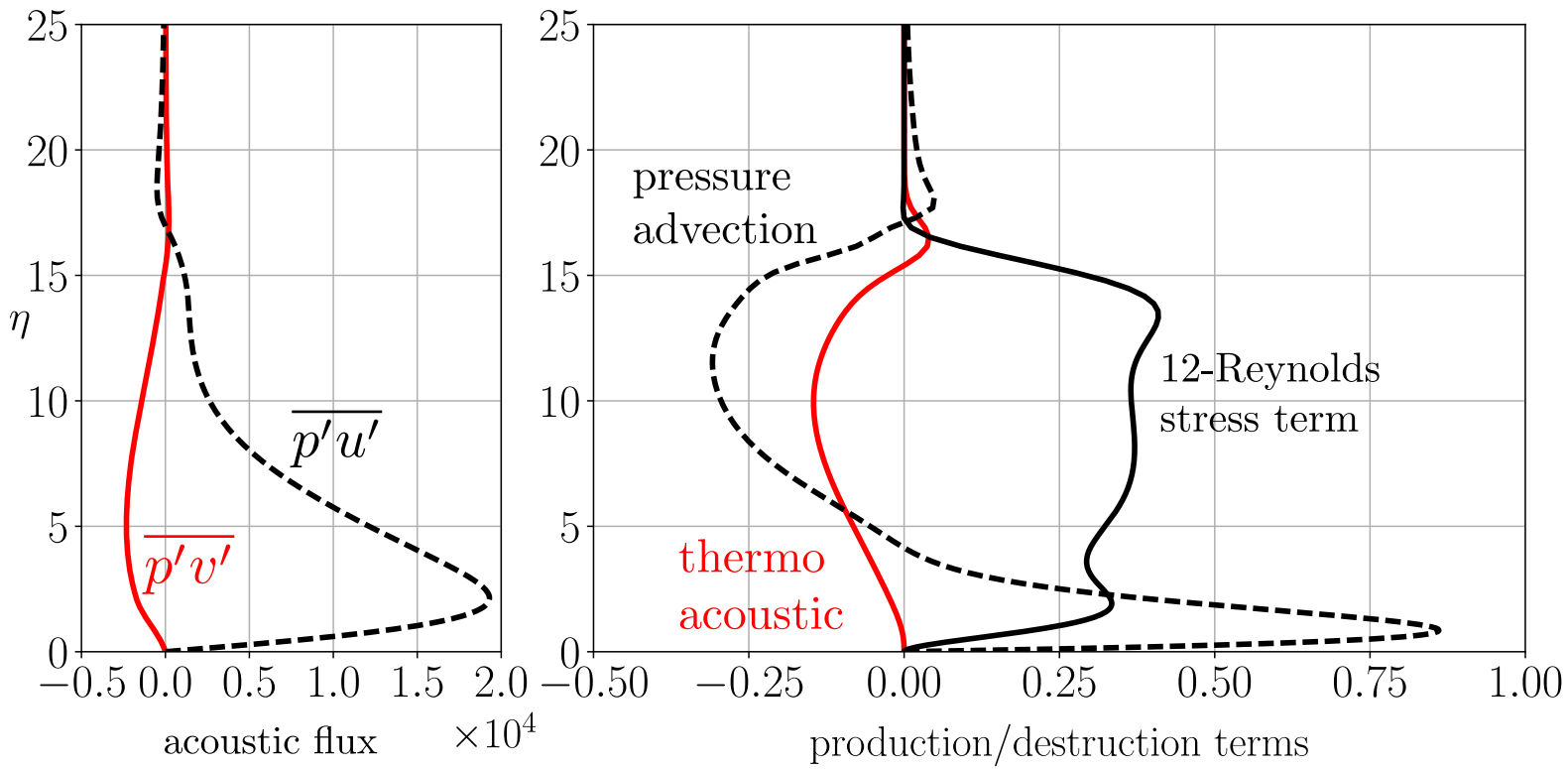
$$u_0 = u_0^*/u_\infty, \quad p' = p^{*\prime}/\rho_0^* \, a_0^{*2}, \quad v' = v^{*\prime}/u_\infty, \quad \eta = y^*/\sqrt{\nu_\infty{}^* \, x^*/u_\infty{}^*}$$



Perturbation Energy Budgets (Kuehl & Scalo, 2017)

- Inviscid acoustic perturbation energy: $\overline{E} = \frac{1}{2}\rho_0\left(\overline{u'^2} + \overline{v'^2}\right) + \frac{1}{2\rho_0 a_0^2}\overline{p'^2}$

$$\frac{D\overline{E}}{Dt} = \underbrace{-\overline{p'\,v'}\,\frac{1}{T_0}\,\frac{d\,T_0}{d\,y}}_{\text{thermoacoustic}} \underbrace{-\overline{u'\,\frac{\partial p'}{\partial x}} - \overline{v'\,\frac{\partial p'}{\partial y}}}_{\text{pressure-advection}} \underbrace{-\rho_0\overline{u'v'}\,\frac{d\,u_0}{d\,y}}_{\text{12-Reynolds stress}}$$



PURDUE UNIVERSITY

Harmonic Excitation

- Impedance Boundary Condition (IBC):

$$\hat{p} = Z(\omega)\hat{v}$$

is imposed via Time-Domain technique by Scalo *et al.* 2015 [10]

- A three-parameter impedance model:

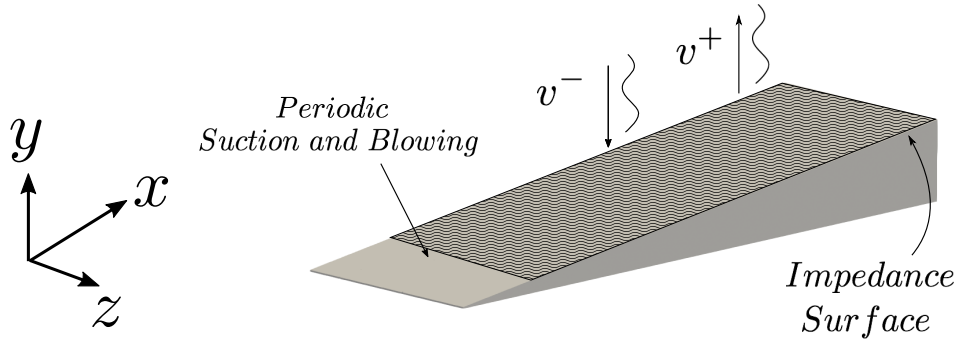
$$Z(\omega) = R + i\left(X_{+1}\omega - X_{-1}/\omega\right)$$

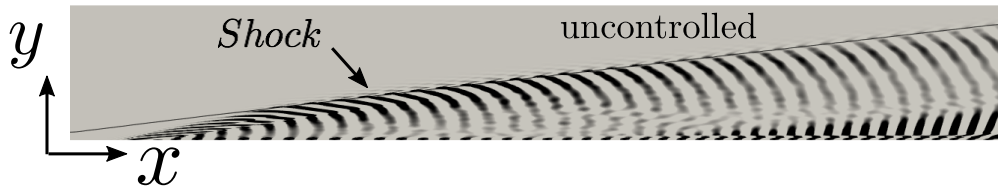
tuned to the most amplified frequency

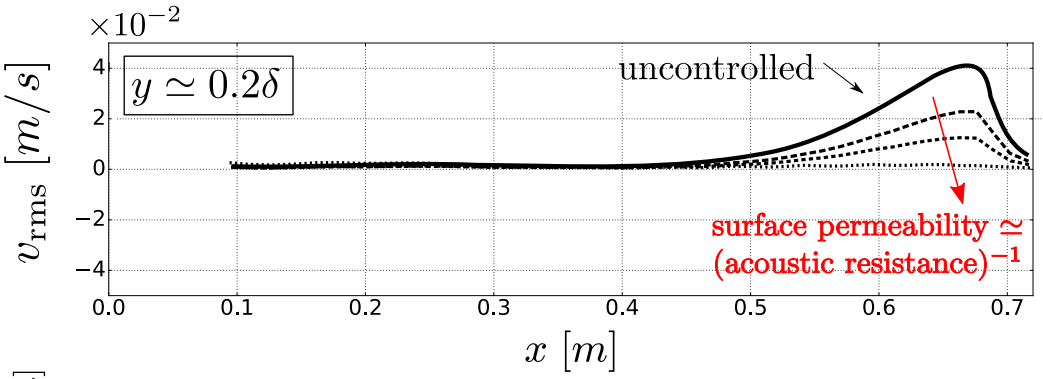
$$f_{\text{res}} = \frac{1}{2\pi}\sqrt{\frac{X_{-1}}{X_{+1}}} \simeq 149\text{kHz}$$

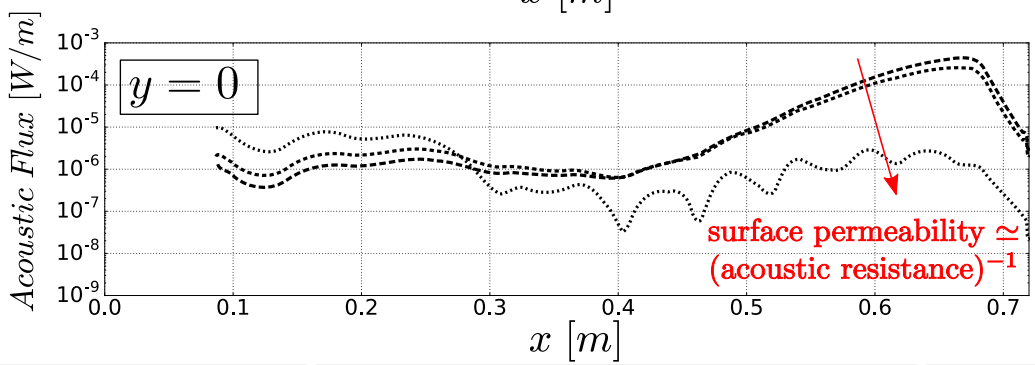
effectively damps acoustic energy.

- Idealized Impedance $\Rightarrow$ not representative of realistic porous surfaces









PURDUE UNIVERSITY

Harmonic Excitation

- Impedance Boundary Condition (IBC):

$$\hat{p} = Z(\omega)\hat{v}$$

is imposed via Time-Domain technique by Scalo *et al.* 2015 [10]

- A three-parameter impedance model:

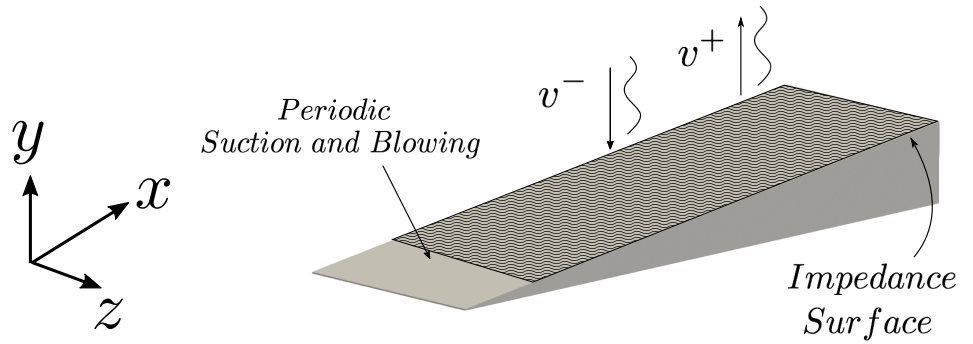
$$Z(\omega) = R + i\left(X_{+1}\omega - X_{-1}/\omega\right)$$

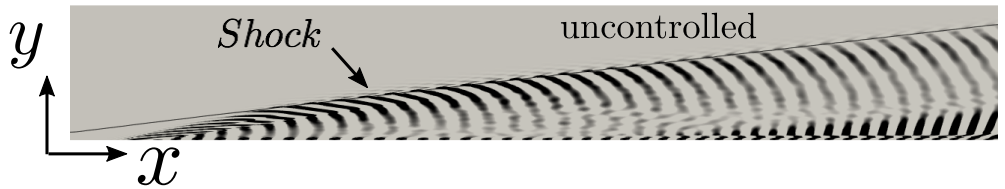
tuned to the most amplified frequency

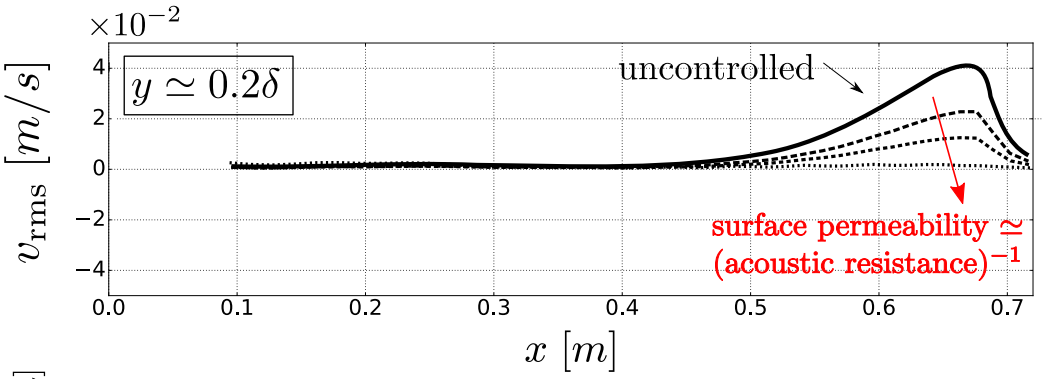
$$f_{\text{res}} = \frac{1}{2\pi}\sqrt{\frac{X_{-1}}{X_{+1}}} \simeq 149\text{kHz}$$

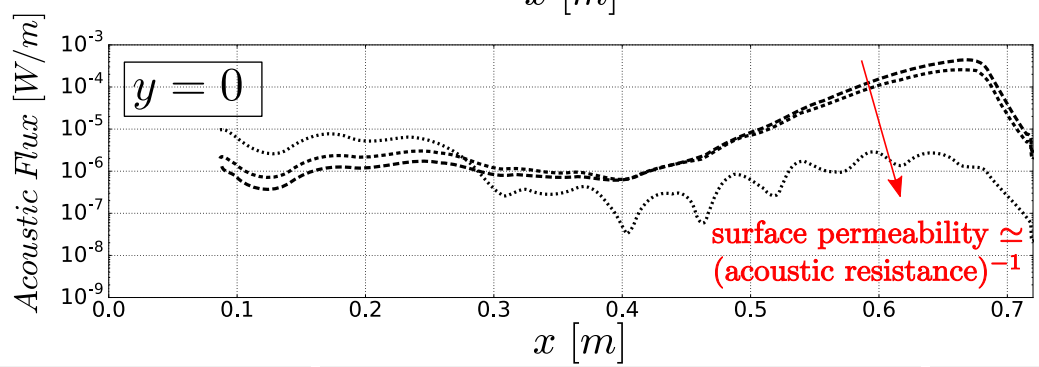
effectively damps acoustic energy.

- Idealized Impedance $\Rightarrow$ not representative of realistic porous surfaces
- Any given impedance can be represented as a linear superposition of three-parameter models





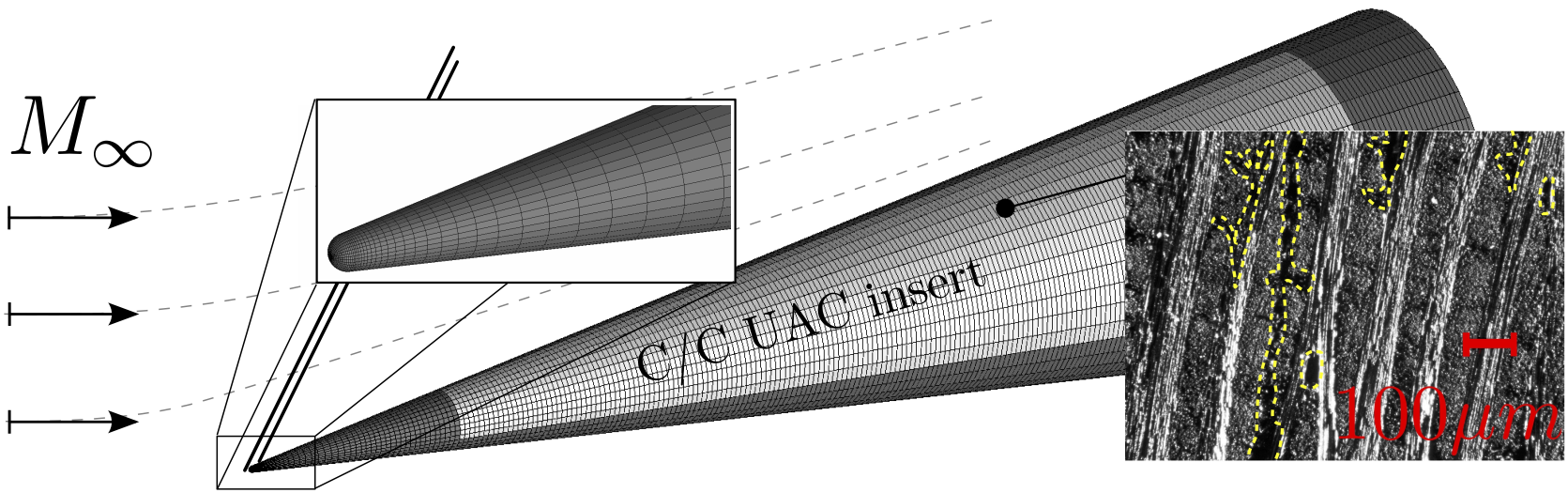




Objectives

Short Term: Modeling of Transition Control over C/C UACs

1. *Ultrasonics*: Characterization of acoustic response of porous C/C UACs
2. *Aerodynamics*: DNS of transition delay experiments of Wagner *et al.* [12, 13]



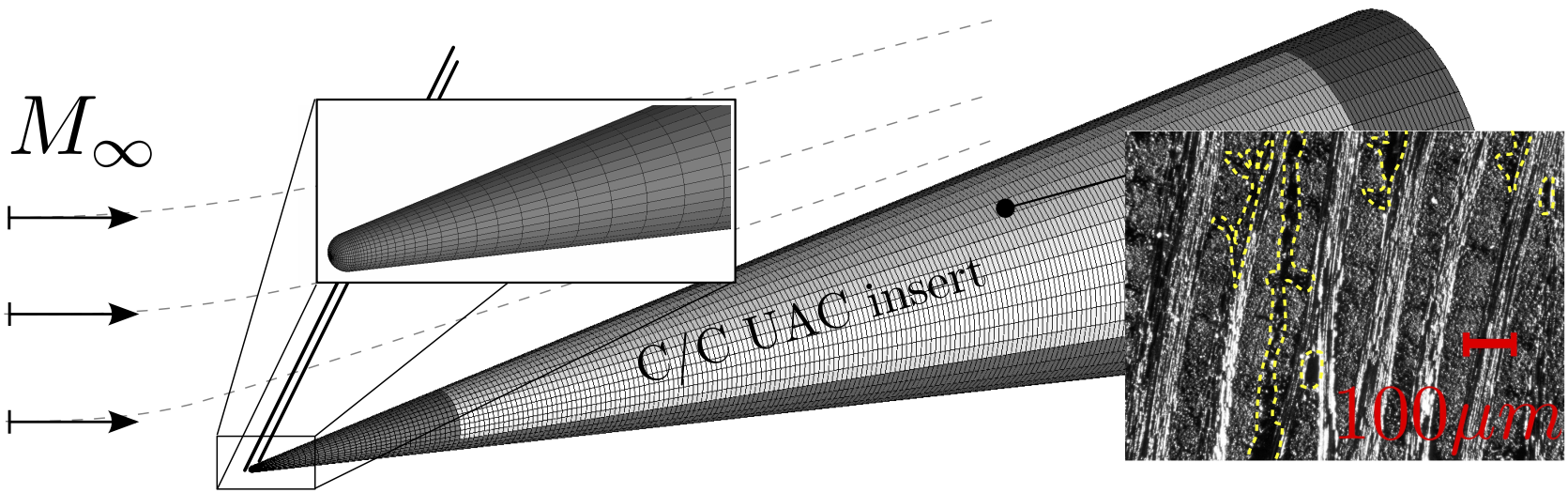
Objectives

Short Term: Modeling of Transition Control over C/C UACs

1. *Ultrasonics*: Characterization of acoustic response of porous C/C UACs
2. *Aerodynamics*: DNS of transition delay experiments of Wagner *et al.* [12, 13]

Long Term: Sub-Task on C/C UACs for NATO AVT-240 (2018)?

- USA: Carlo Scalo (Purdue), Erica Corral (U. Arizona / Sandia)
- DLR: A. Wagner (Göttinghen), V. Wartemann (Braunschweig), M. Kuhn (Stuttgart)
- Prospective AF funding: Conversations with Ivett Leyva and Ali Sayir



References I



Jean-Baptiste Chapelier, Carlo Scalo, and Bono Wasistho.

Development of adaptive subgrid scale models based on a large-scale vorticity sensor.

American Institute of Aeronautics and Astronautics, 2017/07/29 2017.



K. Y. Fung and H. Ju.

Broadband Time-Domain Impedance Models.

AIAA Journal, 39(8):1449–1454, 2001.



K. Y. Fung and H. Ju.

Time-domain Impedance Boundary Conditions for Computational Acoustics and Aeroacoustics.

Int. J. Comput. Fluid D., 18(6):503–511, 2004.



Andreas C Laible, Christian S.J. Mayer, and Fasel F. Hermann.

Numerical Investigation of Transition for a Cone at Mach 3.5: Oblique Breakdown.

In *39th AIAA Fluid Dynamics Conference*, June 2009.



Sanjiva K. Lele.

Compact finite difference schemes with spectral-like resolution.

Journal of Computational Physics, 103(1):16–42, 1992.



J. Lin, C. Scalo, and L. Hesselink.

High-fidelity simulation of a standing-wave thermoacoustic–piezoelectric engine.

Journal of Fluid Mechanics, 808:19–60, Dec 2016.

References II



Santhanam Nagarajan, Sanjiva K Lele, and Joel H Ferziger.

A robust high-order compact method for large eddy simulation.

Journal of Computational Physics, 191(2):392–419, 2003.



Iman Rahbari and Carlo Scalo.

Bi-Global stability analysis of compressible channel flow over complex impedance walls.

In *55th AIAA Aerospace Sciences Meeting*, page 1879, January 2017.



Iman Rahbari and Carlo Scalo.

Linear Stability Analysis of Compressible Channel Flow over Porous Walls, pages 451–467.

Springer International Publishing, Cham, 2017.



C. Scalo, J. Bodart, and S. K. Lele.

Compressible turbulent channel flow with impedance boundary conditions.

Phys. Fluids, 27(035107), 2015.



Jayahar Sivasubramanian and Hermann F. Fasel.

Numerical investigation of the development of three-dimensional wavepackets in a sharp cone boundary layer at Mach 6.

J. Fluid Mech., 756:600–649, 10 2014.

References III



A. Wagner.

Passive Hypersonic Boundary Layer Transition Control Using Ultrasonically Absorptive Carbon-Carbon Ceramic with Random Microstructure.

PhD thesis, Katholieke Universiteit, Leuven, 2014.



A. Wagner, K Hannemann, and M. Kuhn.

Experimental investigation of hypersonic boundary-layer stabilization on a cone by means of ultrasonically absorptive carbon-carbon material.

In *18th AIAA/3AF International Space Planes and Hypersonic Systems and Technologies Conference*, 2012.

AIAA-2012-5865.



A. Wagner, K Hannemann, and M. Kuhn.

Ultrasonic absorption characteristics of porous carbon–carbon ceramics with random microstructure for passive hypersonic boundary layer transition control.

Experiments in Fluids, 55(6):1750, 2014.